ENGINEERING COLLAGEN MIMETIC PEPTIDE AMPHIPHILE HYDROGELS BY TUNING MECHANICAL PROPERTIES FOR BIOMEDICAL APPLICATIONS

SUSHMITHA SUNDAR
(M.Tech., ***Indian Institute of Technology, Kharagpur*****)**

A THESIS SUBMITTED

FOR THE DEGREE OF DOCTOR OF PHILOSOPHY
DEPARTMENT OF BIOMEDICAL ENGINEERING
NATIONAL UNIVERSITY OF SINGAPORE

2015

DECLARATION

I hereby declare that this thesis is my original work and it has been written by me in its entirety. I have duly acknowledged all the sources of information which have been used in this thesis.

This thesis has also not been submitted for any degree in any university previously.

Sushmitha Sundar
30 June 2015

ACKNOWLEDGEMENTS

It is a joy to express my gratitude to all the people who were in my thick and thin phases of PhD journey from the beginning to the end.

First and foremost, I would like to express my deepest and most sincere gratitude to my supervisor, Professor Tong Yen Wah, for giving me this precious learning opportunity. His passion in scientific research, guidance and good will during these challenging but wonderful years are the key motivating factors behind my successful completion of this thesis. I am sincerely grateful to his invaluable patience and advice that aided in enhancing the quality of this research. I also want to show my appreciation to the Department of Biomedical Engineering, National University of Singapore for providing the research opportunity and research scholarship. In addition, I also want to show my appreciation to Department of Chemical and Biomolecular Engineering for the facilities provided that made this study possible.

I would also like to thank Dr. Luo Jingnan for mentoring me in the initial phase of my PhD. In addition, I would like to thank Dr. Chen Wenhui, Dr. Liang Youyun and Dr. Anjaneyulu Kodali for teaching me various cell culture and immunofluorescence techniques as well as for taking part in some stimulating discussions on tissue engineering along with Mr. Chen Yiren which immensely helped in expanding my knowledge. My special thanks to all my fellow lab mates

Dr. Niranjani Sankarakumar, Dr. Xie Wenyuan, Dr. He Fang, Dr. Guo Zhi, Dr. Ingo Wolf, Dr. Zhou Danhua, Dr. Jee Yeon, Ms. Ajitha Sundaresan, Mr. Lee Jonathan, Ms. Zhu Meiling, Ms. Gan Hui Xian and others for all the valuable advices and fun times! In addition, I would like to thank our lab officers, Ms. Li Fengmei, Dr. Yang Liming, Ms. Li Xiang, Mr. Evan Stephen Tan, Mr. Ang Wee Siong, Mr. Lim You Kang and Mrs. Siew Woon Chee for helping with various technical, administrative and safety issues.

Last but not least, I would like to thank my parents for their unconditional support and love which made me successfully overcome all the difficulties and challenges in this PhD journey. Finally, I would like to thank my dearest husband, Mr. Praveen Pothala, for his selfless support and love.

Above all, I would like to express my heartfelt gratitude to God for providing and leading me through this journey of learning and experience.

TABLE OF CONTENTS

SUMMARY

The ultimate aim of this work is to design and engineer a collagen mimetic peptide amphiphile hydrogel with appropriate mechanical cue for the culture of fibroblast cells for biomedical applications. In order to achieve this aim, we employed three design strategies to fabricate collagen mimetic peptide amphiphile (CM-PA) nanofiber hydrogels with varying mechanical cues.

In the initial parts of the study, collagen mimetic peptide amphiphile nanofiber hydrogels are investigated for the fibroblast cell culture with the preferred nano-topographical and biochemical cues (Chapter 4). This study led to the need of tuning the mechanical properties of the collagen mimetic peptide amphiphile nanofiber hydrogels.

The first strategy employed to tune the mechanical properties of the collagen mimetic peptide amphiphile nanofiber hydrogels is to fabricate a semi-interpenetrating network hydrogels consisting of collagen mimetic peptide amphiphile and poly(ethylene glycol) diacrylate with varying mechanical cues (Chapter 5). After the fabrication, the hydrogels were physically and biologically characterized. This study led to the conclusion that biochemical cue of collagen mimetic peptide amphiphile is essential for fibroblast cell viability, however, mechanical cue for fibroblast culture is required in a nanoscale level.

The second strategy employed is to tune the mechanical properties of the collagen

mimetic peptide amphiphile nanofiber hydrogels at the nanoscale level by mimicking the *in vivo* mechanism of enzyme mediated covalent cross-linking of collagen fibrillogenesis by employing a chemical cross-linker, glutaraldehyde (Chapter 6). After the fabrication, the hydrogels were physically and biologically characterized. This study led to the conclusion that, indeed, fibroblast cells respond to the nanoscale level mechanical cue. However, the design limits the use of collagen mimetic peptide amphiphile hydrogels for in-situ gelling.

Finally, the third strategy is to tune the mechanical properties of the collagen mimetic peptide amphiphile nanofiber hydrogels by tapping the advantage of the modular nature of the single tail peptide amphiphile system (Chapter 7). Collagen mimetic peptide amphiphile nanofiber hydrogel with a novel design was fabricated and characterized by physical and biological techniques. This study led to the conclusion that mechanically stiffer collagen mimetic peptide amphiphile nanofiber hydrogels in the nano-scale level can be obtained by changing the amino acid sequence and can expand the use of collagen mimetic peptide amphiphile nanofiber hydrogels for in-situ three dimensional cell culture for other cell and tissue types.

This research only serves as groundwork in the proposed design strategy for collagen mimetic peptide amphiphile nanofiber hydrogels. Hence, use of this design for other cell and tissue types will raise new issues and challenges. This area will be examined by other members of our group.

LIST OF TABLES

LIST OF FIGURES

LIST OF SYMBOLS AND ABBREVIATIONS

θ	Ellipticity in millidegrees
$[\theta]$	Molar ellipticity
α	Alpha
β	Beta
c	Concentration in mg/ml
G’	Storage modulus
G”	Loss modulus
l	Path length of the cuvette in cm
m	Molecular weight in g/mol
m_0	Dry weight of the semi-interpenetrating network hydrogel constructs
m_{eq}	Equilibrium wet weight of the semi-interpenetrating network hydrogel constructs
T_m	Melting temperature
x	Wavelength at positive CD peak maxima
y	Wavelength at negative CD peak maxima.
2D	Two dimensional
3D	Three dimensional
ATCC	American type culture collection
bFGF-2	Basic fibroblast growth factor 2
BMP-2	Bone morphogenetic protein 2
BSA	Bovine serum albumin
CD	Circular dichroism

CLSM	Confocal laser scanning microscope
CMP	Collagen-mimetic peptide
CM-PA	Collagen mimetic peptide amphiphile
Cryo-SEM	Scanning Electron Microscope in cryo mode
DMEM	Dulbecco's modified Eagle's medium
DMSO	Dimethyl sulfoxide
ECM	Extracellular matrix
ESI MS	Electrospray ionization mass spectrophotometer
EWC	Equilibrium water content
FBS	Fetal bovine serum
FTIR	Fourier Transform – Infra-red
Glt	Glutaraldehyde
HPLC	High performance liquid chromatography
KBr	Potassium bromide
K-PA	Spacer peptide amphiphile
LLC	Limited liability company
ME	Molar ellipticity
MTT	Thiazolyl Blue Tetrazolium Bromide
Na_3PO_4	Trisodium phosphate
NIH	National Institutes of Health
PA	Peptide amphiphile
PBS	Phosphate buffered saline
PEG	Poly(ethylene glycol)
PEGDA	Poly(ethylene glycol) diacrylate
PPII	Polyproline II-type

PTA	Phosphotungstic acid
S-IPN	Semi-interpenetrating network
TEM	Transmission Electron Microscope
TRITC	Tetramethylrhodamine isothiocyanate
UV	Ultra-violet
VEGF	Vascular endothelial growth factor

CHAPTER 1

INTRODUCTION

A brief background, motivation, hypothesis along with the research objectives and novelty of this thesis work will be presented in this chapter.

1.1. Background and motivation

Modern era since the Second World War has been an age of paradox in medicine. On one hand, ground breaking milestones for the treatment of diseases, illness and injury have been effectuated, thus, immeasurably benefitting mankind by meager untimely death and lavishly improved living standard. But, on the other hand advent of newer diseases, failure and limitations of existing therapeutics, lifestyle habits and several other factors have impacted adversely on the physical health conditions of the mankind. This adversity and need for a better quality of life for all paved way to novel technologies like nano-medicine, tissue engineering and regenerative medicine. In addition to therapeutic value, tissue engineering and regenerative medicine aims to provide diagnostic value especially as a tool for drug testing. Tissue engineering and regenerative medicine requires the perfect interplay between scaffold, cells and signals for tapping its full potential.

Scaffold plays a prominent role in tissue engineering and regenerative medicine and is required to provide the desirable environment that favors the natural behavior of cells. Cell adhesion and spreading over a substratum plays a pivotal role in many biological processes such as organogenesis, wound healing etc. *In vivo*, this pivotal role of the substratum is played by the extracellular matrix (ECM) components. Many ECM components like collagen, elastin, fibronectin, laminin and others facilitate attachment, spreading and proliferation of cells by presenting required tissue specific cues. Increasingly, it is intended to design the

scaffold to mimic the natural niche of the target cells or tissue as close as possible. In order to serve this goal the scaffold has to fulfill a wide list of requirements derived from the ECM environment of the target cells in their native tissue or organs in the human body. These tissue specific requirements include cues like topographical, biochemical, mechanical, structural and so on. Hence, over the years, conceptualizing and designing of ECM mimicking biomaterials as a scaffold for tissue engineering and regenerative medicine has become imperative and attractive. ECM mimicking biomaterials as scaffolds have the potential to encourage cell adhesion and proliferation, subsequently, leading to tissue regeneration and tissue integration required for the healing of the tissue. So, while mimicking the *in vivo* environment by designing a synthetic material, it is also important to elucidate the features by which the target cell can bind to an artificial substratum and, thus, activate a cascade of events leading to attachment, spreading and proliferation.

With this aim, our group designed a collagen mimetic peptide amphiphile (CM-PA) design that provides biochemical cue inherent of the most abundant ECM component, collagen, in a nano-architecture (Luo et al. 2011). In continuation, in this thesis, we aim to design various ECM mimicking three dimensional (3D) scaffolds by employing CM-PA to impart mechanical cue to the target fibroblast cells. In particular, this study focuses to understand the cell-matrix interactions in particular to the combined role of biochemical and mechanical cues provided by the CM-PA in the form of a functional 3D scaffold,

i.e. hydrogel, in the cell spreading and proliferation of fibroblast cells.

1.2. Hypothesis

The plasticity behavior of fibroblast cells to various matrix stiffness can be exploited to design collagen mimetic peptide amphiphile 3D scaffolds i.e. hydrogel with appropriate biochemical and mechanical cues for fibroblast proliferation. Also, it is hypothesized that collagen mimetic peptide amphiphile hydrogels can be tuned for varying mechanical properties to influence cell behavior, in particular to fibroblast cells.

1.3. Research objective

The objective of this thesis is to develop a CM-PA hydrogel with appropriate mechanical strength for the proliferation of L929 fibroblast cells to further the application of CM-PA for biomedical applications. L929 fibroblast cells are employed because of its robust nature and plasticity to modulate behavior by the biochemical and mechanical cues provided by the ECM molecules.

Therefore, the specific research objectives of this thesis include:

1) To develop and study the effect of semi-interpenetrating network hydrogels consisting of CM-PA and poly(ethylene glycol) diacrylate (PEGDA) with varying mechanical cues on the behavior of fibroblasts. (Chapter 5)

2) To develop and study the effect of cross-linked CM-PA hydrogels with varying mechanical cues on fibroblasts behavior. (Chapter 6)

3) To develop a CM-PA hydrogel with a novel design by tuning the peptide

amphiphile sequence for providing appropriate mechanical cue and to study the proliferation behavior of fibroblasts on the designed scaffold. (Chapter 7)

1.4. Novelty

This study to the best of my knowledge is the first study to focus on the biological cellular behavior of fibroblasts on the shorter fragment of collagen i.e. collagen mimetic peptide containing the collagen specific cell binding region i.e. “glycine (G) – phenylalanine (F) – hydroxyproline (O) – glycine (G) – glutamine (E) – arginine (R)” (GFOGER) incorporated in a functional design of a nanofiber in a hydrogel. This study is also the first to study the effect of CM-PA hydrogels with varying mechanical strength on the behavior of fibroblasts.

The novelty of the study is also in the design strategy of the hydrogel in the form of semi-interpenetrating network of PEGDA and CM-PA to study the effect of varying mechanical cues.

This study is also the first study to understand the effect of tunable mechanical properties of CM-PA with varying peptide sequences in the form of a hydrogel for the cellular interactions with fibroblasts.

CHAPTER 2

LITERATURE REVIEW

A description of the unmet tissue engineering needs with a focus on cell instructive extracellular matrix mimetic scaffolds, particularly of collagen mimetic peptide amphiphile hydrogels is provided in this chapter.

2.1. Tissue engineering and Regenerative medicine

Increasingly, millions of people on an annual basis damage their organs like kidneys, liver, lungs, pancreas, brain, heart, skin, bone, cornea and so on due to diseases or accidents. However, the survival and quality of these people is dependent on the current gold standard medical technique i.e. organ transplantation. The need of this technique is the availability of appropriate organ from a donor that meets all the necessary requirements. This quest is plagued with the serious issue of organ shortage and transplant rejection, thus, lowering the survival rate of the patient. This demand for survival and improved quality of living has led to the development of many novel and promising therapeutics. One such therapeutics that came to existence few decades ago is tissue engineering and regenerative medicine to solve the unmet need in the field of organ failures, tissue repair and replacement (Langer et al. 1993). The term tissue engineering was first introduced by Langer and Vacanti in 1993 to the scientific community (Langer et al. 1993).

Yet another unmet need is in the field of drug screening for therapeutics where current drug testing methods are done *in vivo* either using animal models or cadaver specimens. Both these models for drug testing methods have severe limitations in mimicking the human physiological conditions. Hence, there is a need to develop novel testing tools that closely mimic the native cells, tissues, organs or human on the whole. Interestingly, tissue engineering offers a remarkable platform to develop devices resembling human cells, tissues, organs (Huh et al. 2010) or human on the

whole (Huh et al. 2012). This opportunity is also seized to design several tissue engineering products modeling the diseases and disorders such as arrhythmia (Thompson et al. 2012), skin fibrosis (Moulin. 2013) and cancer (Bhowmick et al. 2004; Kim. 2005) and so on.

To sum up, tissue engineering and regenerative medicine is defined and fashioned in numerous ways. On such definition which aptly describes the purpose and benefits of tissue engineering and regenerative medicine is by National Institutes of Health (NIH). NIH defines Tissue Engineering as, "An emerging multidisciplinary field involving biology, medicine, and engineering that is likely to revolutionize the ways we improve the health and quality of life for millions of people worldwide by restoring, maintaining, or enhancing tissue and organ function. In addition to having a therapeutic application, where the tissue is either grown in a patient or outside the patient and transplanted, tissue engineering can have diagnostic applications where the tissue is made in vitro and used for testing drug metabolism and uptake, toxicity, and pathogenicity. The foundation of tissue engineering for either therapeutic or diagnostic applications is the ability to exploit living cells in a variety of ways. Tissue engineering research includes biomaterials, cells, biomolecules, engineering design aspects, biomechanics, informatics to support tissue engineering and stem cell research".

Overall, tissue engineering and regenerative medicine promises to offer next generation therapeutics and diagnostics beneficial for mankind. One of the

evidence of this realizable promise is the increase clinical trials in the field of tissue engineering and regenerative medicine in US i.e. from 38 in 2007 to 83 in 2011 (Fisher et al. 2013).

2.2. Tissue engineering triad

The classical definition of tissue engineering (Williams. 1999), "the persuasion of the body to heal itself, through the delivery to the appropriate sites of molecular signals, cells and supporting structures", highlights the three main components of tissue engineering i.e. scaffolds, signal and cells, also denoted as the “Tissue Engineering Triad”, as shown in Figure 2.1.

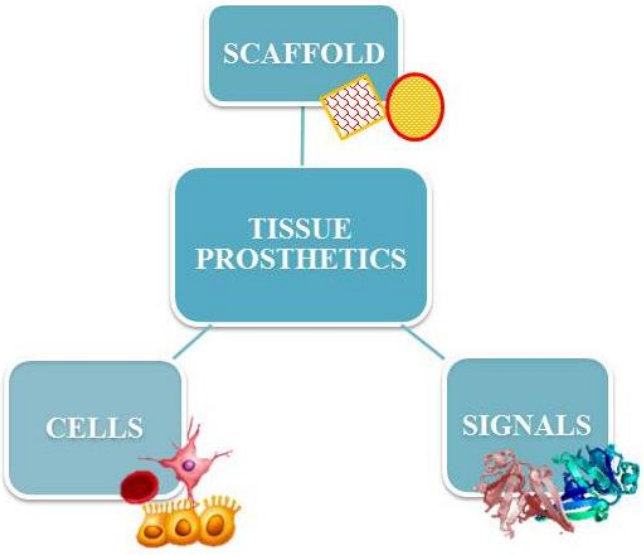

Figure 2.1: Schematic showing the three major components of a tissue engineered prosthetics i.e. scaffold, cells and signals. These three together are known as the tissue engineering triad.

2.3. Scaffolds - Biomaterials

Scaffold plays a prominent role in the tissue engineering as one of the major pillar. Over the years the role of scaffold has been changing from a bio-inert material to a biomaterial with cell stimulating effect. Several authors have listed the

requirements for an ideal biomaterial scaffold; however, these lists are not exhaustive.

In a recent review (Edalat et al. 2012), authors have competently enlisted and reviewed the material parameters for the design of a scaffold along with few material choices and design options. In brief, the material design criteria includes the following: (i) ability to provide 3D nano-topography within the scaffold including porosity, pore size, and inter-pore connectivity to satisfy adequate mass transfer of gases, nutrients and waste as well as cell attachment, proliferation and tissue formation; (ii) ability to possess mechanical parameters such as linearity or non-linearity, elasticity, viscoelasticity, or anisotropy that must be tailored to the specific tissue in mind; and (iii) ability to deliver successfully molecular signaling biologics such as cells, growth factors, cytokines etc.

Moving on, in a perspective review paper (Williams. 2014), the author made a bold attempt to summarize the mandatory and the optional specifications for biomaterial scaffolds. In brief, the review highlights the following specifications as mandatory, namely: (i) capability of biomaterial scaffold to recapitulate the architecture of the niche of the target cells; (ii) capability of the material to adapt to constantly changing microenvironment of the target cells; (iii) capability of the material to possess mechanical signaling properties particularly, stiffness to favor the proliferation of the target cells; (iv) material to possess optimal surface energy to facilitate cell adhesion; (v) capability of the material to orchestrate molecular

signaling to the target cells; (vi) ability of the material to form appropriate shape and size to the regenerated tissue; (vii) capability of the material to form architecture that optimizes cell, nutrient, gas and bio-molecule transport in culture and body conditions; (viii) noncytotoxic, nonimmunogenic and minimally proinflammatory material. In addition, he also highlights few optional specifications for the biomaterials like degradability, injectability and so on.

Indeed, both papers highlight the need for the biomaterial scaffold to mimic the target cell niche as closely as possible. Hence, meeting these requirements led to revisiting the traditional biomaterials and scaffold designs used in tissue engineering and regenerative medicine applications and designing novel biomaterial scaffolds specific to the target cells niche. The need to derive knowledge to design target cell specific supportive scaffold paved way to study, understand and re-create the complex cell niche called as, the extracellular matrix (ECM).

2.4. Extracellular matrix (ECM)

ECM is the non-cellular part of all types of cells and is specific to each type of the cells, tissues and organs. Traditionally, ECM was considered as bio-inert with only the role of a supportive scaffold. However, the role of ECM expanded over the few decades and is considered as crucial for an appropriate cell behavior. In essence, in addition to acting as physical structural support, ECM is now considered to be a source of crucial cell instructive signals such as biochemical

nano-topography, and mechanical. ECM also acts as a reservoir for soluble chemical cues like growth factors, cytokines, enzymes and so on. ECM communicates biochemical cues to the cells either through the binding and controlling the local concentration of a wide variety of soluble chemical cues and/or by exposing certain cell specific motifs that are recognized by cellular adhesion receptors present on the cells (Frantz et al. 2010; Juliano et al. 1993; Kim et al. 2011). ECM communicates the nano-topography cue to the cells as its inherent component matrix structure. In addition, ECM communicates mechanical cues to cells through its inherent matrix stiffness. Through a process known as mechanotransduction, cells convert this mechanical cue into a chemical response for the behavior of cells (Wozniak et al. 2009; Janmey et al. 2011). Overall, ECM is dynamically and imperatively integrated with cell morphology and cell function.

Hence, before designing an ECM mimicking scaffold, it is essential to understand the structure and function of various ECM components. Fundamentally, ECM comprises water and two main classes of biomacromolecules, namely, proteoglycans and fibrous proteins like collagens, elastins, fibronectins and laminins (Frantz et al. 2010). Components of the ECM are produced by specific resident cells where they integrate with the existing matrix. Of all the biomacromolecules, collagen is the most abundant component of the ECM in all types of the tissues and making up to 25% - 35% of the entire protein content of the body (Di Lullo et al. 2002).

2.5. Collagen

Collagen is a family of insoluble fibrous multi-functional protein in the ECM in all tissue types' especially connective tissue. In fact, it is the single most abundant protein in animals with at least 28 types of variants. Of all the types of collagen in the body, types I, II, and III are the major fibrillar collagens comprising 80 – 90 percent (Hulmes. 2002; Kadler. 1995; Van der Rest et al. 1991). Collagen provides the structural and physiological functions like cell attachment, proliferation, migration and also, transmission of mechanical forces between cells in tissues such as liver, skin and neurons (Faassen et al. 1992; Grzesiak et al. 1992; Scharffetter-Kochanek et al. 1992; Perris et al. 1993).

The typical structure of collagen is the triple-helical structure comprising three polypeptide chains and each chain possessing around 1000 amino acid residues. The three polypeptide chains consist a left-handed, polyproline II-type (PPII) helical conformation, in turn, the three chains are supercoiled to form a right-handed triple-helix around a central axis. The unique triple-helical structure arises from an unusual abundance of three amino acids: glycine (G), proline (P), and 4-hydroxyproline (O) (Fraser et al. 1979). These amino acids make up the characteristic repeating motif Glycine-X-Y, where X are mostly proline and Y are mostly hydroxyproline or hydroxylysine in humans (Sakakibara et al, 1973). Glycine being the smallest amino acid fits into the internal crowded center spaces of the triple-helix and also stabilizes the triple-helix structure by forming a hydrogen bond between its peptide bond (N-H) and a peptide bond carbonyl

group (C═O) in the adjacent polypeptide chains. Another force which facilitates each polypeptide chain to fold together to form a triple-helix is the fixed angle of the C – N peptidyl-proline or peptidyl-hydroxyproline bond. Further, Triple-helix structure is reinforced by the hydrogen bonds between the hydroxy groups (–OH) of 4-hydroxyproline and water molecules (Shoulders et al, 2009). The unique amino acids, hydroxyproline and hydroxylysine, are the result of post translational modification of the polypeptide chains after being translated.

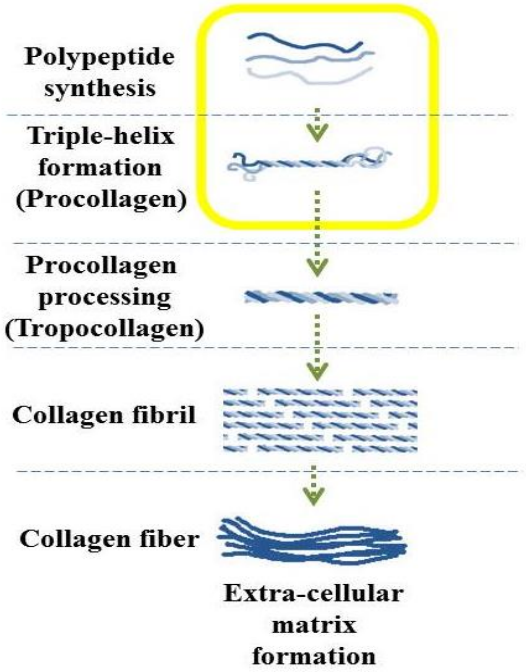

Figure 2.2: Schematic sketch showing the formation of collagen ECM. The typical structure of collagen is the triple-helical structure comprising three polypeptide chains and each chain possessing around 1000 amino acids. The three polypeptide chains after post translational modification form a super coiled triple-helical unit, called, procollagen. Upon release into the extracellular space, procollagen molecules undergo processing to form tropocollagen. Then, tropocollagen molecules assemble to form collagen fibrils. Then, collagen fibrils self-assemble to form collagen fibers or bundles. These collagen fibers then self-assemble to form the ECM collagen fibers of the cells.

In the case of most abundant fibrillar type I collagen as illustrated in Figure 2.2, self-assembly begins by the formation of a basic unit called procollagen, which is

a supercoiled trimer, with three polypeptide strands that adopt the PPII-type helical conformation. The formed triple-helical procollagen is secreted from cells in soluble form, then, procollagen is processed by several enzymes like procollagen metalloproteinases to form tropocollagen. One of the processing steps includes removal of N- and C-terminal propeptides resulting in the formation of tropocollagen. Then, the formed tropocollagen molecules pack against one another in a staggered fashion to form nanofibrous structure known as collagen fibrils (Ottani *et al.* 2001; Ottani *et al.* 2002). Collagen fibrils in turn form collagen fibers with larger diameter by self-assembling both linearly and laterally. The ECM of the cells is composed of these collagen nanofibers. The structural integrity of the ECM is attributed to the multiple levels of collagen's structural hierarchy which is also necessary to provide binding sites for other proteins and cells (O'Leary *et al.* 2011).

Collagen along with providing structural support also provides certain biochemical cues for the cells to adhere to the ECM e.g. the triple-helical sequence "GFOGER" corresponding to residues 502 to507 of collagen α1(I) is identified as the major integrin receptor binding locus within type I collagen (Knight et al. 1998). This sequence is recognized by the integrins α2β1, α1β1, α10β1 and α11β1 present as the cell surface receptors to cascade the intracellular signaling pathways, thereby, resulting in cellular functions like adhesion, spreading, proliferation, migration and differentiation (Emsley et al. 2004).

Hence, the unique and specific amino acid sequence in the collagen leads to the formation of the unique signature structure of collagen which is required for its function as an ECM structure.

2.6. ECM structural mimic – hydrogels

One such scaffold design amenable to favoring tissue engineering and regenerative medicine applications is hydrogels. Hydrogels are a cross-linked network of monomers, oligomers, or polymers that contain 90–95% water in volume and structurally mimic the ECM of the natural tissue (Wichterle et al. 1960). Hydrogels exhibit many unique physicochemical properties which are advantageous for biomedical applications such as tissue engineering, regenerative medicine and drug delivery (Kopecek. 2007; Lutolf. 2009; Chung 2009; Oh. 2010; Lee et al. 2008; Geckil et al. 2010). In addition, they are excellent candidates for encapsulating biomacromolecules including proteins and DNA (Peppas et al. 2000), thus, acting as good carriers for molecular signaling cues. Hydrogel are attractive scaffold design for cell encapsulation because of their good biocompatibility and high permeability and mass transfer for oxygen, nutrients and other water-soluble metabolites (Hunt et al. 2010; Drury et al. 2003; Liu et al. 2010; Slaughter et al. 2009). The capability of fabricating hydrogels in relatively mild conditions like ambient temperature and no requirement of organic solvents (Lin et al. 2006) also led to its preference for biological applications.

Hydrogels based on their cross-linking mechanism can be classified into physical and chemical hydrogels (Chung et al. 2009; Slaughter et al. 2009). Physical crosslinks are not permanent cross-links but include crosslink mechanisms such as entangled chains, hydrogen bonding, hydrophobic interaction and crystallite formation (Zhu et al. 2009). On the other hand, chemical (or covalent) crosslinks, are formed by covalent bonds which are permanent junctions (Hoffman. 2002).

Hydrogels are prepared from natural, synthetic or their hybrid polymers (Davis et al. 2002; Zhu et al. 2011). Hydrogels made from natural polymers like polysaccharides (Sechriest et al. 1999), cellulose derivatives (Hirsch et al. 2002) and proteins (Kennedy et al. 2001) exhibit several advantageous properties such as inherent biocompatibility and biodegradability but may not provide sufficient mechanical properties, may possess limited tunability and may lead to immune reactions due to the source it is obtained. Albeit, hydrogels prepared from proteins are of particular interest, due to their ability to form complex hierarchical structures (Trabbic-Carlson et al. 2003). Hydrogels fabricated using natural polymer biomaterials possess the capability to mimic the target tissue more closely and usually these natural polymers are components of the ECM.

Synthetic hydrogels, on the other hand, offer the advantage of well-defined structures with well-defined mechanical strength that can be modified to yield tailorable degradability specific to the tissue but lack the inherent bioactive properties (Lin and Metters, 2006). Hydrogels are made up of various polymers

like synthetic hydrophobic polymers such as poly(lactic acid) or poly(glycolic acid) or synthetic hydrophilic polymers like poly(ethylene glycol) (PEG) (El-Sherbiny et al. 2013). Networks of hydrophobic polymers have limited water absorption capabilities whereas hydrophilic polymer hydrogels are useful because of their high water content and rubbery state, which mimic the natural tissue. However, the hydrogel material should strike an optimum hydrophobic and hydrophilic balance to allow cell adhesion and subsequently leading to cell spreading and cell proliferation (Zhu. 2010).

The need for functional hydrogels exhibiting both biocompatibility and biodegradability with sufficient mechanical strength led to the formation of hybrid hydrogels with both natural and synthetic polymers (Hoffman. 2002). One such strategy is the semi-interpenetrating network hydrogels (S-IPNs). S-IPNs are fabricated either by sequentially polymerizing one monomer in the presence followed by polymerizing the second monomer or by polymerizing both the monomers together provided the polymerization mechanism of two polymer are significantly different processes (Zhu et al. 2011; Burke et al. 2012).

2.7. ECM component mimic - collagen hydrogels

The almost ubiquitous presence of collagen *in vivo* for all tissue types led to its most popularity as the natural tissue specific polymer for tissue engineering and regenerative medicine scaffold biomaterial. In addition, collagen possesses several comprehensive advantages such as biodegradability, biocompatibility,

ease of availability and moderate tunability. Collagen-based functional scaffold are derived through two fundamental techniques namely, decellularized collagen matrix which retains the native tissue ECM structure and composition and processed collagen obtained by extraction, purification and polymerization of collagen and its diverse components from various animal sources like bovine, porcine, equine and fish.

Collagen-based scaffolds in the form of hydrogels are used for experimental and few commercial clinical applications in cartilage (Schulz. 2008; Zheng et al. 2009), bone (Du et al. 2000, Liao et al. 2009) cardiac (Park et al. 2005), skeletal muscle (Beier et al. 2009), vascular (Boccafoschi et al. 2007; Tedder et al. 2009), skin (Trottier et al. 2008; Karr. 2008), corneal (Griffith et al. 2009; Rafat et al. 2009) urogenital (Akbal et al. 2006; Liu et al. 2009), neural (Sun et al. 2007; Bozkurt et al. 2009) tissue engineering and regenerative medicine and so on.

Although, natural collagen-based scaffolds are widely used in clinics and in research for various tissue engineering and regenerative medicine applications, yet, it is plagued with several deleterious properties. Namely, immunogenicity and antigenicity associated with the source of collagen; batch to batch variability due to processing control difficulties; limited flexibility and modifiability in terms of mechanical and biochemical properties; and above all, presence of unique amino acids in the structure leading to deprived recombinant production technologies. Thus, speedily the quest for collagen mimics has gained momentum.

2.8. ECM mimic - collagen mimetic peptide amphiphile hydrogels

Even though collagen derived components provide a good biomaterial scaffold, the inherent deleterious properties led to the need for alternative biomaterials negating these deleterious properties and possessing required properties arose. Hence, over the years, conceptualizing and designing of ECM mimicking materials became imperative and attractive. Thus, mimics of ECM of the tissue natural polymers like collagen, fibronectin, laminin and so on have gained importance and popularity.

Almost for a century now, collagen is the focus of study for several research groups either to decipher its structure, stability, hierarchical assembly or biochemical properties. Natural collagen due to its inherent variants and large molecular weight poses a difficulty for the purpose of the study, hence increasingly, smaller synthetic collagen like triple-helical folding peptides are used. Recent review presents an exhaustive outlook on the various synthetic collagen mimics, called collagen mimetic peptides (CMPs), with a focus on their primary structure and hierarchical self-assembly to form higher order structures Fallas et al. 2010). The CMPs also aid in identifying the specific sequences in collagen facilitating the adhesion. The abundant wealth of knowledge regarding collagen using CMPs led to the substitution of CMPs in place of collagen for biological applications.

The use of CMPs as a scaffold or biomaterial is still at its infancy and research is

ongoing to tap the enormous potentiality of CMPs for this purpose. The pioneering studies using CMP for tissue engineering and regenerative purposes employed composite scaffold designs with synthetic polymer providing the structural support of the scaffold and CMP providing the biological signal cues for the cells. Khew et al. (2007) designed Poly (3-hydroxybutyrate-co-3-hydroxyvalerate) microspheres functionalized with CMP incorporated with GFOGER sequence for culturing Hep3B cells for liver tissue engineering. This study marked a significant breakthrough in tapping the biomolecular signaling cues present in collagen. However, the use of microspheres to provide the mechanical cue and the form for the scaffold failed to achieve the tissue like microenvironment. Further on, Lee et al (2008) designed a new type of synthetic hydrogel scaffold employing polymer-peptide hybrid. The scaffold was fabricated as collagen mimetic peptide – conjugated poly(ethylene oxide) diacrylate hydrogel and was employed for encapsulation of mesenchymal stem cells for chondrogenic differentiation. Thus, this study as well taps the use of collagen mimetic peptide for biomolecular signaling only. Hence, there is need to design a novel scaffold biomaterial that can mimic collagen both structurally and functionally to fully and more closely resemble the ECM of target cells. This need led to the development of peptide based hydrogels.

Peptide based hydrogels have the potential to be designed according to the target cell niche synthetically yet biochemically mimicking the natural cell niche. Solid phase peptide synthesis is the main technique for the preparation of peptides. One

such peptide scaffold biomaterial design is based on self-assembling peptide amphiphiles. The design of single-tail peptide amphiphiles (PAs) was first developed by Hartgerink and Stupp (Hartgerink et al. 2001). Moving on, several self-assembling peptide amphiphile designs that can form nanofibers have been created and used for tissue engineering and regenerative medicine applications (Silva et al. 2004; Tysseling-Mattiace et al. 2008; Tysseling et al. 2010; Webber et al. 2010; Zhang et al. 2010; Angeloni et al. 2011; Chow et al. 2011).Single tail peptide amphiphile (PA), as shown in figure 2.3, contains distinct hydrophobic and hydrophilic segments comprising of alkyl or acyl chains (Cui et al. 2010) and other hydrophobic compounds (Tovar et al. 2005) and amino acid residues respectively.

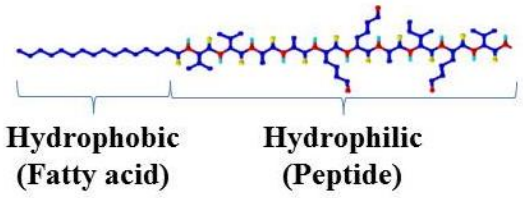

Figure 2.3: Single tail peptide amphiphile (PA) showing distinct hydrophobic and hydrophilic segments. The hydrophobic segment is made up of fatty acid coupling in the N-terminal of hydrophilic peptide segment.

Peptide amphiphiles are capable to spontaneously organize into highly ordered nanostructures in a free-energy driven process in a manner molecularly determined by the peptide sequence. The self assembly process is coordinated by the same forces which are involved in the cells for the process of protein folding. These forces are non-covalent inter- and intra-molecular interactions such as coulomb forces between charged amino acids, hydrogen bonding between side

groups and peptide backbone, pi-pi stacking and hydrophobic interactions. In particular, peptides of certain sequences are capable of forming regular hydrogen bonding between their backbones to give their signature secondary structures of beta-sheet and alpha helixes that facilitate the self-assembly process (Hartgerink et al. 2001). Therefore, the programmability of the peptide sequence by changing the type or/and order of amino acids in the sequence of the peptide enables molecular designers to precisely design various kinds of nanostructures.

In brief, the base configuration of the PA designed by Hartgerink and Stupp (Hartgerink et al. 2001), as shown in figure 2.4, typically has three key structural features in the hydrophilic peptide region. The first region is the consecutive β-sheet forming amino acids like valine (V), alanine (A), etc., followed by a charged region comprising charged amino acids like lysine (K) or glutamic acid (E) and finally, the flexible region which enables displaying of the cell adhesion ligands like isoleucine (I) – lysine (K) – valine (V) – alanine (A) – valine (V) (IKVAV) derived from laminin on the surface.

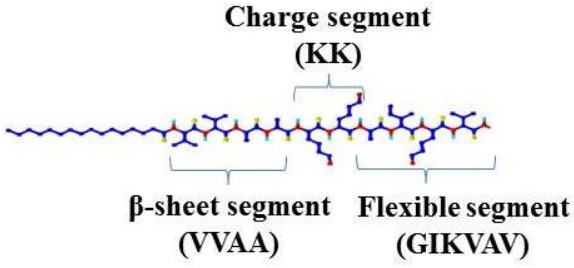

Figure 2.4: Single tail peptide amphiphile (PA) showing distinct hydrophilic segment made up of β-sheet forming amino acids like valine (V) and alanine (A), followed by a charged region comprising charged amino acids like lysine (K) and finally, the flexible region which enables displaying of the cell adhesion ligands like isoleucine-lysine-valine-alanine-valine (IKVAV) derived from laminin on the surface of the PA.

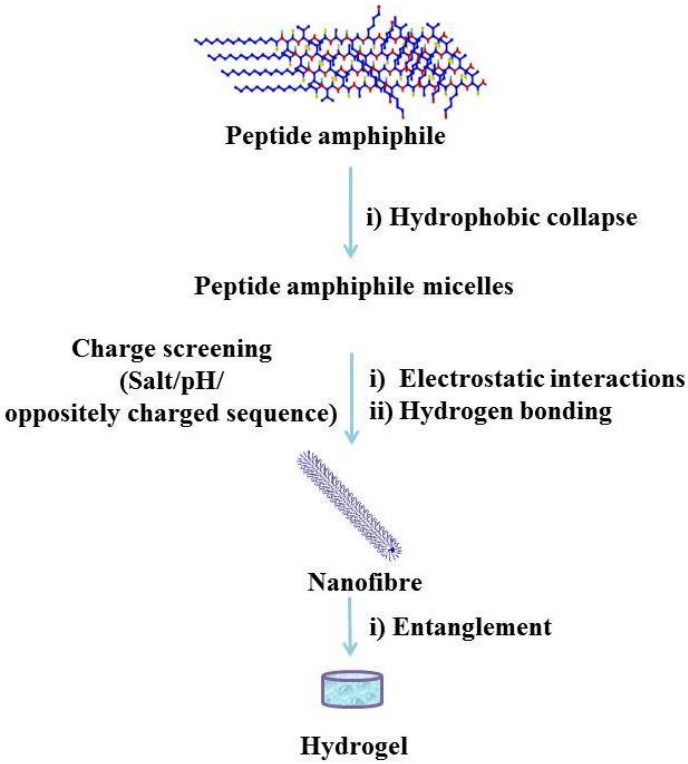

Figure 2.5: Single tail peptide amphiphile (PA) developed by Stupp's group in 2001 is shown to form high-aspect ratio nanofiber when triggered by a pH change or charge screening by appropriate salts. In brief, initially, the hydrophobic moieties collapse into the core of the nanofiber. Then upon trigger of charge screening, the peptide sequence elongates the nanostructure via β-sheet formation. The formed nanofibers entangle to form hydrogels.

The formation of nanofiber by peptide amphiphile is a self-assembly bottom-up process triggered by external stimuli. The theoretical mechanism, as shown in figure 2.5, is as follows, the amphiphilic nature of the peptide amphiphile results in the formation of micelles in the solution, these micelles then form cylindrical nanofiber instead of spherical micelle or vesicle because of dominant electrostatic attractive forces of the hydrophilic head group in presence of charged ions or pH triggers i.e. by charge screening over the hydrophobic force of the tail group (Hartgerink et al. 2002). The cylindrical nanofiber also gets its directionality from the β-sheet segment by forming hydrogen bonds between the PAs. The PA

nanofibers at above certain critical concentration aggregate through physical cross-links to form functional bioactive scaffolds like hydrogels.

The PA system has the potentiality to mimic several ECM molecules based on the sequence in the flexible region like Arginine-Glycine-Aspartic acid *(*RGD*)* or Arginine-Glycine-Aspartic acid-Serine (RGDS) (Mann et al. 2002; Sargeant et al. 2008) sequence to mimic fibronectin, IKVAV (Tysseling et al. 2010) sequence to mimic laminin and heparin binding mimics (Rajangam et al. 2006; Rajangam et al. 2008). In addition, PA system can be employed to design growth factor binding mimics and growth factor mimics such as bone morphogenetic protein 2 (BMP-2) binding mimics (Lee et al. 2014) and vascular endothelial growth factor (VEGF) mimics (Webber et al. 2011) respectively.

Few research groups studied the applicability of PA nanofibers and hydrogels for tissue regeneration applications like neural tissue engineering, bone tissue engineering and liver tissue engineering using different tissue specific ECM mimics. Fibronectin mimetic bioactive PA nanofiber networks were self-assembled into the pores of titanium alloy foams for bone repair (Sargeant et al. 2008). In yet another study, injectable laminin mimetic PA nanofiber hydrogel was used to study the functional recovery of neurons at the site of spinal injury (Tysseling et al. 2010). Novel PA designs possessing heparin-binding mimetic sequence enabled the optimal display of heparin-binding sequence in a large surface area. Thus, the formed nanofibers in turn bound to heparin, a proteoglycan

present in the ECM, which in turn captured growth factors possessing heparin-binding domains such as basic fibroblast growth factor 2 (bFGF-2) and VEGF and eventually, aiding in angiogenesis (Rajangam et al. 2006; Rajangam et al. 2008).

In line with the synthesis of ECM mimicking self-assembling peptides, Raines' group and Koide's group developed a strategy to prepare hydrogel forming self-assembling collagen-mimetic supramolecule peptides (Koide et al. 2005; Kotch et al. 2006; Yamazaki et al.2008). Our group also designed a hydrogel forming self-assembling mimic of collagen to form nanofibrous hydrogels (Luo et al. 2011).

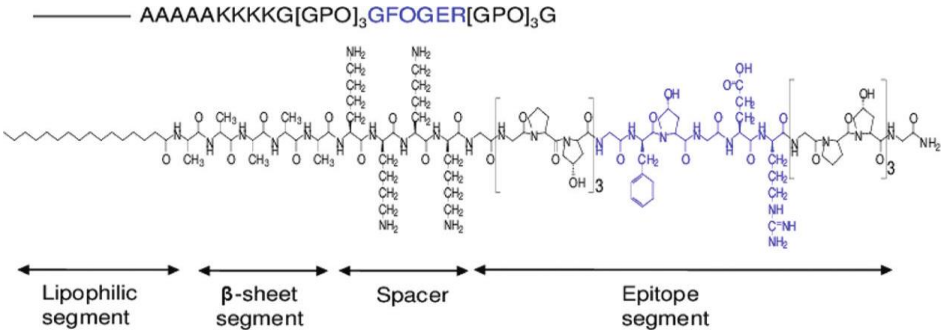

Figure 2.6: Single tail collagen mimetic peptide amphiphile (CM-PA) developed by Luo and Tong in 2011. CM-PA consists of a long alkyl tail of palmitoyl (C_{16}) group that forms the lipophilic segment. Followed by, five consecutive β-sheet forming amino acids alanine (A) that forms the β-sheet segment. Further on, charged region comprising of charged amino lysine (K). Finally, the epitope segment displaying the cell adhesion ligand mimicking the primary sequence of collagen i.e. repeats of Glycine (G)–Proline (P)–Hydroxyproline (O) (GPO) along with the triple-helical cell binding sequence, glycine (G) – phenylalanine (F) – hydroxyproline (O) – glycine (G) – glutamine (E) – arginine (R) (GFOGER).

In brief, as shown in figure 2.6, CM-PA typically has four key structural features. Firstly, a long alkyl tail of palmitoyl (C_{16}) group that conveys hydrophobic character to the molecule forms the lipophilic segment. Followed by, five

consecutive alanine (A) amino acid residues were chosen. Alanine was chosen as it is a weak β-sheet former and has propensity for formation of α-helices (Chou et al. 1974). Further on, charged region comprising of charged amino acid lysine (K). Finally, the epitope segment displaying the cell adhesion ligand mimicking the primary sequence of collagen i.e. repeats of Glycine (G)–Proline (P)–Hydroxyproline (O) (GPO) along with the triple-helical cell binding sequence GFOGER. The repeats of GPO confer the triple-helical nature to the peptide amphiphile. Thus, the CM-PA design provides the required biochemical cue necessary for appropriate cell behavior.

The only disadvantage of such a versatile system is its cost considerations. Though the large-scale synthesis of proteins comprising hundreds of residues still remains a daunting challenge, oligopeptides can be produced rather easily using standard solid-phase synthesis. But, in the light of the abundant benefit provided, these oligopeptides could serve as an effective, low-cost alternative for functional mimicry of large proteins especially like collagen, fibronectin, laminin, growth factors like VEGF, bFGF etc.

The immense advantages of the self-assembling peptide amphiphile system in particular, self-assembling collagen mimetic peptide amphiphile system out weighs in comparison to the economy disadvantage. Hence, the promising self-assembling collagen mimetic peptide system designed by Raines's and Koide's group with the addition of GFOGER sequence between the GPO repeats

was used for human dermal fibroblast culture (Yamazaki et al. 2010). In addition, self-assembling collagen mimetic peptide system designed by our group was also used for culture of Hep3B cells (Luo et al. 2011). Both the designs employed for cell culture on self-assembling peptide employing the technique of coating the nanofibers on the surface of the culture plates for cell adhesion and proliferation studies. Also, both the papers confirm the role of GFOGER sequence for integrin mediated cell adhesion.

2.9. Cells - fibroblasts

L929 fibroblast cells are a mouse subcutaneous connective tissue, areolar and adipose fibroblast cells. L929 fibroblast cells exhibit robust nature and plasticity to modulate behavior by the ECM molecules such as collagen in the stimulation of mechanical and biochemical triggers (Daley et al. 2008; Farahani et al. 2008; Gjorevski et al. 2009; Jiang et al. 2007). Several research works support the plasticity nature of fibroblast e.g. commercial collagen membrane devices, varying in origin of collagen and presence and absence of cross-links and cross-linking agents, used for wound healing and tissue regenerative applications showed different fibroblast cellular behavior (Rothamel et al. 2004). Also, many works are carried out to study the behavior of fibroblasts in 2D (Harris et al. 1984) and 3D (Jiang et al. 2005; Rhee et al. 2007; Da Rocha Azevedo et al. 2012)**.** From earlier studies, it is evident that mouse fibroblast phenotype and gene expression are altered by their adhesion state (Carlson M.A. et al. 2009)**.** Studies performed to understand cell-matrix interaction using collagen scaffolds with several cell

types, especially with fibroblasts, is directly relevant to different aspects of tissue engineering (Briceno P.C. et al, 2011).

CHAPTER 3

MATERIALS AND METHODS

A detailed description of all the materials and methods employed for the work in this thesis will be provided in this chapter

3.1 Materials

All peptide amphiphile sequences were purchased from biopeptek inc. (Malvern, Pennsylvania, United States) with a purity >95%. Table 3.1 tabulates the list of peptide amphiphile design sequences synthesized along with its labels. The sequence is written from the N-terminal to C-terminal of the peptide

Table 3.1: List of all the peptide amphiphile design sequences from the N-terminal to C-terminal of the peptide along with its labels.

Label	Sequence*
CM-PA	C_{16}-AAAAAKKKKG$(GPO)_3$GFOGER$(GPO)_3$G
K-PA	C_{16}-AAAAAKKKKGGK
PGA-CM-PA	C_{16}-GAGAGAGKKKKG$(GPO)_3$GFOGER$(GPO)_3$G
PGA-PA	C_{16}-GAGAGAGKKKK
PA-CM-PA	C_{16}-AAAAAKKKKG$(GPO)_3$GFOGER$(GPO)_3$G
PA-PA	C_{16}-AAAAAKKKK

* C_{16} stands for palmitic acid modification in the N-terminal of the peptide. Standard one-letter amino acid code listed in Appendix B is used to express the sequences of the peptide.

Peptide amphiphile (PA) sample solutions were prepared only with ultrapure water filtered through 0.22 μm filter. Polyethylene glycol di-acrylate, mw 2000 (PEGDA) was purchased from Jenkem Technology, USA. Phosphate buffered saline (PBS), ammonium hydroxide (NH_4OH), trisodium phosphate (Na_3PO_4), irgacure 2959, hoechst 33258, phalloidin-tetramethylrhodamine isothiocyanate (phalloidin-TRITC), thiazolyl Blue Tetrazolium Bromide (MTT), bovine serum

albumin (BSA), saponin, phosphotungstic acid (PTA) and dimethyl sulfoxide (DMSO) were purchased from Sigma Aldrich. Glutaraldehyde was purchased from Merck (USA). Bovine collagen solution, Type I (PureCol®) for cell culture was purchase from Advanced BioMatrix, USA. Coomassie (Bradford) Protein Assay Kit for peptide estimation was purchased from Thermo Scientific, USA. L929 fibroblast cells were obtained from the American type culture collection (ATCC), USA. Dulbecco's modified Eagle's medium (DMEM), fetal bovine serum (FBS), trypsin and antibiotics for cell culture were obtained from Hyclone, USA. Fibroblast Basal Medium and fibroblast Growth Kit-Low serum was obtained from ATCC, USA.

3.2. Hydrogel fabrication techniques

3.2.1. Fabrication of self-assembling peptide amphiphile hydrogels

PA samples of required concentration (say 5 mM) were dissolved in filtered ultrapure water and stored at 4°C for at least 2 days prior to salt induced nanofiber self-assembly. The hydrogel samples were prepared in 96 well plates. PA self-assembly to form nanofiber and subsequently hydrogels was triggered by the addition of equal volume of four times molarity of trisodium phosphate salt (say 20 mM). Mixed PA hydrogels were made up of required concentrations of different PA which includes for example, 10 % of CM-PA and 90% of K-PA in the total concentration of PAs. Mixed PA self-assembly to form nanofiber and

subsequently hydrogels was also triggered using trisodium phosphate salt. This technique of hydrogel fabrication is used in chapters 4 and 7.

3.2.2. Fabrication of semi-interpenetrating network hydrogels

Semi-interpenetrating network hydrogels of PA (individual and mixed) and PEGDA were prepared. In brief, equal volumes of 20% w/v PEGDA and 10 mM PA solutions were mixed with the photo-intiator Irgacure 2959 with final concentration of 0.1% w/v. Photo initiator solution was prepared by diluting 10% w/v Irgacure 2959 in DMSO to 1 % w/v in de-ionized water. PA nanofiber self-assembly was induced using 40 mM trisodium phosphate salt solution. Following the nanofiber formation of the PA, ultra-violet (UV) cross-linking at 10-15 mW/cm^2 for 120 seconds using 365 nm UV light was performed to photo-crosslink PEGDA resulting in the formation of PA-PEGDA semi-interpenetrating network hydrogels. This technique of hydrogel fabrication is used in chapter 5.

3.2.3. Fabrication of cross-linked hydrogels

Covalently cross-linked hydrogels of mixed PAs i.e. 10 % of CM-PA and 90% of K-PA in the total concentration of PAs were prepared by using chemical cross-linker glutaraldehyde. PA samples of required concentration (say 5 mM) containing 10 % of CM-PA and 90% of K-PA were dissolved in filtered ultrapure water and stored at 4°C for at least 2 days prior to salt induced nanofiber self-assembly. The hydrogel samples were prepared in 96 well plates. Then, PA

self-assembly to form nanofiber and subsequently hydrogels was triggered by the addition 20 mM trisodium phosphate salts. Then, the formed nanofibers were allowed to cross-link with glutaraldehyde cross-linker in 1:0.5 and 1:1 Molar ratios of the lysine end group in the PA. The formed cross-linked hydrogels were incubated with glycine overnight to neutralize any active glutaraldehyde cross-linker. Control mixed PA hydrogel construct without glutaraldehyde cross-linking was also prepared. This technique of hydrogel fabrication is employed in chapter 6.

3.3. Physical characterization techniques

3.3.1. Morphological characterization - Transmission Electron Microscope

Transmission Electron Microscope (TEM) images of the nanofibers were taken on a JEOL JEM 2010 TEM operating at 200 kV accelerating voltage. The samples were prepared on a holey carbon copper grid. Negative staining was carried out with 1 w/v% phosphotungstic acid in water. TEM grids were prepared by casting 10 μL of salt induced self-assembled PA nanofibers onto the carbon side of the grid, followed by wicking off the excess moisture with filter paper after 1 min. Negative staining was then performed by placing the grid carbon-side down on a droplet of filtered phosphotungstic acid solution for 30 seconds. Then, the samples were air dried overnight before imaging.

3.3.2. Morphological characterization – Scanning Electron Microscope

Internal structure of the PA-PEGDA semi-interpenetrating network hydrogels were observed using XL30 FEG Scanning Electron Microscope in cryo mode (Cryo-SEM). Swollen PA-PEGDA semi-interpenetrating network hydrogel samples were freezed in liquid nitrogen, fractured and sublimed at 95°C for 10 mins. Then, the constructs were gold sputter coated for 10 mins in pre-chamber of the SEM. Finally, images were obtained by viewing using an electron microscope.

3.3.3. Circular dichroism spectroscopy

Circular dichroism (CD) experiments was performed using the JASCO J-810 spectropolarimeter (Jasco, Tokyo) equipped with a Peltier device for temperature control. The spectra were obtained in water using a 1 mm quartz cuvette (Hellma, Germany) at room temperature over a wavelength range of 190-240 nm at a scan speed of 50 nm/min.. Spectrum is obtained as an average of five scans. A volume of 400 µl of required concentration of PA (individual or mixed) sample self-assembled to form nanofiber using salt trigger is used.

The molar ellipticity (ME) expressed in units degrees cm^2 $dmol^{-1}$ is calculated from the measured ellipticity using the following equation:

$$[\theta] = \frac{\theta \times m}{c \times l} \qquad (1)$$

Where, θ is the ellipticity in milli degrees, m is the molecular weight in g/mol, c is the concentration in mg/ml and l is the path length of the cuvette in cm. Red-shifting for the β-sheet forming PA was calculated by the following equation:

$$\text{Red shift} = \frac{(x - 195) + (y - 215)}{2} \qquad (2)$$

Where, red shift is calculated in nm, x is wavelength at positive CD peak maxima in nm and y is the wavelength at negative CD peak maxima in nm.

3.3.4. Melting curve studies

Melting studies for CM-PAs were also performed on a J-810 spectropolarimeter (Jasco, Great Dunmow, Essex, UK) equipped with a Peltier device for temperature control using a 1 mm quartz cuvette (Hellma, Germany). Melting point curves were obtained by recording the ellipticity at 223 nm, where the CD positive peak signal was maximum, while the temperature was continuously increased between 5°C and 80°C, at a rate of 0.2 °C/min. For samples exhibiting sigmoidal melting curves, the reflection point in the transition region (first derivative) is defined as the melting temperature (T_m). CM-PAs are prepared and stored at 4°C for at least 24 hours prior to the experiment.

3.3.5. Blending test - Fourier Transform – Infra-red spectroscopy

Blending of PA and PEGDA in PA-PEGDA semi-interpenetrating network hydrogels was characterized using Fourier Transform – Infra-red spectroscopy (FTIR) on a Bio-Rad FTIR spectrophotometer (Model FTS135). In brief, PA-PEGDA semi-interpenetrating network hydrogels were freeze dried and powdered. The powdered sample was grinded with potassium bromide (KBr) in a weight ratio 1:49. The ground powder was cast into a pellet using pressure assisted holders. Then the formed pellet was used to obtain a FTIR spectrum from

400 cm^{-1} to 4000 cm^{-1} wavenumber range under ambient conditions in transmission mode. Typically, 16 scans at a resolution of 8 cm^{-1} were accumulated to obtain one spectrum.

3.3.6. Stability testing - Bradford assay

Microplate protocol with working range 1-25µg/mL using Coomassie (Bradford) Protein Assay Kit (Thermo Scientific, USA) was employed to determine the amount of peptide leached from the PA-PEGDA semi-interpenetrating network hydrogel constructs. In brief, 150µL of 48 hours hydrogel incubated de-ionized water was taken in 96 well plates and incubated for 10 minutes at room temperature after addition of equal volume of Bradford reagent. Absorbance was measured at 595 nm on a microplate reader (Tecan infinite M200). Standard curve was prepared for each PA individually.

3.3.7. Swelling characteristics

The swelling behavior of the hydrogels is evaluated using conventional gravimetric methods. Completely freeze dried gels were immersed in deionized water at 37°C. At equilibrium conditions i.e. after 3 days, hydrogels were blotted dry and weighed using an electronic balance. The swollen gels were then again freeze dried and weighed.

Percentage equilibrium swelling degree is determined as the percentage of wet weight over dry weight. Percentage equilibrium water content (EWC) is calculated using the following formula,

$$EWC = \frac{m_{eq} - m_0}{m_{eq}} \times 100 \quad (3)$$

Where, m_{eq} is the equilibrium wet weight and m_0 is the dry weight of the semi-interpenetrating network hydrogel constructs.

Percentage equilibrium swelling degree is calculated using the following formula,

$$\text{Percentage equilibrium swelling} = \frac{m_{eq} - m_o}{m_o} \times 100 \quad (4)$$

Where, m_{eq} is the equilibrium wet weight and m_0 is the dry weight of the semi-interpenetrating network hydrogel constructs.

3.3.8. Rheological characterization

All rheological studies were done using AR G2 Rheometer with a 20" parallel plate configuration with a gap of 50 μm. Peptide amphiphile nanofiber hydrogels induced by the addition of equal volume of four times molarity of trisodium phosphate salt were prepared directly on the rheometer plate. Strain sweeps were done at a frequency of 10 rad/s and frequency sweeps were done at a constant strain of 0.5%. Frequency sweep curves and strain sweep curves for all constructs were obtained as a log-log graph.

3.3.9. Mechanical properties characterization

Mechanical properties of PA-PEGDA semi-interpenetrating network hydrogel and glutaraldehyde cross-linked PA hydrogels were performed using a universal mechanical testing machine (Instron, USA) for compressive tests with a 5N load cell at an compression rate of 0.1mm/min for hydrogels. Vernier caliper was used to measure the diameter and height of the samples and the data was recorded

using the BlueHill^{TM} software. Stress-strain graph was fitted and compressive modulus was calculated from the initial linear range of the graph (~10% strain). Breaking point was determined as the stress at which there was a sudden drastic drop in the compressive stress owing to the breaking of the semi-interpenetrating network hydrogel constructs.

3.4. Biological characterization techniques

3.4.1. Cell culture of L929 fibroblast cells

L929 fibroblast cells were cultured in high glucose Dulbecco's modified Eagle's medium (DMEM) with 10% v/v fetal bovine serum and 1% v/v antibiotic solution (penicillin - 100U/mL and streptomycin - 100μg/mL) at 37°C in an incubator with 5% CO_2.The cells were grown in a T75 flask and the medium was replenished with fresh supply of medium every 3-5 days. Cells were harvested for cell proliferation studies when it was 80-90% confluent. 2000 cells are seeded for each construct for Cell proliferation studies.

3.4.2. Cell viability and cell proliferation assay

Cell viability and cell proliferation was determined using thiazolyl Blue Tetrazolium Bromide (MTT) assay. In brief, medium was removed and gels were washed with PBS to remove unattached cells. Then 1:10 MTT reagent in medium without serum was added and incubated for 4 hours at 37°C in dark. The formed purple crystals were dissolved in DMSO and absorbance was measured at 540 nm

with reference at 690 nm. Standard curve with known cell numbers was plotted to determine the cell number in the sample constructs.

3.4.3. Immunofluorescence staining for cell adhesion and spreading

Attachment of L929 fibroblast cells onto the constructs was visualized using confocal microscopy after immunofluorescence staining. In brief, fibroblasts were cultured for 2 days on various PA-PEGDA semi-interpenetrating network hydrogel constructs in Lab-Tek® chamber slides with glass bottom for direct confocal microscopy visualization. Attached L929 fibroblast cells on various PA-PEGDA semi-interpenetrating network hydrogel constructs were fixed in cold 3.7 v/v% formaldehyde for 15 min and permeabilized with 0.2% saponin solution for 5 mins. Then, constructs were blocked with 1 w/v% bovine serum albumin (BSA) in PBS. Staining of the cell actin cytoskeleton and cell nucleus was done with phalloidin-tetramethylrhodamine isothiocyanate (1:750 dilutions in PBS) and Hoechst (1:3000 dilutions in PBS) for 45 minutes respectively. Finally, the samples were washed for five times with PBS and visualized under a confocal laser scanning microscope (CLSM) (C1 system, Nikon, Singapore).

3.5. Statistical analysis

All the data presented in all the chapters except for cell culture represent mean ± standard deviation values of three experiments for each construct. Cell culture data represents mean ± standard deviation values carried out in triplicates of three

experiments for each construct. Statistical differences between groups were found using Student's t-test. A 95% confidence level was considered significant.

CHAPTER 4

PRELIMINARY EXPERIMENTS

A description of the preliminary experiments that led to the research objectives described in the chapters 5, 6 and 7 of this thesis will be presented in this chapter.

Sometimes by losing a battle you find a new way to win the war.

- **Donald Trump**

4.1. Introduction

With the success of developing a versatile CM-PA nanofiber hydrogel (Luo et al. 2011), the next step was to employ the CM-PA nanofiber hydrogel for tissue engineering and regenerative medicine applications. One of the key and early biomedical applications that has gained commercial importance is wound healing, repair and regeneration with a focus on skin tissue engineering.

4.1.1. Skin

Skin is the largest organ in the human body accounting almost one-tenth of the total body mass (Metcalfe et al. 2007). Skin is extremely important for the survival of human beings. Skin performs several vital functions such as (i) protective barrier from external factors like mechanical impact, micro-organisms, radiation; (ii) regulatory organ against temperature variations; and (iii) organ of sensation provided by the presence of several nerve cells with each acting as receptors for touch, temperature and pain (Proksch et al. 2008; Madison. 2003).

Structurally, skin is one of the complex organs composed of different layers each with diverse kind of cells and ECM architecture. Broadly, skin is made up of three layers namely, the outer epidermis, the middle dermis and the inner hypodermis (Boranic et al. 1999). Each layer has its unique ECM architecture and typical composition of cells and performs precise vital functions. In addition to

these layers, skin also possesses appendages like hair, sweat glands also called as sebaceous glands and so on. Outer epidermis is the cell rich layer with a pool of cells, majorly, the keratinocytes and sparse ECM. Other cells which co-exist with keratinocytes in the epidermis are melanocytes, Langerhans cells and Merkel cells. Keratinocytes produce the keratin, the insoluble fibrous protein, which accounts for almost 95% of all the proteins in epidermis (Watt. 1988). Dermis forms the bulk of the outer skin with almost 10 to 40 times thicker than the outer epidermis. Dermis is majorly made up as bio-macromolecular glycoproteineous gel with 80% water, 70-90% collagen, particularly collagen type I (M.C. Branchet et al, 1990), elastin fibers and other proteins. Fibroblasts are the main cell type in dermis (Huang et al. 1998). Dermis ECM mostly type I collagen fibrils produced by fibroblasts along with elastin fibers provide the structural support for the skin. Unlike epidermis, dermis is vascularized, thus, it is able to provide energy and nutrition to the outer epidermis. In addition, dermis also to play a vital role in temperature regulation and in wound healing. Hypodermis is essentially the energy reserve layer of the skin made up of fat cells, called adipocytes.

4.1.2. The problem: chronic skin wounds

Wound healing is a natural dynamic process (Clark. 1996). Wound healing takes place through an intricate cascade of interactions between various cells to restructure and regenerate the injured skin to its native state. Unfortunately, often times wounds exhibit impaired healing after a long period of time; such wounds are called chronic wounds (Moreo. 2005). Most chronic wounds are deep ulcers

or open sores developed due to conditions like cardiovascular or peripheral vascular disease, diabetes mellitus or obesity (Sen et al. 2009). Chronic skin wounds can be also caused by trauma like burns and cut injuries.

The number of people suffering due to chronic wounds is staggering. According to a medical technology market report globally; approximately 3.5 million people of the 50 million people meeting with burn accidents require wound care products for treatment (MedMarket Diligence, company report, 2011). In addition, approximately 4.5 million people need treatment for pressure ulcers, approximately 9.7 million for venous ulcers, and approximately 10.0 million diabetic ulcers. An increasingly growing aging population is further increasing the probability of people with chronic wounds (MedMarket Diligence, company report, 2011).

Impaired healing of chronic wounds affects the quality of life of a person and puts immense burden on the caregivers. To add on, chronic wound care adds a tremendous burden to health care management system and our global society on the whole (Sen et al. 2009).

4.1.3. The solution: wound care - skin equivalents

One such wound care product that promises to heal the wound completely and allows regaining quality life is tissue engineered skin equivalents. From almost three decades, tissue engineered skin is used for clinical applications. Tissue engineered skin products for wound healing are majorly two kinds: (i) Acellular

and (ii) Cellular (Jimenez et al. 2004). In brief, acellular tissue engineered skin is a scaffold with biomaterials without any cells and cellular tissue engineered skin is a scaffold with cells. Acellular tissue engineered skin functions by integrating to the host through matrix-cell interactions. Most often its the porous and the cell instructive nature of the scaffold that allows host cells to infiltrate and integrate seamlessly (Winterswijk et al. 2007). Cellular tissue engineered skin comprise of scaffold populated with the major skin cells i.e. keratinocytes or/and fibroblasts or other cells like hair follicle cells derived from the patient itself to avoid the risk of immune rejection. Tissue engineered skin acts as an equivalent for either outer epidermis or middle dermis or both. In both acellular and cellular tissue engineered skin, the choice of biomaterial for scaffold for most of the products is either collagen or collagen-based with other ECM macromolecules. Collagen is the choicest material because of its abundance in ECM of skin and availability in abundance. Table 4.1 lists the commercial tissue engineered skin equivalent products along with their design approach. This list by no means is exhaustive one.

Table 4.1: List of commercially available tissue engineered skin equivalent products along with their type, skin mimicking layer and design approach. This table is modified from the articles by Winterswijk et al. 2007 and MacNeil. 2008. Highlighted in red are the scaffolds made with of collagen.

Type and Skin Layer equivalent	**Product**	**Design approach**	
		Cells	**Scaffold**

Acellular Dermal	OASIS		Porcine small intestinal submucosa ECM
	Integra		• Silicone membrane • Bovine tendon collagen • Glycosaminoglycan
	Permacol		Porcine dermal collagen ECM
	EZ-Derm		Aldehyde cross-linked porcine dermal ECM
	Matriderm		Bovine collagen-elastin dermal ECM
	Biobrane		• Silicone membrane • Nylon mesh with peptides from porcine dermal collagen type I
Cellular Epidermal	Hyalomatrix KC (Laserskin)	Autologous keratinocytes	• Benzyl ester of hyaluronic acid • Silicone membrane.
	Myskin	Autologous keratinocytes	Poly(vinyl chloride) polymer coated with a plasma polymerized surface
	EpiDex	Autologous root sheath hair follicle cells	perforated hyaluronic acid membrane
	Epicel	Epidermal autograft	
Cellular Dermal	Dermagraft	Allogeneic human fibroblasts	• Auto - synthesized ECM • Polyglactin mesh
	TransCyte	Neonatal fibroblasts	• Silicone membrane • Porcine collagen coated nylon mesh

	ICX-SKN	Allogeneic human dermal fibroblasts	• Auto - synthesized ECM
	Alloderm	Processed cadaver allograft skin	
Cellular Bilayer	Orcel	Human epidermal keratinocytes and dermal fibroblasts	Bovine collagen sponge
	Apligraf	Neonatal fibroblasts neonatal epidermal keratinocytes	Bovine collagen type I
	Permaderm	Autologous epidermal and dermal graft	

Even though, the current tissue engineered skin equivalent products created a huge milestone in the field of tissue engineering and regenerative medicine, yet, they lack and fail to mimic the natural skin in entirety. In addition to their deficiency as suitable skin equivalent, most of the current tissue engineered artificial skin products are plagued with several problems (MacNeil. 2008). The foremost concern is the safety issue which propels the need to avoid animal derived materials. The other problems are related to cell culture such as attachment of cultured skin cells and development of blood vessels. Finally, the biggest challenge to tackle is the avoidance of contraction and fibrosis. Hence, the quest to find the best biomaterial for skin equivalent that eliminates the existing

problems is still on. Newer scaffold designs with newer biomaterials designed with the knowledge and wisdom gained over the decades in the field of tissue engineering have re-kindled the fire to obtain the best skin equivalent.

One of the promising biomaterials for this purpose is synthetic collagen mimetic materials. The current promising scaffold design is to form nanofiber mesh or nanofibrous hydrogels (Chandrasekaran et al. 2011; Hodgkinson et al. 2014;). The requirement of a nano-topographical surface is met by the self-assemblying peptide system. Hence, Bradshaw et al. (2014) developed an efficient therapeutic approaches to enhance the rate of skin wound healing using self-assemblying peptide nanofiber with a collagen type I motif on the surface. However, the fibroblast cells grown on these scaffolds reflected a rounded morphology which is indicative of lack of matrix stiffness in the scaffold. However, CM-PA hydrogel system offers a promising structural and functional mimic to collagen, thus, resembling the ECM of the skin more closely. Hence, we designed an experimental strategy to study the culture of fibroblast cells on CM-PA hydrogels.

In this study, the effect of fibroblast growth in particular to morphology and proliferation on CM-PA hydrogel was focused on. Firstly, as a collagen mimetic material, a collagen derived biochemical cue was employed. This cue was derived from the triple-helical GFOGER integrin receptor binding sequence of collagen. Our group published couple of articles featuring the specific recognition of GFOGER as peptide templated coatings by Hep 3B and L929 fibroblast cells

(Khew et al. 2008; Khew et al. 2007). Hence, with the evidence of cell instructive ability of GFOGER peptide sequence to L929 fibroblast cells, the same cell line was used for this study. In addition, short length spacer PA (K-PA) was also designed and used in this study to understand the effect of a sequence without collagen cell instructive sequence. Mixing of collagen mimetic PA and spacer PA results in the protrusion of the collagen cell binding epitope to the surface of the nanofiber which enables favorable cell binding activity. Then, the nanostructure and functionality of self-assembled PA (individual and mixed) nanofibers were studied through various characterization methods. Transmission electron microscopy (TEM) was used to study the self-assembled PA nanofiber nanostructure. The secondary structure of CM-PAs was characterized using circular dichroism (CD) spectroscopy and melting curve studies. Subsequently, the PA (individual and mixed) nanofiber hydrogels were prepared and characterized for their mechanical properties using rheology. Finally, the hydrogels were employed to study the effect of fibroblast growth in particular to morphology and proliferation.

4.2. Results and Discussions

4.2.1. Synthesis of peptide amphiphiles

Collagen mimetic (CM-PA) and spacer PA (K-PA) were designed and synthesized based on Luo et al from biopeptek inc. (Malvern, Pennsylvania, United States). The molecular weight was determined using electrospray ionization mass spectrophotometer (ESI MS) for each sequence obtained and was consistent with

that of the desired calculated value. In addition, the purity of the synthesized PA was determined using high performance liquid chromatography (HPLC) and was >95%. The data of the molecular weight and the purity was supplied by the manufacturer. Table 4.2 tabulates the molecular sequences and the molecular weights of the PAs employed in this study.

Table 4.2: List of peptide amphiphile design sequence along with its label and molecular weight.

Label	Sequence*	Molecular Weight
CM-PA	C_{16}-AAAAAKKKKG$(GPO)_3$**GFOGER**$(GPO)_3$G	3502.2
K-PA	C_{16}-AAAAAKKKKGGK	1367.1

* C_{16} stands for palmitic acid modification in the N-terminal of the peptide. Standard one-letter amino acid code listed in Appendix B is used to express the sequences of the peptide.

4.2.2. Morphological characterization – Transmission Electron Microscopy

CM-PA and K-PA molecules spontaneously form micelles in aqueous solution and self-assemble to form nanofibers upon charge screening of the charge segment (Luo et al. 2011; Hartgerink et al. 2001). Figure 4.1 shows the TEM images depicting the morphology of self-assembled CM-PA, K-PA and K-CM-PA (construct with equi-molar ratios of K-PA and CM-PA) after screening the positive charges of the lysine segment using trisodium phosphate (Na_3PO_4) salt. The images confirm that screening the positive charges in the lysine spacer led to the formation of nanofibers. The diameter of the nanofiber was approximately around 15 nm which is consistent with the literature. The images also reveal

marked differences in the length and morphology among CM-PA and K-PA including the combination of CM-PA and K-PA in equal ratios. K-PA forms very long nanofibers in relation to CM-PA and the combination of the two PAs yields nanofibers in intermediate lengths. However, it was difficult to quantify the size of the nanofibers owing to its polydisperse distribution.

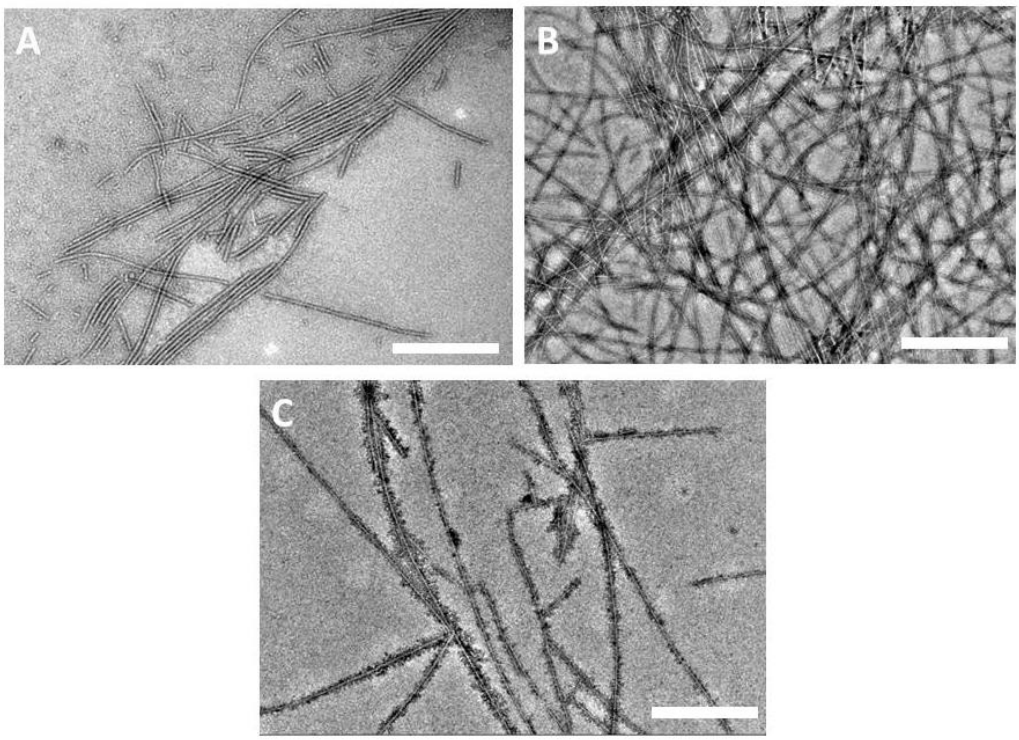

Figure 4.1: TEM micrographs of self-assembled PA nanofibers (A) CM-PA, (B) K-PA, and (C) K-CM-PA (construct with equi-molar ratios of K-PA and CM-PA) after charge screening. All the PA nanofibers are with the diameter of ~15 nm. However, K-PA forms very long nanofibers in relation to CM-PA and K-CM-PA due difference in the hydrophobic and hydrophilic ratio. Scale of the images is 500 nm.

The marked difference in length of CM-PA and K-PA is attributed to the number of amino acids in the peptide amphiphile. From literature (Gore et al. 2001; Xu et al. 2010) it is seen that the hydrophobic interactions of the alkyl tails, steric hindrance effects, electrostatic interactions, and hydrogen bonding orchestrate the self-assembly of PAs in aqueous medium resulting in nanostructures of various

size and shape. In particular, from literature (Meng et al. 2014), it is also observed that the longer the amino acid sequence the shorter the length of the nanofiber in PA with α-helical epitope due to less pronounced hydrophobic effect of the alkyl chain over hydrophilic effect of the peptide length. Hence, CM-PA consisting of 35 amino acids forms a relatively shorter nanofiber than K-PA consisting of only 12 amino acids. However, K-CM-PA forms intermediate length nanofiber due to inter-mixing of long, K-PA and short, CM-PA nanofibers.

4.2.3. Circular dichroism spectroscopy

Structurally, CM-PA and K-PA form markedly different secondary structure. The CM-PA similar to collagen exhibits a typical triple-helix secondary structure. The signature peaks for typical collagen triple-helix is a large negative peak at approximately 197 nm, crossover near 213 nm and a small positive peak at 220-225 nm (Lesley et al. 2011). Thus, the formation of collagen mimetic nanofiber is confirmed by the presence of the characteristic triple-helical peaks. However, the K-PAs in solution assume a micelle configuration over a certain critical micelle concentration which is reflected as a random coil configuration in the CD spectrum. The signature peak for a random coil is a negative peak at around 200nm. Upon trigger of charge screening using high ionic strength using Na_3PO_4 salt, the micelles self-assemble to form β-sheeted nanofiber (Hartgerink et al. 2001). Thus, the formation of nanofiber is confirmed by the presence of characteristic β-sheet peaks. The characteristic β-sheet peaks are negative peak at 215 nm and positive peak at 195 nm in the CD spectrum. Hence, the secondary

structure of the PAs was analyzed for the formation of nanofiber using circular dichroism (CD) spectrum.

The CD spectrum of CM-PA is shown in Figure 4.2 as green line. From the spectrum, it is confirmed that the CM-PA nanofibers are formed and exhibit a typical collagen triple-helix conformation. CM-PA spectrum shows a positive peak around 223 nm, crossover around 216 nm and negative peak around 203 nm. In addition, CM-PA also displays a red shift in band positions with respect to the typical CD spectral band positions of collagen, probably due to the difference in amino acid content (Rippon et al. 1971). This conclusion is consistent with that of the literature (Luo et al. 2011).

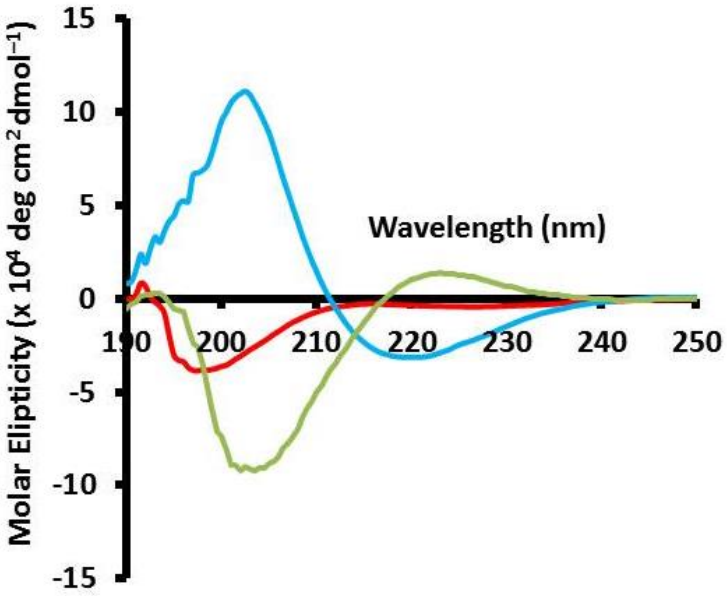

Figure 4.2: CD spectra of CM-PA nanofiber in aqueous solution after charge screening (green line) showing the characteristic CD peaks of collagen triple-helix i.e. a positive peak around 223 nm, crossover around 216 nm and negative peak around 203 nm. CD spectra of K-PA micelle in aqueous solution (red line) showing a dominant negative peak around 198 nm that is typical of random coil conformation. CD spectra of K-PA nanofiber in aqueous solution (blue line) showing a relatively small negative peak at 219 nm and a dominant positive peak at 203 nm that is typical of β-sheet conformation.

The CD spectrum of K-PA is shown in Figure 4.2 as red and blue line. From the spectrum, it is confirmed that the K-PA nanofibers are formed due to β-sheet formation. K-PA micelle represented by red line shows a dominant negative peak around 198 nm, which is typical of random coil conformation. However, K-PA nanofiber represented by blue line shows a relatively small negative peak at 219 nm and a dominant positive peak at 203 nm. The red shift of the CD signal from the signature β-sheet signal is calculated is 6 nm for K-PA nanofiber. The red shift is indicative of the twist in the β-sheet and accounts for the rigidity or stiffness of the nanofiber (Pashuck et al. 2009).

4.2.4. Melting curve studies

Collagen triple-helical conformation is similar to that of the PPII helix conformation in the CD spectrum with positive ellipticity around 215-240 nm wavelength (Leikina et al. 2002; Madhan et al. 2008). A typical triple-helix is stabilized by hydrogen bonds present in the intra- and inter-strand (Shoulders et al, 2009). Thus, collagen is sensitive to temperature. Collagen triple-helix conformation follows a highly cooperative behavior during thermal denaturation unlike PPII helix (Bella et al. 1995; Jefferson et al. 1998). Hence, to further confirm that CM-PA forms a triple-helix and is different from that of PPII helix, a thermal melting curve study using CD spectrum was performed. The thermal unfolding experiment monitors the spectral ellipticity as temperature is increased at 223 nm at the wavelength where the positive ellipticity is maximum for CM-PA. The thermal unfolding curve of CM-PA gave a sigmoidal curve as shown in figure

4.3. The sigmoidal curve is typically associated with the cooperative denaturation of triple-helical conformation to single-stranded structure. In essence, during the temperature transition, the triple-helical structure falls apart by breaking the hydrogen bonds between the three polypeptide chains, thus, assuming a single-stranded structure. The negative ellipticity at higher temperatures in figure 4.3 is indicative of the presence of single-stranded structure. In contrast, PPII helix undergoes a linear thermal transition and its thermal unfolding curve appears as straight line. Hence, it is confirmed that CM-PA forms a triple-helix and is different from that of PPII helix. Melting curve is used to determine the melting temperature.

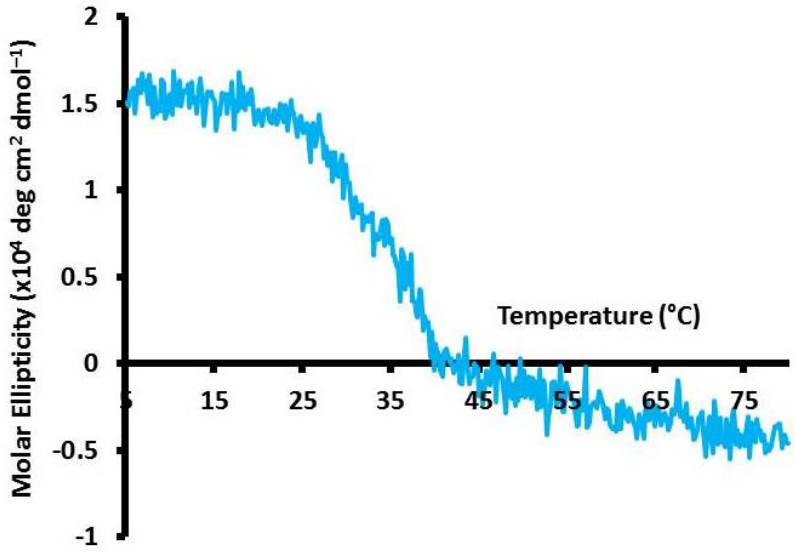

Figure 4.3: CD melting curve spectra of CM-PA showing typical sigmoidal transition associated with the cooperative denaturation of triple-helical conformation to single-stranded structure. Thus, confirming that CM-PA forms a triple-helix.

The first derivative of the melting curve for a CM-PA sample in water was plotted as shown in figure 4.4. From figure 4.4, the temperature at the inflection point i.e.

the negative peak of first derivative ellipticity in the first derivative CD melting curve of CM-PA is defined as the melting temperature (T_m) for CM-PA. T_m indicates the temperature at which 50% of the collagen triple-helices are unfolded to single-stranded random coils. T_m for CM-PA was found to be at 40°C. This result is consistent with that of the literature (Luo et al. 2011). The value of T_m represents the stability of the triple-helix. Triple-helix is more stable when the value of T_m is higher.

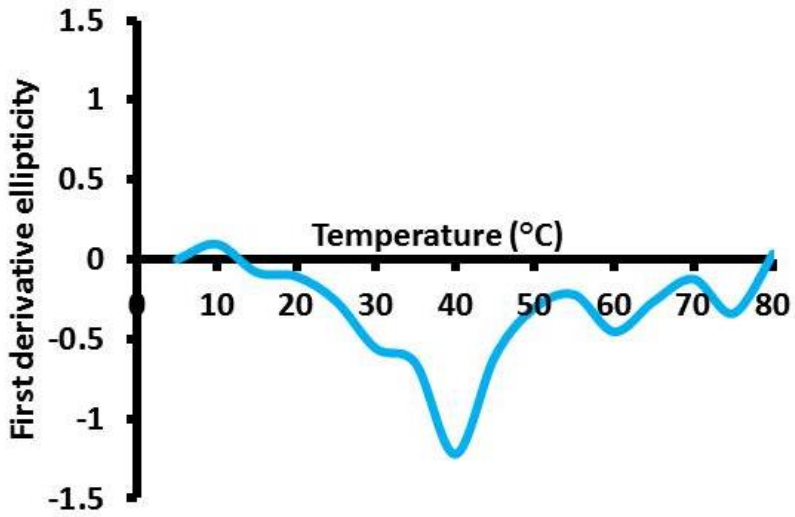

Figure 4.4: First derivative CD melting curve spectra of CM-PA showing the melting temperature for CM-PA as 40°C.

4.2.5. Rheological Characterization

CM-PA, K-PA and K-CM-PA hydrogels were characterized for their mechanical properties by rheological studies using AR-G2 rheometer. Representative strain sweep curves are shown in figure 4.5. Strain sweep graphs were taken to determine the linear visco-elastic region of the hydrogels. Then, frequency sweep tests were also carried out in the linear visco-elastic stain.

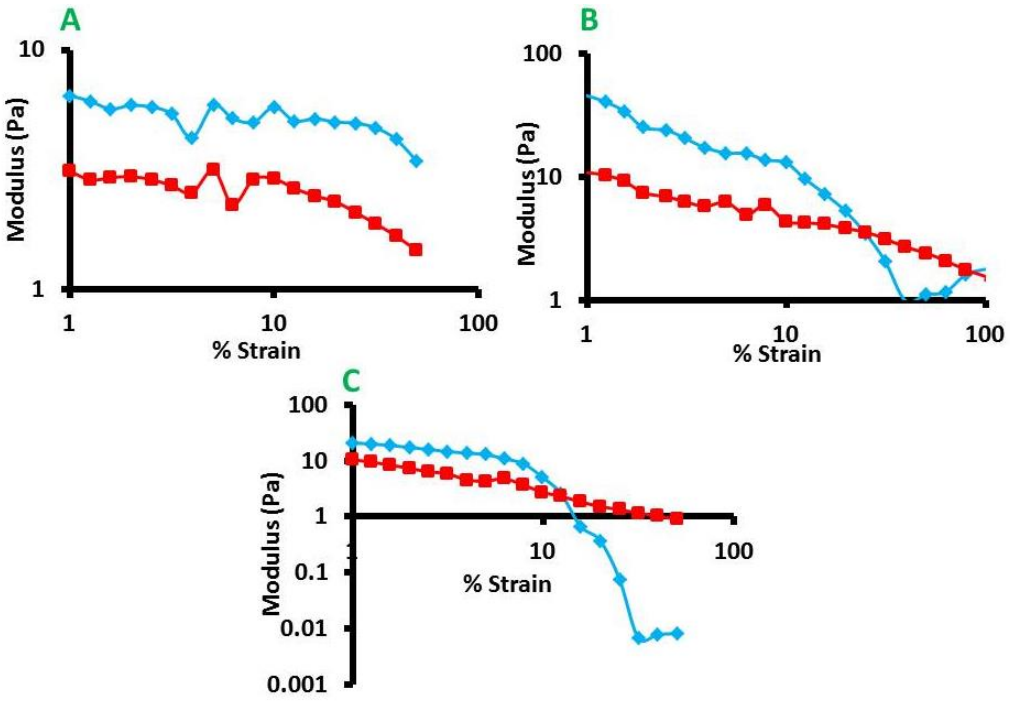

Figure 4.5: Representative strain sweep curves showing storage modulus, G' (blue line) and loss modulus, G" (red line) for rheological characterization of self-assembled PA nanofiber hydrogels (A) CM-PA, (B) K-PA, and (C) K-CM-PA (construct with equi-molar ratios of K-PA and CM-PA) formed after charge screening using salt trigger. Strain sweep curves are used to identify the linear visco-elastic region for the different hydrogels.

From the frequency sweep graphs shown in figure 4.6, it is evident that the PA hydrogels differ in their storage modulus (G') and loss modulus (G"). For CM-PA hydrogel, G' was found to be greater than their respective G" for the lower frequency range and approaching same G' and G" for the higher frequency range close to 10 rad/s. This behavior is indicative of dominant elastic nature at lower frequency but dominant viscous nature at higher frequency (Liu et al. 2013). However, In the PA hydrogels K-PA and K-CM-PA, G' was found to be greater than their respective G" over the entire frequency range studied (1 – 10 rad/s). This indicates that K-PA and CM-PA hydrogels are showing an elastic solid like behavior (Liu et al. 2013).

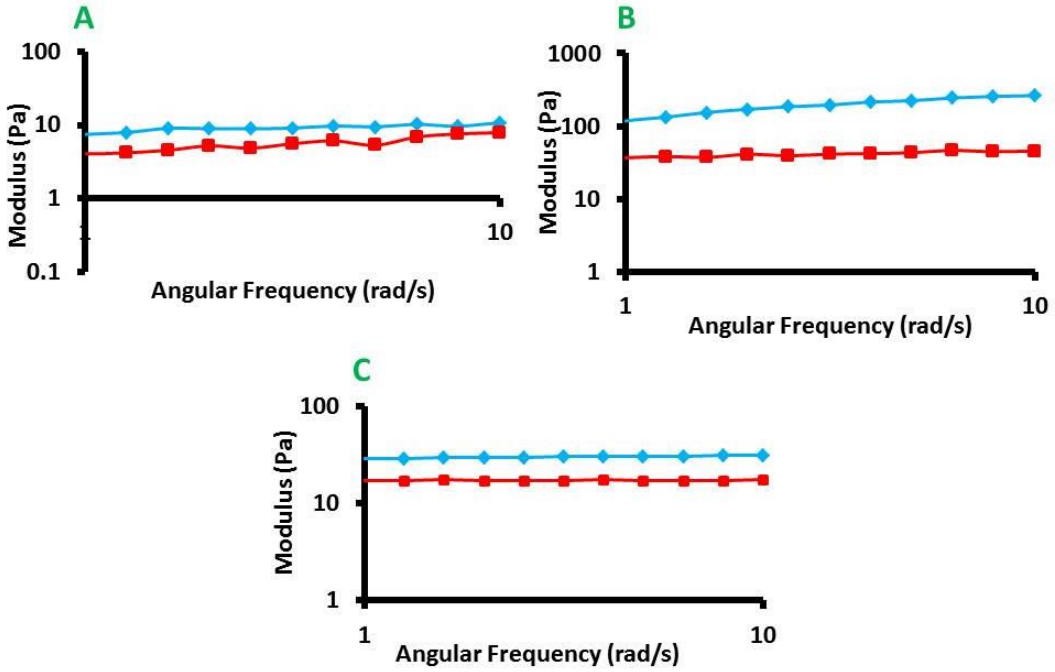

Figure 4.6: Representative frequency sweep curves showing storage modulus, G' (blue line) and loss modulus, G" (red line) for rheological characterization of self-assembled PA nanofiber hydrogels (A) CM-PA, (B) K-PA, and (C) K-CM-PA (construct with equi-molar ratios of K-PA and CM-PA) formed after charge screening using salt trigger. Frequency sweep curves show that the PA hydrogels differ in their G' and G" which in turn indicates the strength of the hydrogels formed.

As shown in figure 4.7, The G' values of all three PA hydrogels at a frequency of 5 rad/s were compared to determine the relative hydrogel strengths. G' of K-PA was found to be significantly higher compared to that of CM-PA and K-CM-PA by about 15 times and 4 times respectively. In addition, G' of K-CM-PA was found to be significantly higher compared to that of CM-PA by almost 4 times. To sum up, CM-PA hydrogels have the least mechanical strength, K-PA hydrogels have the highest strength and K-CM-PA have the intermediate strength. This difference is attributed to difference in nanofiber length. Shorter fiber length leads to lesser entangling to form hydrogels and longer fiber length leads to intricate

entangling to form stronger hydrogels.

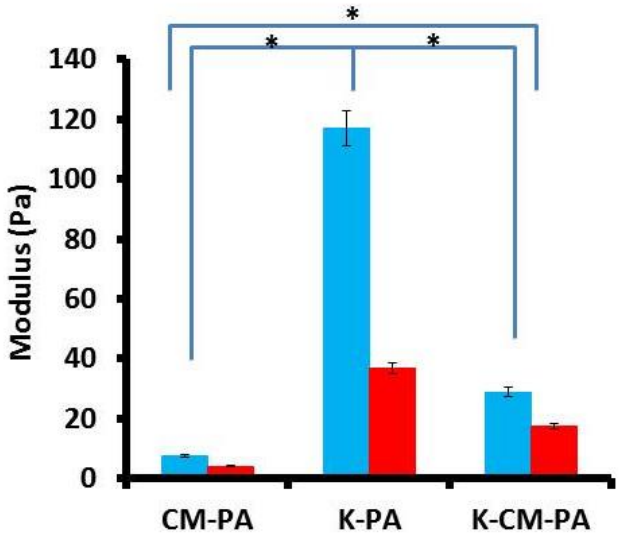

Figure 4.7: Column graph showing the G' values of self-assembled PA nanofiber hydrogels (A) CM-PA, (B) K-PA, and (C) K-CM-PA (construct with equi-molar ratios of K-PA and CM-PA) formed after charge screening using salt trigger at a frequency of 5 rad/s. G' of K-PA was found to be significantly higher compared to that of CM-PA and K-CM-PA by about 15 times and 4 times respectively. *P<0.05 (Student's t-test).

4.2.6. Fibroblast cell culture on peptide amphiphile and collagen coatings

L929 fibroblast cells were cultured on the surface of CM-PA, K-PA and K-CM-PA nanofiber coatings. In brief, PA samples of required dilute concentration (say 0.5 mM) were dissolved in filtered ultrapure water and stored at 4°C for at least 2 days prior to salt induced nanofiber self-assembly. The nanofiber coatings were prepared in 96 wells plate. PA self-assembly to form nanofibers and subsequently hydrogels was triggered by the addition of equal volumes of PA dilute solution (say 20 µl) and four times molarity of trisodium phosphate salt (say 2 mM). Mixed PA hydrogels were made up of equi-molar ratios of K-PA and CM-PA. After the nanofiber formation using salt trigger, the 96 wells plate was air dried overnight and employed subsequently for fibroblast cell culture. The morphology

of the fibroblast cells were studied under optical microscope as shown in figure 4.8. Fibroblast on the CM-PA coatings showed rounded morphology on Day 1. Fibroblasts on the coating of K-PA exhibited typical fibroblast flat spindle shape morphology and K-CM-PA revealed mixed group of fibroblast cells with rounded and typical fibroblast flat spindle shape morphology on Day 1. Subsequently, on Day 5, Fibroblasts on CM-PA displayed clumped colonies along with typical spindle shaped fibroblasts not visible on Day 1.

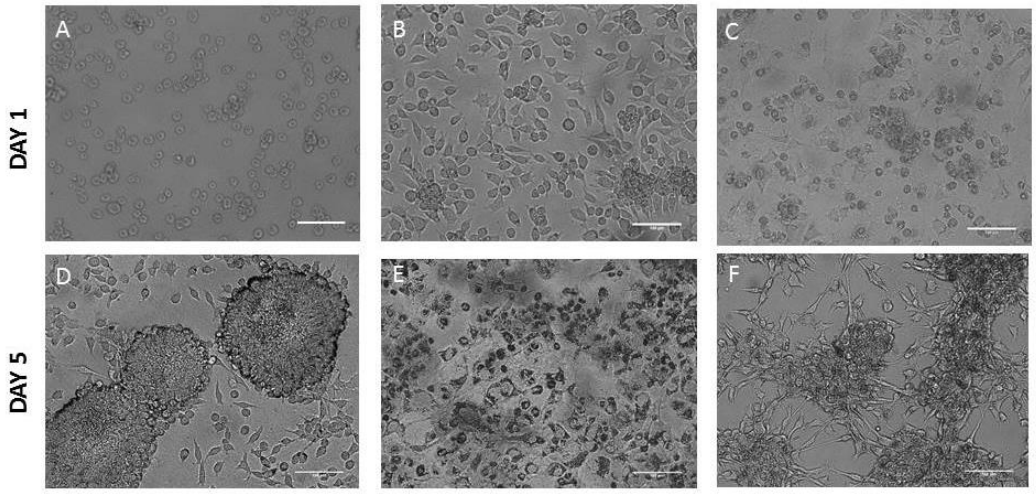

Figure 4.8: Optical light microscope images of fibroblasts on of self-assembled PA nanofiber coatings (A, D) CM-PA, (B, E) K-PA, and (C, F) K-CM-PA (construct with equi-molar ratios of K-PA and CM-PA) formed after charge screening using salt trigger on Day 1 and Day 5 respectively. The scale of the images is 100 microns.

Fibroblasts on K-PA coating exhibited cell death due to apoptosis indicatated by the presence of several dark cells which could be due to lack of cell instructive cue and K-CM-PA coating exhibited both relatively smaller clumps of spindle shaped fibroblasts and apoptosis of cells. The rounded morphology of fibroblast on CM-PA coating can be attributed to lack of mechanical strength (Discher et al. 2005) or suitable biochemical cue (De Rosa et al. 2004; Hamdan et al. 2006) for

cell stretching. The subsequent high proliferation can be attributed to the presence of collagen mimetic GFOGER epitope on the PA which induces the cell receptor signaling, thus, enabling the synthesis of own ECM matrix ,thus, aiding in cell proliferation. The mixed peptide amphiphile nanofiber coating exhibits intermediate behaviour of both individual coatings.

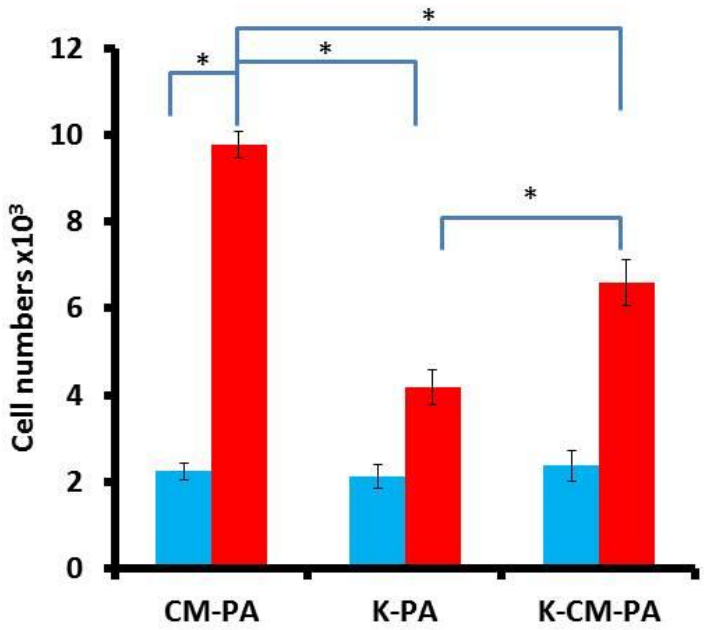

Figure 4.9: Cell proliferation assay of fibroblasts on self-assembled PA nanofiber coatings of CM-PA, K-PA and K-CM-PA (construct with equi-molar ratios of K-PA and CM-PA) formed after charge screening using salt trigger on Day3 (blue columns) and Day 7 (red columns). *P<0.05 (Student's t-test).

The cell proliferation on the above constructs is quantified using MTT assay for Day 3 and Day 7 and plotted in the graph as shown in figure 4.9 and Student's t-test with 95% confidence level was used for the analysis of significance. The significant difference in cell numbers between CM-PA and K-CM-PA coatings is due to the presence of high GFOGER epitope density. This signifies the essential role of GFOGER in cell proliferation. It is observed that there is no significant

difference in the cell numbers on Day 3 and Day 7 in K-PA coating indicating the need for cell adhesion sequences. Thus, the mixed PA biomaterial could provide choice hydrogel scaffold for fibroblast culture as it provides favorable surface biochemical cue for both fibroblast cell spreading and cell proliferation behavior.

L929 fibroblast cells were also cultured on the surface of collagen coated 96 wells culture plate. In brief, 40 µl of 1 mg/ml collagen solution is added into each required number of wells in 96 wells culture plate. Then, the 96 wells plate was air dried overnight and employed subsequently for fibroblast cell culture. The morphology of the fibroblast cells were studied under optical microscope as shown in figure 4.10 (A). Fibroblasts on the coating of collagen exhibited typical fibroblast flat spindle shape morphology from Day 1 and the cell adhesion, spreading and proliferation was relatively higher than that of CM-PA nanofiber coating as shown in figure. 4.8 (A, D) and figure 4.9. By Day 5 as shown in figure 4.10 (A), fibroblast cells reached almost 90% confluency which wasn't observed in CM-PA nanofiber coatings. The cell proliferation on the collagen coatings was quantified using MTT assay for Day 3 and Day 5 and plotted in the graph as shown in figure 4.10 (B). The cell numbers were significantly higher than CM-PA nanofiber coatings. This signifies that collagen contains several other essential biological cell instructive sequences like DGEA and RGD (Khew et al. 2007) inaddition to GFOGER along with mechanical and nano-topographical cues required for L929 fibroblast cells proliferation, which are not present in CM-PA nanofibers.

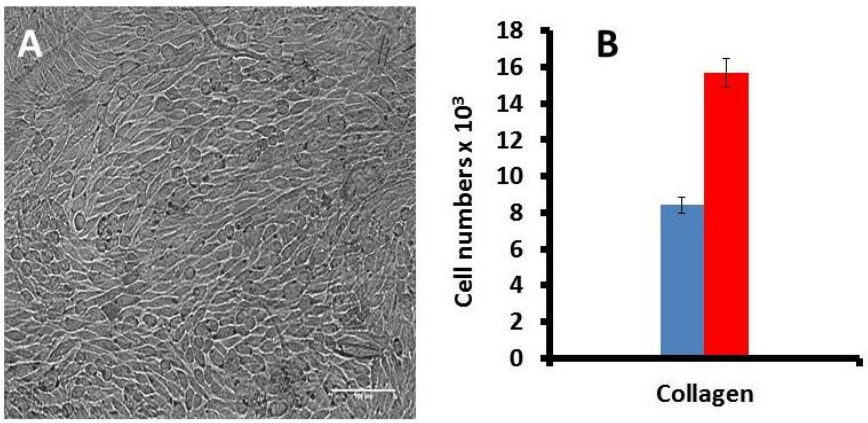

Figure 4.10: (A) Optical light microscope image of fibroblasts on collagen coated 96 wells culture plate on Day 5. The scale of the images is 100 microns. (B) Cell proliferation assay of fibroblasts on collagen coated 96 wells culture plate on Day 3 (blue columns) and Day 5 (red columns).

4.2.7. Fibroblast cell culture on peptide amphiphile hydrogels

L929 fibroblast cells were then cultured on the surface of CM-PA, K-PA and K-CM-PA nanofiber hydrogels. The morphology of the fibroblast cells were studied under optical microscope as shown in figure 4.10 . Fibroblast cells cultured on all the PA hydrogels showed rounded morphology after 24 hours of culture irrespective of the different surface biochemical cues. Hence, the lack of cell spreading and cell proliferation behavior can be inferred due to the lack of sufficient mechanical strength for the culture of fibroblast cells (Discher et al. 2005). On hind sight, fibroblast cells on the PA coatings might have exhibited the various cell behaviors due to the cumulative effect of mechanical strength derived from the bottom of the well plates and the topography and biochemical cue derived from the nanofiber. However, the effect of the biochemical cue i.e. collagen mimetic GFOGER sequence on cell spreading and cell proliferation is inconclusive.

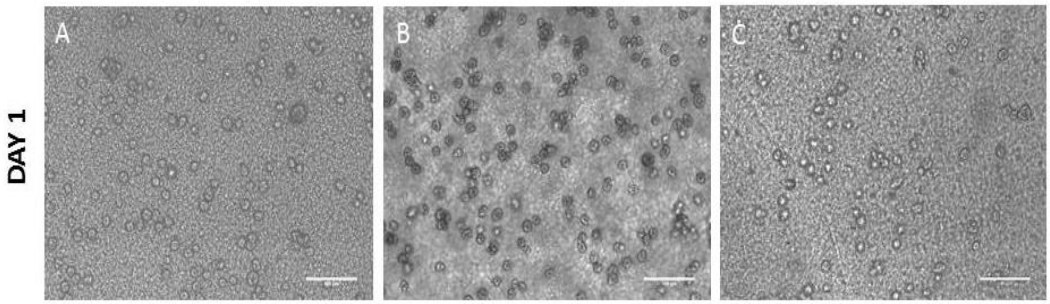

Figure 4.11: Optical light microscope images of fibroblasts on of self-assembled PA nanofiber hydrogels (A) CM-PA, (B) K-PA, and (C) K-CM-PA (construct with equi-molar ratios of K-PA and CM-PA) formed after charge screening using salt trigger on Day1. The scale of the images is 100 microns.

4.3. Conclusion

As mentioned, scaffolds play a major role in providing the necessary signals such as surface biochemical cue, topography, and mechanical property required for proper cell behavior. Based on the above findings, it is evident that CM-PA, K-PA and K-CM-PA nanofiber hydrogels have the potential to provide required surface biochemical cue, but, lack the required mechanical strength for the fibroblast culture. Unfortunately, this failure also pushed the goal to use the CM-PA hydrogel as skin equivalent biomaterial to the back stage for some time.

However,

"Success is neither magical nor mysterious. Success is the natural consequence of consistently applying the basic fundamentals."

- Jim Rohn

In vivo, fibroblasts cell binding to the collagen fibrils is a result of dual properties primarily, presence of cell instructive receptors on collagen fibrils for cell surface

integrin binding (Brakebusch et al. 2003; Delon et al. 2007) and secondarily, mechanical tension existing between collagen fibrils and fibroblasts (Alenghat et al. 2002; Reed et al. 2001; Wang et al. 1994; Grinnell. 2003). One straightforward indication of the mechanical tension existing between collagen fibrils and fibroblasts is flattening and spreading of fibroblast. Reduced mechanical tension is reflected by reduced fibroblast spreading with a collapsed appearance with little cytoplasm. Hence, it is evident that the critical determinants for cellular function are mechanical tension and cell shape (Lecuit et al. 2007; Peyton et al. 2007; Eckes et al. 2006).

Hence, learning from the nature, the study focused to the design CM-PA hydrogels with appropriate mechanical cues for L929 fibroblast cell culture. The following three approaches were employed:

1) To develop and study the effect of semi-interpenetrating network hydrogels consisting of CM-PA and poly(ethylene glycol) diacrylate (PEGDA) with varying mechanical cues on the behavior of fibroblasts. (Chapter 5)

2) To develop and study the effect of cross-linked CM-PA hydrogels with varying mechanical cues on fibroblasts behavior. (Chapter 6)

3) To develop a CM-PA hydrogel with a novel design by tuning the peptide amphiphile sequence for providing appropriate mechanical cue and to study the proliferation behavior of fibroblasts on the designed scaffold. (Chapter 7)

CHAPTER 5

SEMI-INTERPENETRATING NETWORK HYDROGELS

This chapter describes the strategy of semi-interpenetrating network hydrogels consisting of CM-PA and poly(ethylene glycol) diacrylate (PEGDA) to study the effect of varying mechanical cues on the fibroblast cell morphology and proliferation.

The work in this chapter addresses research objective 1 described in chapter 1.

5.1. Introduction

To re-emphasize, natural polymers particularly, collagen type I is the commonly used biomaterial for tissue engineering and regenerative medicine applications. The abundant use of collagen type I is primarily due to its abundant presence in the ECM of all tissue types. For biomedical applications, usually collagen hydrogels are formed through physical crosslinking of collagen fibrils with each at 37°C and neutral pH in aqueous solutions (Wright et al. 2002; Liang et al. 2011) However, the formed collagen gels possess weak mechanical properties, thus, limiting their use for wide range of applications. Hence, to overcome the limitation in the mechanical strength several approaches are followed. One such approach is to form composite hydrogels in combination with other polymers, called interpenetrating networks (IPNs) or semi-IPNs (S-IPNs) (Brigham et al. 2009; Chan et al. 2012)

S-IPNs are formed by mixing two different types of polymers such as one natural polymer and one synthetic polymer and physically crosslinking them to obtain woven-like structures. S-IPNs possess complementary properties of both the polymers (Vendamme et al. 2006). Usually, synthetic polymers contribute towards mechanical properties and natural polymers towards biochemical cell instructive properties (Lee et al. 2001; Weng et al. 2008) Hence, semi-IPNs exhibit tunability for both mechanical and biochemical properties.

Similarly, CM-PA also forms hydrogels with weak mechanical strength, thus,

limiting its application as a scaffold for fibroblast culture. Hence, the approach to form S-IPNs is employed to meet fibroblast tissue-specific mechanical strength requirements.

The synthetic polymer employed is poly(ethylene glycol) (PEG). PEG is an FDA-approved synthetic hydrophilic polymer and various kinds of PEG based hydrogels are widely used for drug delivery and tissue engineering applications (Guarino et al. 2010; Robinson et al. 2012; Jonker et al. 2012; Santos et al. 2012). PEG offers advantages like bio-inertness, biocompatibility, low immunogenicity, low protein adsorption and tunability for chemical modifications (Peppas et al. 2006; Ma. 2008; Mellott et al. 2001). Commercially, PEG is available in various forms namely, linear or multi-arm PEGs or homo-bi-functional or hetero-bi-functional PEGs with hydroxyl, acrylate, amine, maleimide or aldehyde end groups. Even though, PEG offers wide range of tunability as a synthetic polymer, it has to be modified for cell culture applications because of its bio-inertness. PEG hydrogels are highly hydrophilic and have high wettability, thus, have difficulty in protein absorption and in turn for cell adhesion and proliferation. Hence, PEG hydrogels require specific cell binding motifs usually done by functionalizing with peptides or combining with other natural polymers to provide biochemical cell instructive property for cell receptor mediated cell adhesion or electrostatic charge based protein adsorption to facilitate cell attachment and proliferation (Guarino et al. 2010; Jin et al. 2010; Cushing et al. 2007).

In this study, S-IPNs comprising CM-PA and poly(ethylene glycol) diacrylate (PEGDA) is fabricated. PEGDA being non-adhesive polymer only imparts the mechanical cue for the scaffold and CM-PA is provides the biochemical cue as collagen mimetic. The whole system is formed as a self-assembling photo-cross linked system as shown in figure 5.1, thus, has in-situ gelling capability (Sawhney et al. 1993; Gobin et al. 2002; Mahn et al. 2002; Shoichet et al. 2010; Gaharwar et al. 2011). Subsequently, the prepared S-IPNs were characterized for their internal morphology using scanning electron microscope in cryo mode. The blending of the two polymers was confirmed using Fourier Transform – Infra-red Spectroscopy. Further, stability was tested using Bradford protein quantification assay. Then, swelling and mechanical properties were characterized for the formed S-IPNs. Finally, the hydrogels were employed to study the effect of fibroblast growth in particular to morphology and proliferation.

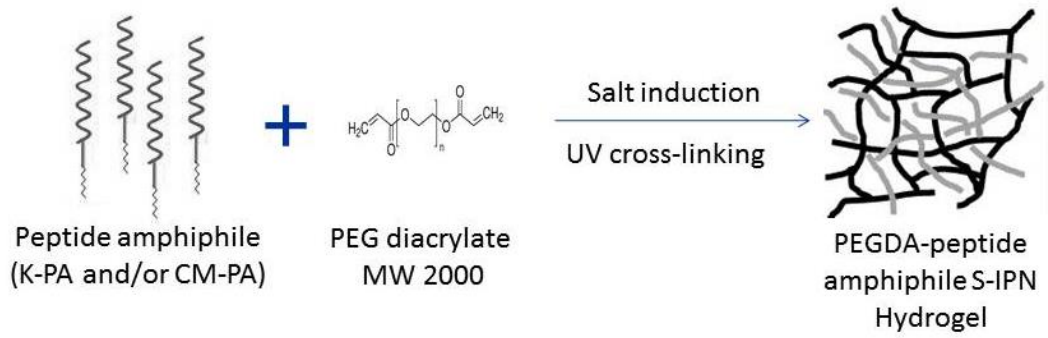

Figure 5.1: Schematic diagram of fabrication of semi-interpenetrating networks (S-IPNs) of PA (CM-PA and/or K-PA) and poly(ethylene glycol) diacrylate (PEGDA). PA-PEGDA S-IPN hydrogels are synthesized by salt induction to for PA nanofiber hydrogel followed by photo crosslinking of PEGDA with 365 nm UV at 10-15 mW/cm^2 for 120 seconds.

5.2. Results and discussion

5.2.1. Design and synthesis of peptide amphiphiles

Collagen mimetic (CM-PA) and cross-linking spacer (K-PA) PAs were designed and synthesized based on Luo et al from biopeptek inc. (Malvern, Pennsylvania, United States). The molecular weight determined using electrospray ionization mass spectrophotometer (ESI MS) for each sequence obtained was consistent with that of the desired calculated value. In addition, the purity of the synthesized PA was determined using HPLC and was >95%. The data of the molecular weight and the purity was supplied by the manufacturer. Table 5.1 tabulates the molecular sequences and the molecular weights of the PAs employed in this study.

Table 5.1: List of peptide amphiphile design sequence along with its label and molecular weight.

Label	Sequence*	Molecular Weight
CM-PA	C_{16}-AAAAAKKKKG$(GPO)_3$**GFOGER**$(GPO)_3$G	3502.2
K-PA	C_{16}-AAAAAKKKKGGK	1367.1

* C_{16} stands for palmitic acid modification in the N-terminal of the peptide. Standard one-letter amino acid code listed in Appendix B is used to express the sequences of the peptide.

5.2.2. Fabrication of semi-interpenetrating network hydrogels

S-IPNs of CM-PA with PEGDA (CM-PA-PEGDA) are fabricated along with two control S-IPNs with K-PA (K-PA-PEGDA) and mixed PA of CM-PA and K-PA (construct with equi-molar ratios of K-PA and CM-PA). In addition, PEGDA hydrogel without PA is fabricated as control. The final composition of the construct is 10% by weight of PEGDA and 7.5 molar concentration of PA. The

self-assembly of PA is initiated with salt induction before the photo crosslinking of PEGDA with 365 nm UV at 10-15 mW/cm^2 for 120 seconds. Table 5.2 lists the composition of the PA-PEGDA S-IPN hydrogel constructs.

Table 5.2: Composition of semi-interpenetrating networks (S-IPNs) of PA (CM-PA and/or K-PA) and poly(ethylene glycol) diacrylate (PEGDA).

Construct	PA Sequence* (1 wt. %)
PEGDA	-
CM-PA-PEGDA	C_{16}-AAAAAKKKKG$(GPO)_3$**GFOGER**$(GPO)_3$G
K-PA-PEGDA	C_{16}-AAAAAKKKKGGK
K-CM-PA-PEGDA	C_{16}-AAAAAKKKKG$(GPO)_3$ **GFOGER**$(GPO)_3$G C_{16}-AAAAAKKKKGGK

* C_{16} stands for palmitic acid modification in the N-terminal of the peptide. Standard one-letter amino acid code listed in Appendix B is used to express the sequences of the peptide.

5.2.3. Morphological characterization – Scanning Electron Microscope

Scanning electron microscope in cryo mode is used to visualize the internal morphology of the swollen S-IPN constructs. S-IPNs with PA show the presence of nanofibers as indicated by white arrows in figure 5.2. B, C and D. Image J software is used to analyze the pore size as listed in table 5.3. From the analysis it is observed that PEGDA hydrogel has significantly smallest pore size in comparison to S-IPNs: CM-PA-PEGDA, K-PA-PEGDA and K-CM-PA-PEGDA. The relatively higher pore size of S-IPNs relative to control PEGDA is due to presence of hydrophilic PA in addition to hydrophilic PEG. Higher hydrophilicity prevents cell adhesion and eventually, cell proliferation. Hence, for favorable cell

behavior S-IPNs must possess cell binding sequences (Guarino et al. 2010; Jin et al. 2010; Cushing et al. 2007). In addition, K-PA-PEGDA has significantly higher pore size, this could be because of the formation of long nanofibers by K-PA which could hinder the polymerization of PEGDA upon UV cross-linking.

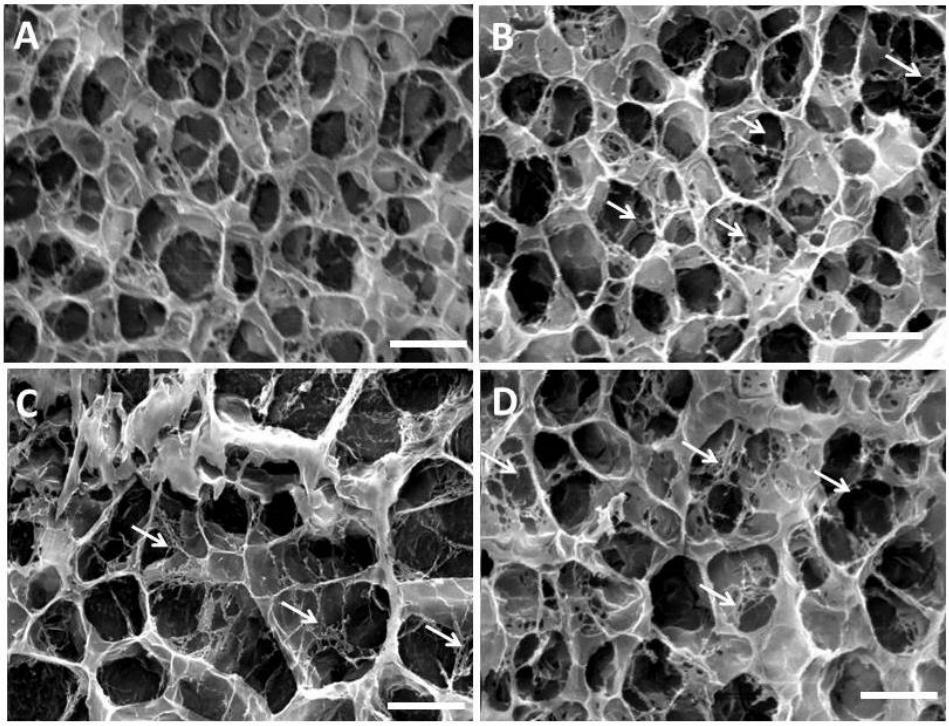

Figure 5.2: Cryo SEM images of semi-interpenetrating networks (S-IPNs) of PA (CM-PA and/or K-PA) and poly(ethylene glycol) diacrylate (PEGDA) (A) PEGDA, (B) CM-PA-PEGDA, (C) K-PA-PEGDA and (D) K-CM-PA-PEGDA in swollen state. PA nanofibers are indicated by white arrows (scale: Images A, B, D - 1µm and Image C -2 µm).

Pore diameter is smaller than the optimal pore diameter for fibroblast i.e. 5-15 microns (Annabi et al. 2010). This pore size can be achieved with higher molecular weight of PEG. However, in this we used smaller molecular weight PEG i.e. 2000 Da to form small pores so as to contain the CM-PA nanofibers within the PEGDA gel. However this pore size is sufficient for cell migration because it is filled with the softer PA hydrogels.

Table 5.3: Pore diameter of semi-interpenetrating network (S-IPNs) hydrogels of PA (CM-PA and/or K-PA) and poly(ethylene glycol) diacrylate (PEGDA) in swollen state.

Construct	Pore Diameter (μm)
PEGDA	0.69±0.15
CM-PA-PEGDA	1.25±0.23
K-PA-PEGDA	1.91±0.53
K-CM-PA-PEGDA	0.83±0.23

5.2.4. Blending test - Fourier Transform – Infra-red Spectroscopy

Blending test using Fourier Transform – Infra-red Spectroscopy (FTIR) confirms the blending in S-IPNs: CM-PA-PEGDA, K-PA-PEGDA and K-CM-PA-PEGDA by the presence of individual polymer i.e. peptide and PEGDA components. The FTIR spectrum of pure PA (Figure 5.3: CM-PA – navy blue line and K-PA – green line) and PEGDA (Figure 5.3: black line) were collected. The signature peaks of both PA are at 1,655 and 1,540 cm^{-1}, which corresponds to the vibrations of amide (-CO-NH) I and II bands, respectively (Zhu et al. 2009). The signature peaks of PEGDA are at 1,098, 1,342 and 1,726 cm^{-1}, which correspond to -C-O-symmetric stretching, -C-H_2 bending and -C=O stretching from ester bonds, respectively (Zhu et al. 2009). The FTIR spectra of S-IPNs: CM-PA-PEGDA (Figure 5.3: magenta line), K-PA-PEGDA (Figure 5.3: blue line) and K-CM-PA-PEGDA (Figure 5.3: red line) were collected to identify the signature peaks of the individual polymer. In all the three S-IPNs, signature peaks of both PA and PEG is observed confirming the formation of polymer blends.

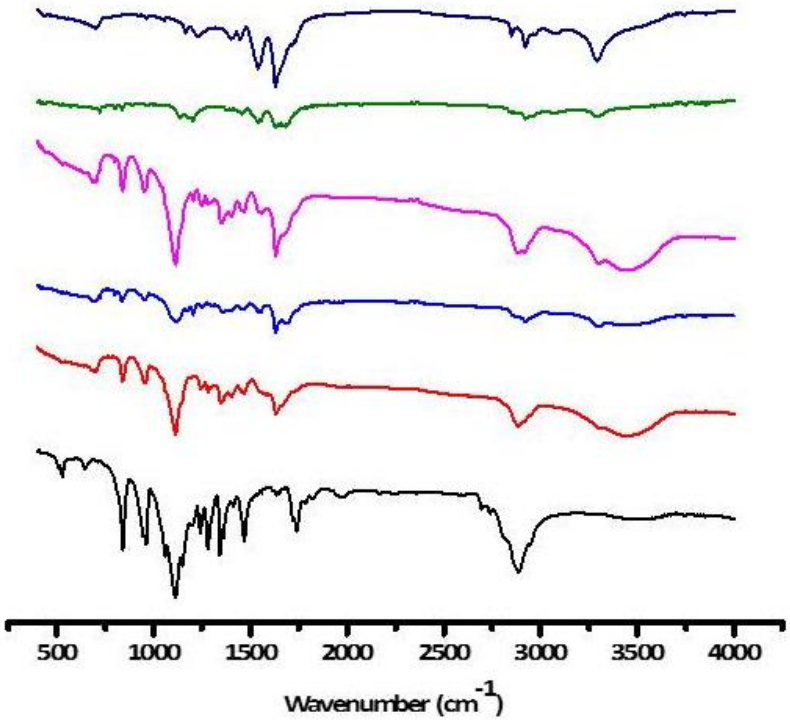

Figure 5.3: Fourier Transform – Infra-red (FTIR) spectrum of semi-interpenetrating networks (S-IPNs) of PA (CM-PA and/or K-PA) and poly(ethylene glycol) diacrylate (PEGDA): CM-PA – navy blue line; K-PA – green line; CM-PA-PEGDA - magenta line; K-PA-PEGDA - blue line; K-CM-PA-PEGDA - red line and PEGDA – black line. The signature peaks of both PA are at 1,655 and 1,540 cm^{-1} and PEGDA are at 1,098, 1,342 and 1,726 cm^{-1}. S-IPNs exhibit the signature peaks of both PA and PEGDA.

5.2.5. Stability testing - Bradford assay

The stability of the hydrogels in particular to the containment of PA nanofibers within PEG network was analyzed using Bradford assay. PEGDA hydrogel and S-IPNs: CM-PA-PEGDA, K-PA-PEGDA and K-CM-PA-PEGDA were incubated in de-ionized water and the amount of peptide leached in the de-ionized water is analyzed by using Bradford assay. The results as shown in figure 5.4 indicate that S-IPN CM-PA-PEGDA has significantly higher leaching of PA in comparison to PEGDA hydrogel and S-IPNs: K-PA-PEGDA and K-CM-PA-PEGDA constructs. The higher percentage of peptide leach from CM-PA-PEGDA can be attributed to

shorter nanofiber lengths formed by CM-PA (Chapter 4 - Figure 4.1) and significantly larger pore size which prevents to contain the nanofiber within the PEG network.

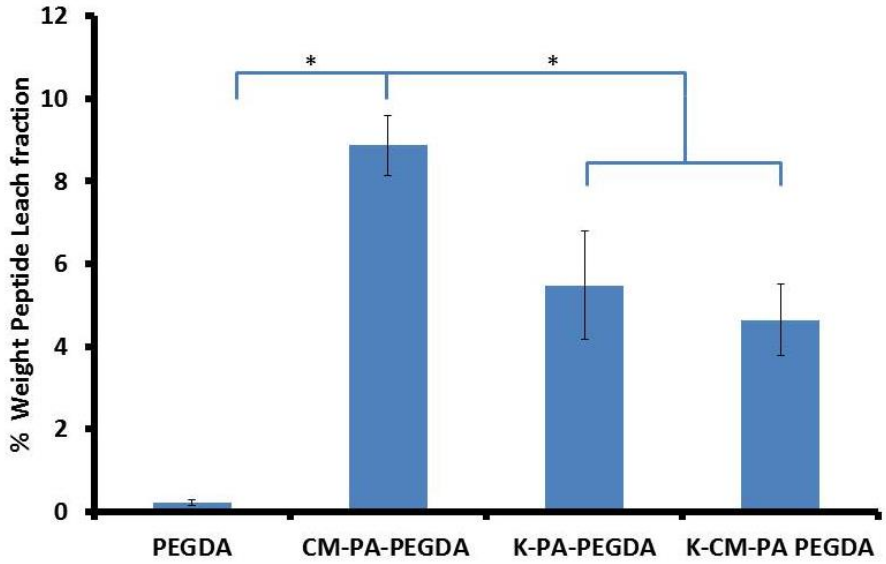

Figure 5.4: Peptide leach percentage determined by Bradford assay for various constructs of semi-interpenetrating network (S-IPNs) hydrogels of PA (CM-PA and/or K-PA) and poly(ethylene glycol) diacrylate (PEGDA) - PEGDA, CM-PA-PEGDA, K-PA-PEGDA and K-CM-PA-PEGDA in swollen state. *P<0.05 (Student's t-test).

5.2.6. Swelling Characteristics

Hydrogels are preferred scaffold design because of their high water content. The high water content of around 90% resembles that of native tissue. Table 5.4 shows the percentage equilibrium water content and percentage swelling degree of various S-IPN hydrogel constructs. All the constructs exhibit greater than 90% water content mimicking native tissue matrix. However, the hydrogel constructs show a trend in swelling characteristics, the increasing order of percentage equilibrium swelling degree is PEGDA, followed by K-CM-PA-PEGDA, then,

K-PA-PEGDA and finally, CM-PA-PEGDA. This indicates that PEGDA is significantly more rigid than CM-PA-PEGDA and K-PA-PEGDA. The increase in the swelling of the various S-IPN hydrogel constructs over PEGDA alone construct can be attributed to the presence of additional hydrophilic PA component.

Table 5.4: Percentage equilibrium water content and percentage swelling degree of semi-interpenetrating networks (S-IPNs) of PA (CM-PA and/or K-PA) and poly(ethylene glycol) diacrylate (PEGDA).

Construct	**% Equilibrium Water Content**	**% Equilibrium Swelling degree**
PEGDA	90.8 ± 0.4	992 ± 8.4
CM-PA PEGDA	93.0 ± 0.3	1326.3 ± 15.7
K-PA PEGDA	93.3 ± 0.2	1384.2 ± 10.8
K-CM-PA PEGDA	91.6 ± 0.3	1085.7 ± 6.4

5.2.7. Mechanical properties characterization

Mechanical properties of the constructs were analyzed using Instron compressive studies and results are depicted in figure 5.5 and table 5.5. In consistent with the findings from swelling characteristics (Section 5.2.6), PEGDA hydrogel has higher compressive modulus than S-IPNs: K-PA-PEGDA and CM-PA-PEGDA. However, all the constructs are significantly stiffer than that is required for L929 fibroblast cells to have the typical fibroblast spindle morphology i.e. greater than 1 KPa (Elter et al. 2010). Thus, all the constructs possess the required mechanical cue for fibroblast growth.

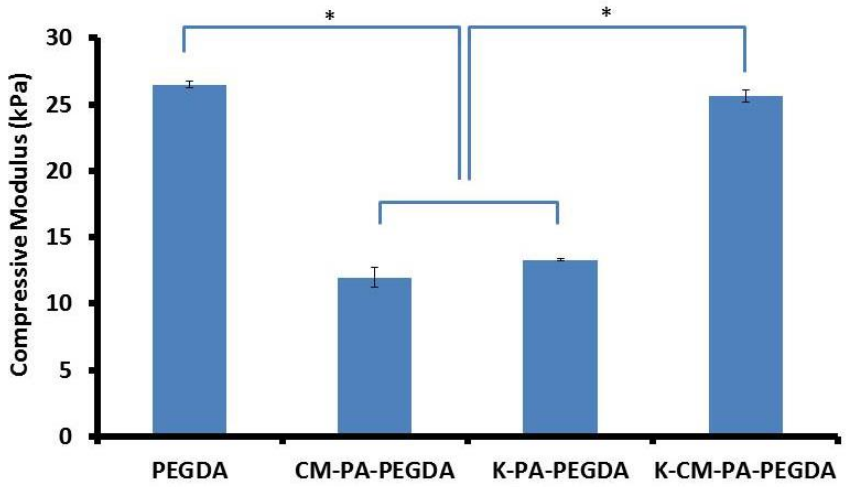

Figure 5.5: Column graphs showing compressive modulus of semi-interpenetrating networks (S-IPNs) of PA (CM-PA and/or K-PA) and poly(ethylene glycol) diacrylate (PEGDA) in swollen state. *P<0.05 (Student's t-test).

Table 5.5: Compressive modulus and breaking strengths of semi-interpenetrating networks (S-IPNs) of PA (CM-PA and/or K-PA) and poly(ethylene glycol) diacrylate (PEGDA) in swollen state.

Construct	Compressive Modulus (kPa)	Breaking Stress (kPa)
PEGDA	26.46± 0.25	2.11 x 10^2± 1.31
K-PA PEGDA	13.3± 0.12	1.85 x 10^2± 1.23
CM-PA PEGDA	11.96± 0.73	1.61 x 10^2± 2.64
K-CM-PA PEGDA	25.62± 0.45	2.03 x 10^2± 1..51

5.2.8. Fibroblast cell culture on semi-interpenetrating network hydrogels

L929 fibroblast cells were cultured on the surface of PEGDA hydrogel and S-IPNs: CM-PA-PEGDA, K-PA-PEGDA and K-CM-PA-PEGDA. The morphology of the fibroblast cells were studied under optical microscope as shown in figure 5.6. Fibroblast cells cultured on the surface of PEGDA hydrogel as control and S-IPNs showed similar trend as fibroblasts on 0.1% PA nanofiber coatings (Chapter 4 – Figure 4.8). Fibroblast cells on PEGDA hydrogel showed

rounded morphology on day 1 and remained in the same morphology until day 5. Fibroblasts on the CM-PA-PEGDA S-IPN exhibited rounded morphology on day 1 and further on day 5, exhibited a clumped colonies of mixed rounded and typical spindle shaped fibroblasts not visible on Day 1. S-IPNs: K-PA-PEGDA and K-CM-PA-PEGDA revealed typical fibroblast flat spindle shape morphology on day 1. However, on day 5, fibroblasts on K-CM-PA-PEGDA displayed clumped colonies of flat spindle shaped fibroblasts. The rounded morphology of fibroblast on CM-PA-PEGDA S-IPN can be attributed to lack of mechanical strength in the nanoscale architechture as cells sense mechanical signals at this level (Discher et al. 2005; Elter et al. 2011).

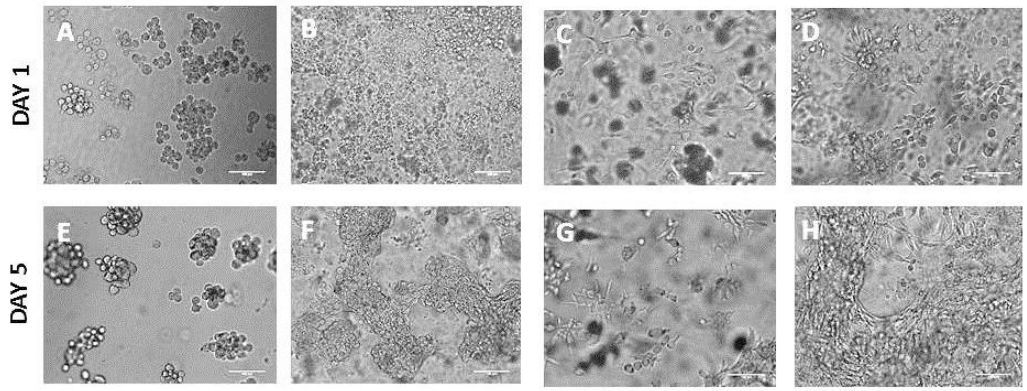

Figure 5.6: Optical light microscope images of fibroblasts on semi-interpenetrating networks (S-IPNs) of PA (CM-PA and/or K-PA) and poly(ethylene glycol) diacrylate (PEGDA): (A, E) PEGDA, (B, F) CM-PA-PEGDA, (C, G) K-PA-PEGDA and (D, H) K-CM-PA-PEGDA (construct with equi-molar ratios of K-PA and CM-PA) on Day1 and Day 5 respectively. The scale of the images is 100 microns.

The cell proliferation on the above constructs is quantified using MTT assay for Day 3 and Day 7 and plotted in the graph as shown in figure 5.7 and Student's t-test with 95% confidence level was used for the analysis of significance. Fibroblast cell proliferation is significantly higher in S-IPNs than PEGDA

hydrogel. This confirms that PEG scaffold alone cannot take part in cell adhesion and proliferation and requires the presence of cell instructive biochemical cues. The significantly high proliferation of fibroblasts in S-IPNs: CM-PA-PEGDA and K-CM-PA-PEGDA than K-PA-PEGDA can be attributed to the presence of collagen mimetic GFOGER epitope on the PA which induces the integrin based cell receptor signaling for cell adhesion and subsequent cell proliferation. Thus, in CM-PA-PEGDA enabling the synthesis of own ECM matrix ,thus, aiding in cell stretching on day 5. The mixed peptide amphiphile nanofiber S-IPN, K-CM-PA-PEGDA exhibits intermediate behaviour of both individual peptide amphiphile S-IPNs. Thus, K-CM-PA-PEGDA offers the appropriate biochemical cue for cell adhesion and proliferation, however, the construct shows clumped cell colonies which is similar to fibroblasts growth in fibrosis. The formation of fibrosis is attributed to high mechanical strength of the matrix (Karamichos et al. 2007; Liu et al. 2010).

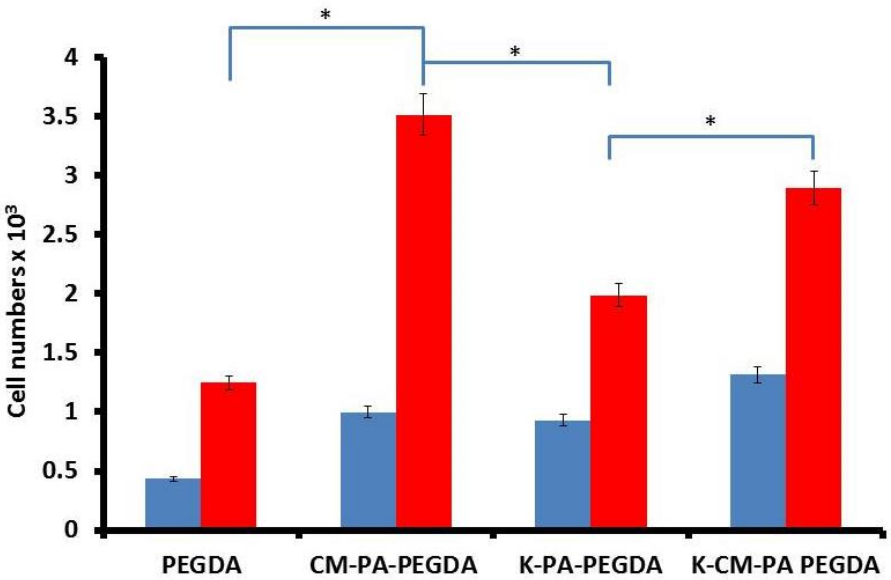

Figure 5.7: Cell proliferation assay of fibroblasts on semi-interpenetrating networks (S-IPNs) of PA (CM-PA and/or K-PA) and poly(ethylene glycol) diacrylate (PEGDA) on Day3 (blue columns) and Day 7 (red columns). *P<0.05 (Student's t-test).

5.2.9. Immunofluorescence staining for cell adhesion and spreading

Immunofluorescence staining was used to observe the cell adhesion and spreading of fibroblast cells on CM-PA-PEGDA and K-CM-PA-PEGDA S-IPN hydrogels. Figure 5.8, re-emphasizes the morphology of fibroblast as rounded clumped morphology on CM-PA-PEGDA S-IPN hydrogel (figure 5.8 A) and typical fibroblast flat spindle shape morphology on K-CM-PA-PEGDA hydrogel (figure 5.8 B). In addition, figure 5.8A shows the lack of stretching in the actin filament stained with phalloidin-TRITC (pink colour) on CM-PA-PEGDA S-IPN, however, fibroblasts on K-CM-PA-PEGDA S-IPN (figure 5.7 B) are observed to possess stretching in the actin filament indicating the sensing of mechanical tension by fibroblasts on this surface. The nucleus is stained using Hoechst (blue colour).

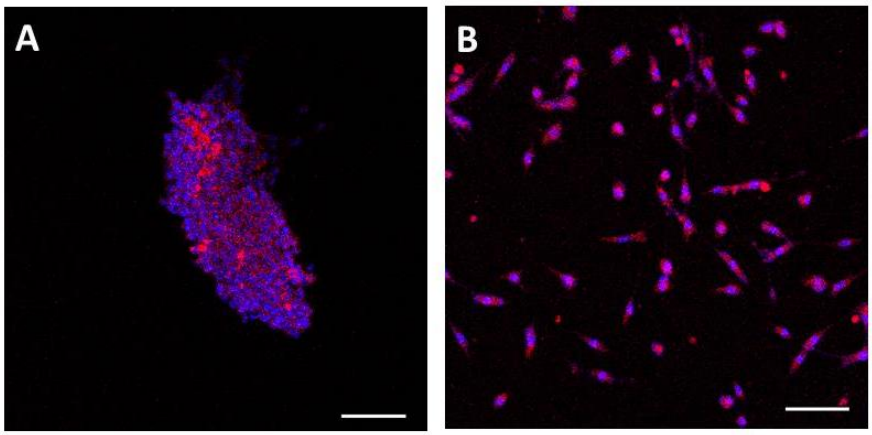

Figure 5.8: Confocal image of fibroblast on Day 2 of of fibroblasts on semi-interpenetrating networks (S-IPNs) of PA (CM-PA and/or K-PA) and poly (ethylene glycol) diacrylate (PEGDA): (A) CM-PA-PEGDA and (B) K-CM-PA-PEGDA. Actin filaments of the cells are stained with phalloidin-TRITC (pink colour) and nucleus is stained using Hoechst. The scale of the images is 100 microns.

5.3. Conclusion

Semi-interpenetrating network hydrogels of collagen mimetic peptide amphiphile and poly(ethylene glycol) diacrylate are excellent scaffold design to study the effect of the cell instructive sequence carried by the collagen mimetic peptide amphiphile as they are able to de-couple mechanical and biochemical cues. Thus, from the results of fibroblast culture with and without collagen mimetic peptide amphiphile sequences, it is clear that the cell instructive collagen sequence, GFOGER, is essential for cell adhesion and subsequent, proliferation of the fibroblast cells. However, presence of cell instructive collagen sequence alone doesn't ensure favourable fibroblast cell growth. Semi-interpenetrating network hydrogel scaffolds highlight that appropriate tissue specific mechanical properties along with cell instructive cue are required for favourable cell culture. In addition, the scaffold design also reveals the importance of mechanical cue in nanoscale level to be favorable for fibroblast cells than microscale level.

CHAPTER 6

CHEMICAL CROSS-LINKED HYDROGELS

This chapter describes the strategy of chemical cross-linked collagen mimetic peptide amphiphile nanofiber hydrogels to study the effect of varying mechanical cues on the fibroblast cell morphology and proliferation.

The work in this chapter addresses research objective 2 described in chapter 1.

6.1. Introduction

In nature, from biomechanical view point, fibrillar collagen in particular collagen type I is of prime importance. Collagen type is the most abundance ECM protein found in skin, tendon, lung, bone, cornea and the vasculature. *In vivo*, collagen type I is initially synthesized as soluble precursor molecules, called procollagen (Myllyharju, 2005). Then, procollagen is processed with the help of enzymes to assemble into collagen fibrils during transport inside the cell organelles and at the plasma membrane before being secreted out of the cells. Further, extracellularly, the final step of collagen biosynthesis, i.e. supramolecular assembly of collagen fibrils to form collagen fiber by introducing covalent cross-links, takes place. In fibrillar collagen, covalent cross-linking is carried out by lysyl oxidase enzyme family (Lucero et al. 2006; Molnar et al. 2003) and tissue transglutaminase enzyme (Verderio et al. 2005). Lysyl oxidase converts lysines or hydroxylysines residues in the N- and C-terminal end regions to corresponding peptidyl aldehydes. Spontaneously, upon formation, these aldehydes condense with each other or with unreacted lysines and hydroxylysines to form a variety of intra- and intermolecular covalent cross-links (Kuhn. 1987). Tissue transglutaminase enzyme forms covalent cross-links between the γ-carboxyamide group of specific peptidyl glutamine residues and ε-amino group of peptidyl lysines (Grenard et al., 2001). Hence, these covalent cross-links aid in the formation of collagen fibril bundle, i.e. collagen fiber.

In this study, we have mimicked the *in vivo* collagen fiber formation by covalent

cross-links with enzymes using a chemical cross-linker, glutaraldehyde. The chemical cross-linker, glutaraldehyde creates covalent cross-links in CM-PA and K-PA mixed hydrogels to enhance mechanical properties of the hydrogels. Glutaraldehyde is a linear di-aldehyde with 5-carbon atoms. Glutaraldehyde is a clear water soluble cross-linker used extensively to cross-link collagen to obtain collagen-based scaffolds with enhanced mechanical and enzymatic resistance. In literature, collagen cross-linking with glutaraldehyde indicated maximum reactivity in comparison to other mono- and di-aldehydes and the formed cross-links are thermally and chemically stable (Migneault et al. 2004). Glutaraldehyde can react with amine, thiol, phenol, and imidazole functional groups of amino acids, but, usually cross-linking of protein with glutaraldehyde implies the ε-amino group of lysine amino acid (Olde Damink et al. 1995). However, the reaction mechanism of glutaraldehyde cross-linking with amino groups of peptide or protein is not yet clearly understood.

In brief, glutaraldehyde cross-linked collagen mimetic peptide amphiphile nanofiber hydrogels were fabricated as shown in figure 6.1. Subsequently, the prepared hydrogels were characterized for their internal morphology using transmission electron microscope. Further, mechanical properties were characterized for the formed cross-linked collagen mimetic peptide amphiphile nanofiber hydrogels using Instron. Finally, the hydrogels were employed to study the effect of fibroblast growth in particular to morphology and proliferation.

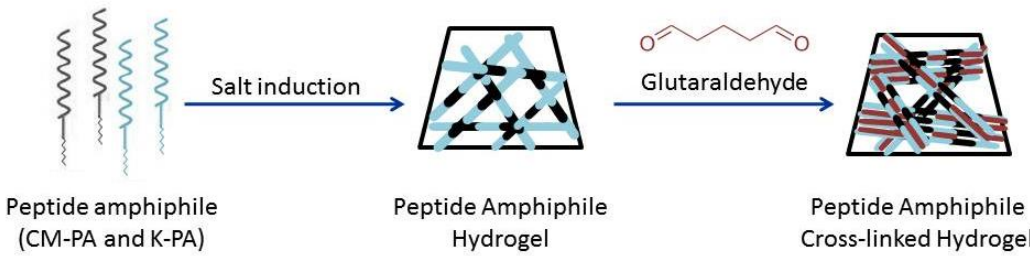

Figure 6.1: Schematic diagram of fabrication of covalently cross-linked hydrogels of mixed PAs i.e. 10 % of CM-PA and 90% of K-PA using chemical cross-linker, glutaraldehyde. PA hydrogels are synthesized by salt induction followed by cross-linking using glutaraldehyde.

6.2. Results and Discussions

6.2.1. Design and synthesis of peptide amphiphiles

Collagen mimetic (CM-PA) and cross-linking spacer (K-PA) PAs were designed and synthesized based on Luo et al from biopeptek inc. (Malvern, Pennsylvania, United States). The molecular weight determined using electrospray ionization mass spectrophotometer (ESI MS) for each sequence obtained was consistent with that of the desired calculated value. In addition, the purity of the synthesized PA was determined using HPLC and was >95%. The data of the molecular weight and the purity was supplied by the manufacturer. Table 6.1 tabulates the molecular sequences and the molecular weights of the PAs employed in this study.

Table 6.1: List of peptide amphiphile design sequence along with its label and molecular weight.

Label	Sequence*	Molecular Weight
CM-PA	C_{16}-AAAAAKKKKG$(GPO)_3$**GFOGER**$(GPO)_3$G	3502.2
K-PA	C_{16}-AAAAAKKKKGG**K**	1367.1

* C_{16} stands for palmitic acid modification in the N-terminal of the peptide. Standard one-letter amino acid code listed in Appendix B is used to express the sequences of the peptide.

6.2.2. Fabrication of cross-linked hydrogels

Cross-linked CM-PA hydrogels are fabricated along with a control of uncross-linked CM-PA hydrogel. K-PA is used as the spacer and cross-linking PA. The lysine in the N-terminal of the K-PA provides the amino group (-NH_2) for glutaraldehyde cross-linking. The final peptide amphiphile composition of the construct is 10% of CM-PA and 90% of K-PA of the total PA concentration. Table 6.2 lists the composition of the glutaraldehyde cross-linked CM-PA hydrogel constructs. The self-assembly of PA is initiated with salt induction before the chemical cross-linking with appropriate concentration of glutaraldehyde. The formed hydrogels are soaked in 1% w/v glycine solution to quench any reactive aldehyde groups to prevent cyto-toxicity to fibroblast cells.

Table 6.2: Composition of glutaraldehyde cross-linked CM-PA hydrogel constructs.

Construct	**Peptide Amphiphile Concentration (mM)**		**Glutaraldehyde Concentration (mM)**
	CM-PA	**K-PA**	
1 PA : 0 Glt	0.55	5	0
1 PA : 0.5 Glt	0.55	5	2.5
1 PA : 1 Glt	0.55	5	5

6.2.3. Morphological characterization – Transmission Electron Microscopy

TEM images of figure 6.2 show the morphology of nanofibers cross-linked with glutaraldehyde after salt induced self-assembly of mixed CM-PA and K-PA PAs along with uncross-linked control. The cross-linked constructs with half molar glutaraldehyde concentration with respect to K-PA (1 PA : 0.5 Glt) and equi-molar glutaraldehyde concentration with respect to K-PA (1 PA : 1 Glt) as shown in

figure 6.2 B and C respectively depict the formation of nanofiber bundles. These nanofiber bundles are not seen in the uncross-linked control, figure 6.2. A.

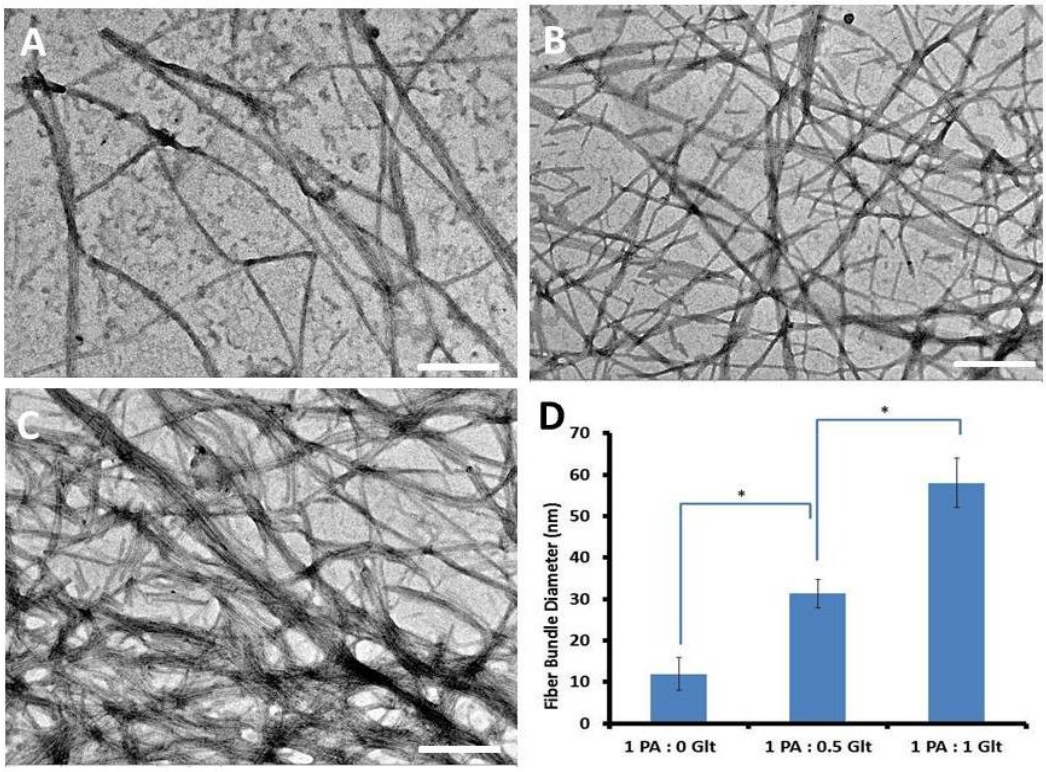

Figure 6.2: TEM micrographs of (A) uncross-linked CM-PA hydrogel and glutaraldehyde cross-linked CM-PA hydrogel constructs (B) 1 PA : 0.5 Glt (cross-linked with half molar glutaraldehyde concentration with respect to K-PA) and (C) 1 PA : 1 Glt (cross-linked with equi-molar glutaraldehyde concentration with respect to K-PA). Images show that the diameter of the fiber bundle increased with the increase in the concentration of glutaraldehyde. (D) Diameter of the fiber bundle of each construct measured using ImageJ software. Scale of the images is 500 nm. *P<0.05 (Student's t-test).

The nanofiber bundles are formed with the cross-linked constructs because of the glutaraldehyde cross-linking of the ε-amino groups of the lysine amino acid present on the surface of the K-PA after the nanofiber self-assembly. The lysine amino acid exposed on the surface of the nanofiber in addition to forming inter-nanofiber cross-linking may also form intra-nanofiber cross-links, thus, stabilizing the nanofiber. It is observed that greater the concentration of

glutaraldehyde greater is the diameters of the fiber bundle as shown in figure 6.2 D. The fiber bundle diameter with equi-molar concentration of glutaraldehyde is significantly bigger than that of half-molar concentration of glutaraldehyde i.e. around two times.

6.2.4. Mechanical properties characterization

Mechanical properties of the glutaraldehyde cross-linked CM-PA hydrogel constructs were analyzed using Instron compressive studies as mentioned in section 3.3.9. Uncross-linked CM-PA hydrogel didn't form a self-standing uniform dimensional hydrogel, hence, its mechanical properties couldn't be tested using Instron compressive testing. Figure. 6.3 shows the compressive modulus of the various glutaraldehyde cross-linked CM-PA hydrogel constructs.

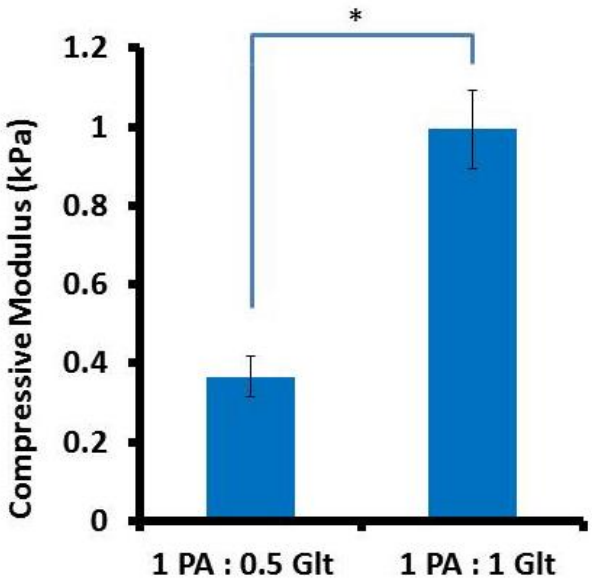

Figure 6.3: Column graph showing compressive modulus of 1 PA : 0.5 Glt (cross-linked with half molar glutaraldehyde concentration with respect to K-PA) and 1 PA : 1 Glt (cross-linked with equi-molar glutaraldehyde concentration with respect to K-PA) hydrogel constructs. *P<0.05 (Student's t-test).

In addition, table 6.3 shows the breaking of the various glutaraldehyde

cross-linked CM-PA hydrogel constructs. Hydrogel cross-linked with equi-molar glutaraldehyde concentration with respect to K-PA (1 PA : 1 Glt) has significantly higher compressive modulus of around two and half times than hydrogel cross-linked with half molar glutaraldehyde concentration with respect to K-PA (1 PA : 0.5 Glt). In addition, only the construct cross-linked with equi-molar glutaraldehyde concentration with respect to K-PA (1 PA : 1 Glt) has compressive modulus favorable for L929 fibroblast cells to have the typical fibroblast spindle morphology i.e. greater than 1 KPa (Elter et al. 2010).

Table 6.3: Breaking strengths of of 1 PA : 0.5 Glt (cross-linked with half molar glutaraldehyde concentration with respect to K-PA) and 1 PA : 1 Glt (cross-linked with equi-molar glutaraldehyde concentration with respect to K-PA) hydrogel constructs.

Constructs (PA : Glt) (Molar Ratio)	**Compressive Modulus (kPa)**	**Breaking Strength (kPa)**
1:0	-	-
1:0.5	0.36 ± 0.05	0.36 ± 0.15
1:1	0.99 ± 0.11	1.91 ± 0.21

6.2.5. Fibroblast cell culture on chemical cross-linked PA hydrogels

L929 fibroblast cells were cultured on the surface of cross-linked and uncross-linked hydrogels. The morphology of the fibroblast cells were studied under optical microscope as shown in figure 6.4. Fibroblast cells on the uncross-linked hydrogel showed clumped rounded morphology on Day 3, figure 6.4 A. However, fibroblast cells on 1 PA : 1 Glt (cross-linked with equi-molar glutaraldehyde concentration with respect to K-PA) exhibited typical spindle

shaped morphology on Day 3. Also, fibroblast cells on 1 PA : 0.5 Glt (cross-linked with half molar glutaraldehyde concentration with respect to K-PA) exhibited cells of both rounded and spindle shaped morphology. The rounded morphology of fibroblast on uncross-linked and 1 PA : 0.5 Glt hydrogel constructs can be attributed to lack of mechanical strength in the nanoscale architechture as cells sense mechanical signals at this level (Discher et al. 2005; Mason et al. 2012).

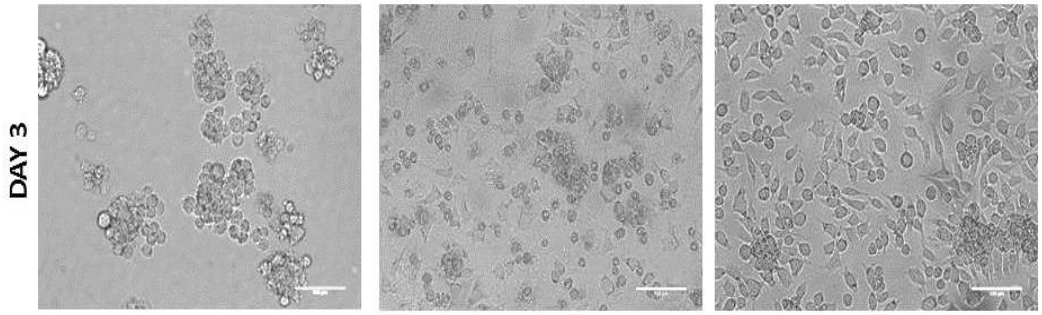

Figure 6.4: Optical images showing the morphology of L929 fibroblast cells cultured on (A) uncross-linked CM-PA hydrogel and glutaraldehyde cross-linked CM-PA hydrogel constructs (B) 1 PA : 0.5 Glt (cross-linked with half molar glutaraldehyde concentration with respect to K-PA) and (C) 1 PA : 1 Glt (cross-linked with equi-molar glutaraldehyde concentration with respect to K-PA) at Day 3. Scale on the images is 100 microns.

The fibroblast cell proliferation on the cross-linked and uncross-linked hydrogels is quantified using MTT assay for Day 3 and Day 7 and plotted in the graph as shown in figure 6.5 and Student's t-test with 95% confidence level was used for the analysis of significance. Fibroblast cell proliferation is significantly higher in cross-linked hydrogel constructs over uncross-linked hydrogel constructs on Day 7. This confirms that appropriate mechanical cue alone with cell instructive biomechanical cue is necessary for cell adhesion. In addition, the significantly

higher cell numbers in 1 PA : 1 Glt hydrogel construct over 1 PA : 0.5 Glt on Day 7 emphasizes that the mechanical cue of the scaffold should be tissue-specific i.e. exactly same mechanical properties as the *in vivo* tissue ECM.

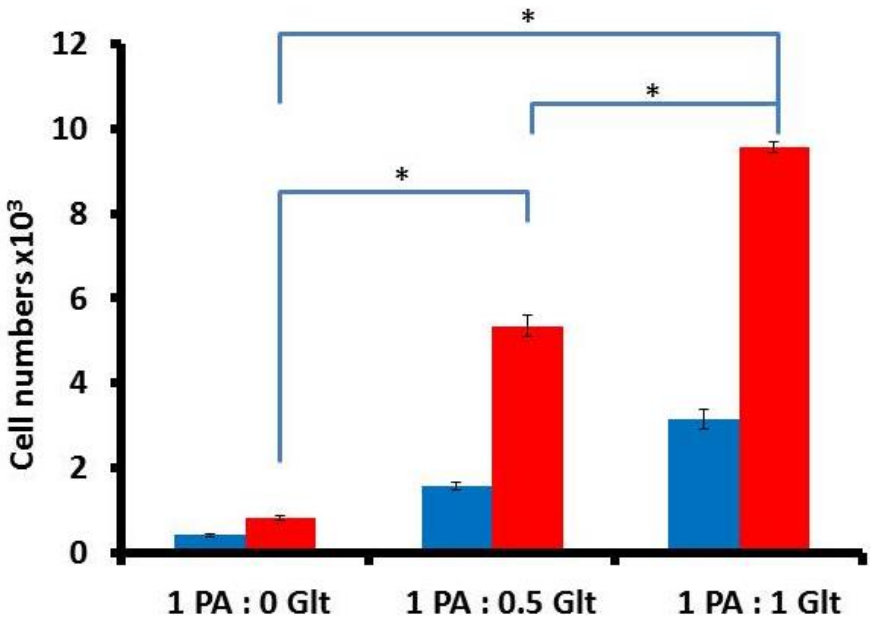

Figure 6.5: Column graph showing cell proliferation assay of fibroblasts on uncross-linked CM-PA hydrogel and glutaraldehyde cross-linked CM-PA hydrogel constructs - 1 PA : 0.5 Glt (cross-linked with half molar glutaraldehyde concentration with respect to K-PA) and 1 PA : 1 Glt (cross-linked with equi-molar glutaraldehyde concentration with respect to K-PA) at Day 3 (blue columns) and Day 7 (red columns). *P<0.05 (Student's t-test).

6.3. Conclusion

Chemical cross-linked collagen mimetic peptide amphiphile hydrogel scaffold design has the capability to present the fibroblast cells with both biochemical cue and mechanical cue at the nanoscale level. Both biochemical and mechanical cue components of the scaffold were de-coupled enabling to understand each cue individually. Biochemical cue is presented by the cell instructive sequence derived from collagen on the surface of nanofiber. The results from fibroblast culture emphasizes the importance of the cell instructive sequence for cell

adhesion and cell proliferation. The nanoscale mechanical cue was achieved by cross-linking the nanofibers to each other and forming fiber bundles. Fibroblast cultured on these scaffold with varying mechanical strength displayed varied morphology in terms of cell spreading. The results emphasize the essential and imperative role of mechanotransduction of the fibroblast cells in the nanoscale level for cell spreading. In brief, the *in vitro* drug testing tools mimic the *in vivo* tissue or disease as models using a biomaterial scaffold platform to grow cells, thus, in essence, chemical cross-linked collagen mimetic peptide amphiphile hydrogel scaffold design has the capability to be used as a scaffold for *in vitro* drug testing tool designs. In addition, it has the capability to be used as a implantable scaffold for biomedical applications, in particular to skin tissue engineering and regenerative medicine for wound healing applications.

CHAPTER 7

SEQUENCE MODIFIED HYDROGELS

This chapter describes the strategy of sequence modified collagen mimetic peptide amphiphile nanofiber hydrogels to study the effect of varying mechanical cues of CM-PA hydrogels on the fibroblast cell morphology and proliferation. The work in this chapter addresses research objective 3 described in chapter 1.

7.1. Introduction

Designing hydrogels with tissue specific mechanical and biochemical properties is extremely important for the success of tissue engineering and regenerative medicine. Time and again, several studies have emphasized that mechanical properties of the hydrogels control cellular behavior (Discher et al. 2005; Elter et al. 2011). Hence, over the years several strategies are employed to alter the mechanical properties of a hydrogel such as combining different materials with favorable mechanical properties and covalent cross-linking (Chan et al. 2012; Liang et al. 2011). Apart from the general strategies employed, mechanical properties of the peptide based hydrogels can be tuned by other methods such as phospholipid inclusions (Paramonov et al. 2006), chemical ligation (Jung et al. 2008), varying type of cross-linkers (Li et al. 2014; Seow et al. 2013), combination of peptides (Taraban et al. 2012) and changing the sequence of the peptides (Pashuck et al. 2010).

The strategy employed in this study is based on the versatile modular advantage of the PA design. From literature it is shown that the sequence of amino acids in the β-sheet forming region of the single tail PA can influence the mechanical strength of the nanofiber which in turn can modulate the mechanical strength of the hydrogel (Pashuck et al. 2010). This strategy was conceived by designing PAs differing in their β-sheet region with varying combinations of valine (V) and alanine (A) amino acids. Amino acid valine was chosen because of its highest propensity among natural amino acids to form β-sheet than any other secondary

structure and alanine was chosen as it is a weak β-sheet former and has propensity for formation of α-helices (Chou et al. 1974). Upon salt induced self-assembly, the hydrogels formed possessed varying gel stiffness. It was observed that the stiffer gels were formed with higher number of strong β-sheet forming amino acid, valine located close to the hydrophobic region of the PA (Pashuck et al. 2010).

In other studies, silk-mimetic approaches were employed to enhance the mechanical strength of the hydrogels (Sun et al. 2012; Guo et al. 2013). Silk from spider drag-line silk and cocoon silk from the silkworm Bombyx mori are increasingly being used as a natural biomaterial scaffold because of their exceptionally high mechanical strength with a modulus around 10 GPa and 11-13 GPa respectively (Altman et al. 2003; Cunniff et al. 1994). The strong mechanical strength is attributed to highly ordered β-sheet rich crystalline units. The β-sheets are formed by the repeat units of alanine or of alternating alanine and glycine amino acids for spider and Bombyx mori silk, respectively (Xiao et al. 2009). These repeats are usually six to nine amino acids in length (Takahashi et al. 1999). These β-sheet regions form highly ordered crystalline structure in the silk by cross-linking the protein chains in the silk fiber via hydrogen bonding. In addition, the uncrystalline regions interspersed between the crystalline region also contribute to the mechanical strength of the silk fibroin fiber (Gosline et al. 1999; Rousseau et al. 2007). Hence, to tap the immense potentiality of the silk fiber's mechanical strength, Guo et al. (2013) fabricated and characterized the robust pH sensitive single tail peptide amphiphile hydrogel based on silk fibroin with

alternating alanine and glycine amino acid sequence. It was observed that the hydrogels reached rheological moduli of around 10^5 Pa. In another popular self assemblying peptide hydrogel design i.e. RADA16-I, repeating units from the uncrystalline region of silk have been grafted to obtain hydrogels with enhanced mechanical strength (Sun et al. 2011). Also, in yet another study, the mechanical properties of short silk-mimetic single tail PA sequences with both crystalline and non-crystalline motifs was studied (Chen et al. unpublished). They observed that the rheological modulus of the single tail PA with alternating alanine and glycine amino acid repeat sequence in the β-sheet region was 50% higher than that of the single tail PA with alanine alone repeat sequence in the β-sheet region.

In this study, in brief, single tail CM-PAs with alternating alanine and glycine amino acid repeat sequence in the β-sheet region and alanine alone repeat sequence in the β-sheet region were synthesized. Along with CM-PA, spacer PAs were also synthesized. These PAs were self-assembled into nanofibers using salt induction. Then, the nanostructure and functionality of the self-assembled PA nanofibers were studied through various characterization methods. Transmission electron microscopy (TEM) was used to study the self-assembled PA nanofiber nanostructure. The secondary structure of CM-PAs was characterized using circular dichroism (CD) spectroscopy and melting curve studies. Subsequently, the PA nanofiber hydrogels were prepared and characterized for their mechanical properties using rheology. Finally, the hydrogels were employed to study the effect of fibroblast growth in particular to morphology and proliferation.

7.2. Results and Discussions

7.2.1. Design and synthesis of peptide amphiphiles

CM-PAs with alternating alanine and glycine amino acid (PGA-CM-PA) repeat sequence in the β-sheet region and alanine alone (PA-CM-PA) repeat sequence in the β-sheet region and spacer PAs (PGA-PA and PA-PA) were designed and synthesized based on Luo et al from biopeptek inc. (Malvern, Pennsylvania, United States). The molecular weight determined using electrospray ionization mass spectrophotometer (ESI MS) for each sequence obtained was consistent with that of the desired calculated value. In addition, the purity of the synthesized PA was determined using HPLC and was >95%. The molecular weight and purity data was supplied by the manufacturer. Table 7.1 tabulates the molecular sequences and the molecular weights of the synthesized PAs.

Table 7.1: List of peptide amphiphile design sequence along with its label and molecular weight.

Label	Sequence*	Molecular Weight
PGA-CM-PA	C_{16}-GAGAGAGKKKKG$(GPO)_3$GFOGER$(GPO)_3$G	3588.25
PGA-PA	C_{16}-GAGAGAGKKKK	1209.90
PA-CM-PA	C_{16}-AAAAAKKKKG$(GPO)_3$GFOGER$(GPO)_3$G	3501.25
PA-PA	C_{16}-AAAAAKKKK	1123.95

* C_{16} stands for palmitic acid modification in the N-terminal of the peptide. Standard one-letter amino acid code listed in Appendix B is used to express the sequences of the peptide.

7.2.2. Fabrication of collagen mimetic peptide amphiphile hydrogels

PGA hydrogel are fabricated by salt induced gelling of 10% of PGA-CM-PA and

90% of spacer PGA-PA in total concentration of the peptide. Similarly, PA hydrogel are fabricated by salt induced gelling of 10% of PA-CM-PA and 90% of spacer PA-PA in total concentration of the peptide. Table 7.2 tabulates the composition of the hydrogel constructs.

Table 7.2: Composition of self-assembled collagen mimetic peptide amphiphile hydrogel design sequences.

Construct	**Peptide Amphiphile**			
	Collagen-mimetic		Spacer	
	Composition	Concentration (mM)	Composition	Concentration (mM)
PGA	PGA-CM-PA	0.55	PGA-PA	4.95
PA	PA-CM-PA	0.55	PA-PA	4.95

7.2.3. Morphological characterization – Transmission Electron Microscopy

PA molecules spontaneously form micelles in aqueous solution and self-assemble to form nanofibers upon charge screening of the charge segment ((Luo et al. 2011; Hartgerink et al. 2001). TEM images of figure 7.1 A and B show the morphology of self-assembled PGA-CM-PA and PA-CM-PA nanofibers respectively after screening the positive charges of the lysine spacer using trisodium phosphate (Na_3PO_4) salt. The images confirm that screening the positive charges in the lysine spacer led to the formation of nanofibers. The diameter of the nanofiber was approximately around 15 nm which is consistent with the literature. The images also reveal marked differences in the length and morphology among PGA-CM-PA and PA-CM-PA construct. PGA-CM-PA forms very long nanofibers in relation to PA-CM-PA. However, it was difficult to quantify the size of the nanofibers owing to its polydisperse distribution. The marked difference in length of PGA-CM-PA and PA-CM-PA is attributed to strong β-sheet formation of

alternating alanine and glycine amino acid in PGA-CM-PA nanofibers which aids in fiber elongation.

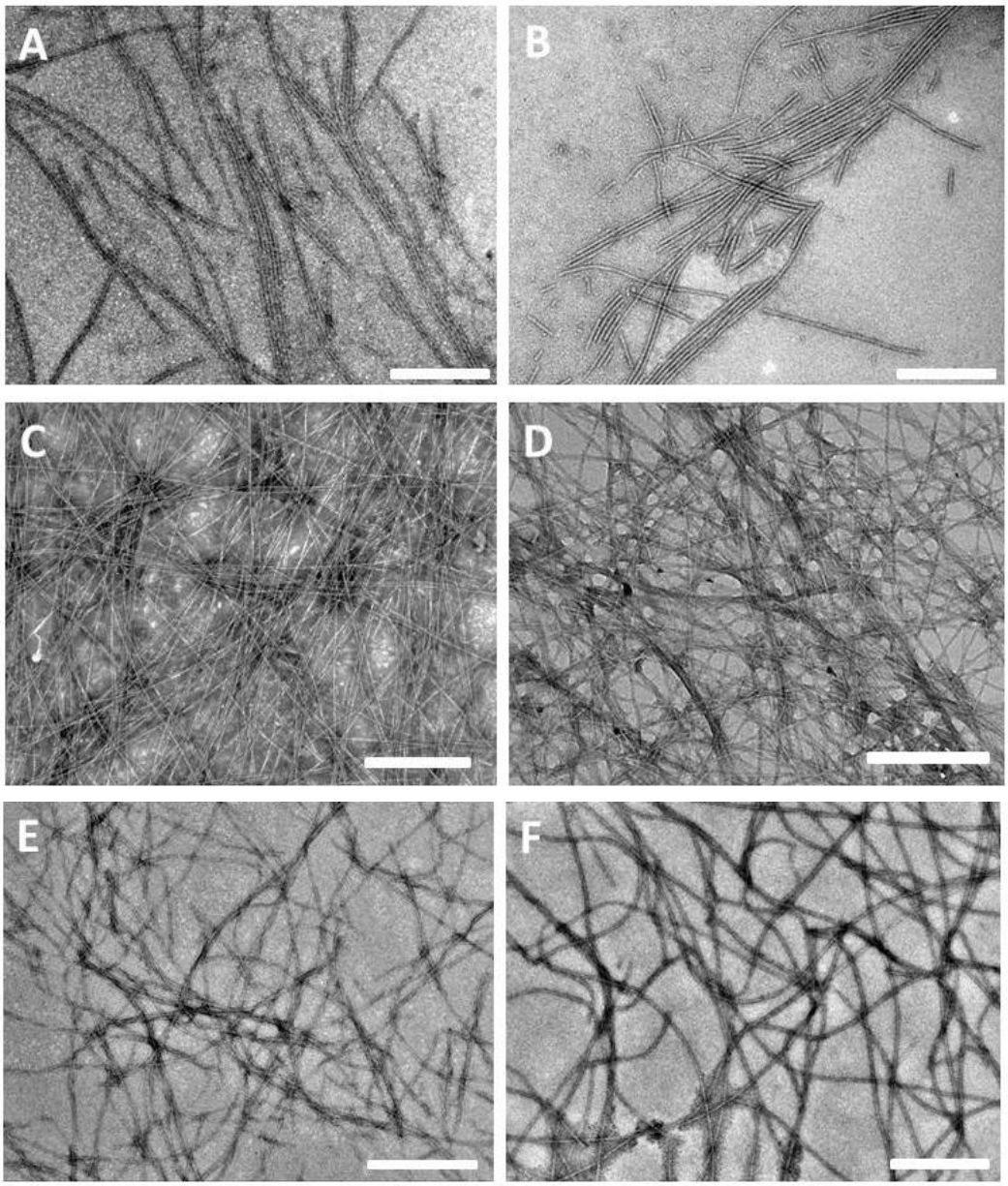

Figure 7.1:TEM micrographs of self-assembled PA nanofibers (A) PGA-CM-PA, (B) PA-CM-PA, (C) PGA-PA, (D) PA-PA, (E) PGA (construct with 10% of PGA-CM-PA and 90% of PGA-PA) and (F) PA (construct with 10% of PA-CM-PA and 90% of PA-PA) after charge screening. All the PA nanofibers are with the diameter of ~15 nm. However, they vary in their nanofiber lengths. Scale of the images is 500 nm.

TEM images of figure 7.1 C and D show the morphology of self-assembled PGA-PA and PA-PA nanofibers respectively after salt induced charge screening.

Both the sequence of PA owing to relatively shorter peptide length than CM-PA form long nanofibers. The diameter of the nanofiber was approximately around 10 nm which is consistent with the literature. There isn't any significant difference in the morphology of the PGA-PA and PA-PA nanofibers.

TEM images of figure 7.1 E and F show the morphology of self-assembled PGA (construct with 10 % PGA-CM-PA and 90 % PGA-PA) and PA (construct with 10 % PGA-CM-PA and 90 % PGA-PA) nanofibers respectively after screening the positive charges of the lysine spacer using salt. The diameter of the nanofiber was approximately around 10 nm which is consistent with the literature. In comparison to the both CM-PAs, mixed PA constructs formed nanofibers of longer length; this difference is due to the presence of spacer PA in the mixed PAs that aids in fiber elongation. Also, in comparison to both spacer PAs, the mixed PAs formed less dense nanofiber networks; this difference is attributed to the presence of CM-PA component in the mixed PAs that interferes with formation of nanofibers.

7.2.4. Circular dichroism spectroscopy

Secondary structure of CM-PAs and spacer PAs was analyzed using circular dichroism spectroscopy (CD). Structurally, CM-PAs (PGA-CM-PA and PA-CM-PA) and spacer PAs (PGA and PA) form markedly different secondary structure. The CM-PAs similar to collagen exhibits a typical triple-helix tertiary structure. The signature peaks for typical collagen triple-helix is a large negative

peak at approximately 197 nm, crossover near 213 nm and a small positive peak at 220-225 nm (Lesley et al. 2011). Thus, the formation of collagen mimetic nanofiber is confirmed by the presence of characteristic triple-helix peaks. The CD spectrum of PGA-CM-PA and PA-CM-PA is shown in figure 7.2 as red and blue line respectively.

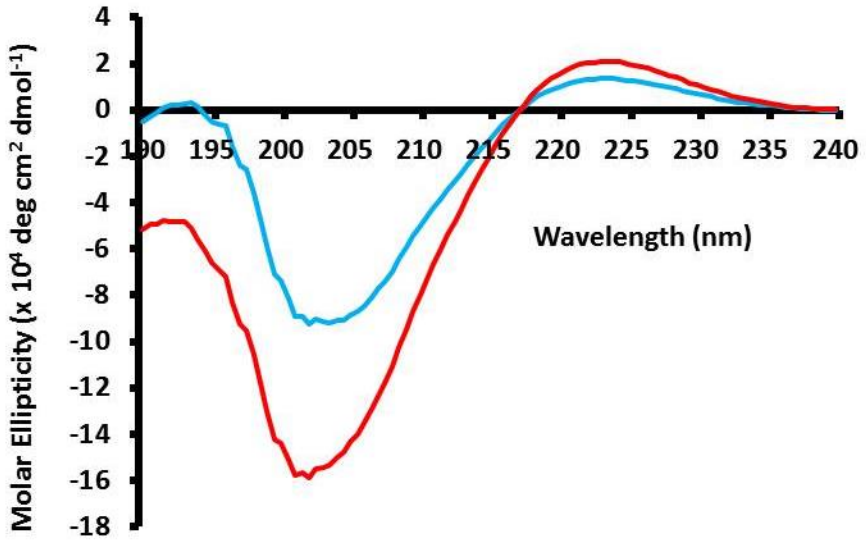

Figure 7.2: CD spectra of CM-PAs: PGA-CM-PA (red line) and PA-CM-PA (blue line) nanofiber in aqueous solution after charge screening showing the characteristic CD peaks of collagen triple helix i.e. a positive peak around 223 nm, crossover around 216 nm and negative peak around 203 nm.

From the spectrum, it is confirmed that the both CM-PAs nanofibers exhibit a typical collagen triple-helix conformation. CM-PA spectrum shows a positive peak around 223 nm, crossover around 216 nm and negative peak around 200 nm. In addition, both CM-PAs display a red shift in band positions with respect to the typical CD spectral band positions of collagen, probably due to the difference in amino acid content (Rippon et al. 1971). This conclusion is consistent with that of the literature. The increase in dichroic intensity in PGA-CM-PA construct than PA-CM-PA construct could be due to the increase of hydrogen bond cross-links

between alternating alanine and glycine amino acid in the β-sheet region of PGA-CM-PA (Xiao et al. 2009).

However, the spacer PAs upon trigger of charge screening using high ionic strength self-assemble to form β-sheeted nanofiber. Thus, the formation of nanofiber is confirmed by the presence of characteristic β-sheet peaks. The characteristic β-sheet peaks are negative peak at 215 nm and positive peak at 195 nm in the CD spectrum (Hartgerink et al. 2001). The CD spectrum of PGA-PA and PA-PA is shown in figure 7.3 as red and blue line respectively.

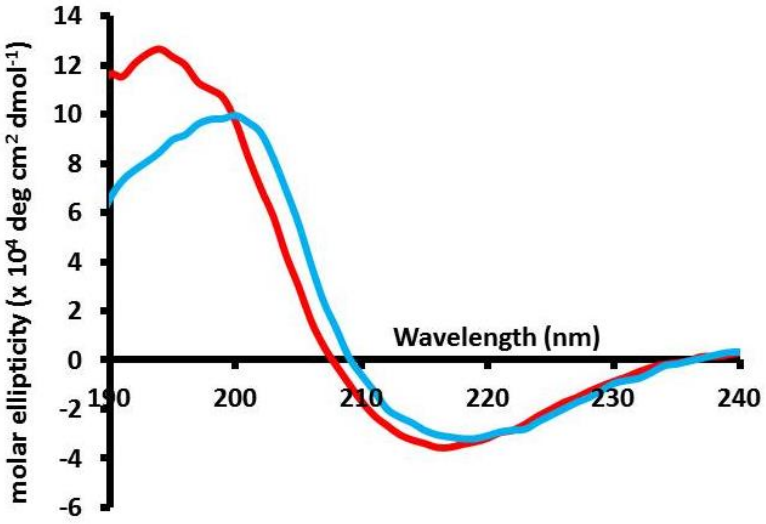

Figure 7.3: CD spectra of spacer PAs: PGA-PA (red line) and PA-PA (blue line) nanofiber in aqueous solution (blue line) showing a relatively small negative peak at 219 nm and a dominant positive peak at 203 nm that is typical of β-sheet conformation.

From the spectrum, it is confirmed that the both spacer PA nanofibers are formed due to β-sheet formation. PGA-PA nanofiber represented by red line shows a relatively small negative peak at 216 nm and a dominant positive peak at 194 nm. The red shift of the CD signals from the signature β-sheet signal is calculated as 0.

In addition, PA-PA nanofiber represented by blue line shows a relatively small negative peak at 218 nm and a dominant positive peak at 200 nm. The red shift of the CD signals from the signature β-sheet signal is calculated as 4. The red shift is indicative of the twist in the β-sheet and accounts for the rigidity or stiffness of the nanofiber (Pashuck et al. 2009). The greater the red shift the greater is the twist in the β-sheet and less rigid or stiffer is the nanofiber (Pashuck et al. 2009). Hence, it is confirmed from the difference in the red shift values between PGA-PA and PA-PA that PGA forms rigid β-sheet conformation than PA-PA.

7.2.5. Melting curve studies

As mentioned before, collagen triple-helical conformation is similar to that of the PPII helix conformation in the CD spectrum with positive ellipticity around 215-240 nm wavelength ((Leikina et al. 2002; Madhan et al. 2008).A typical triple-helix is stabilized by hydrogen bonds present in the intra- and inter-strand (Shoulders et al, 2009). Thus, collagen is sensitive to temperature. Collagen triple-helix conformation follows a highly cooperative behavior during thermal denaturation unlike PPII helix (Bella et al. 1995; Jefferson et al. 1998). Hence, to further confirm that CM-PA forms a triple-helix and is different from that of PPII helix, a thermal melting curve study using CD spectrum was performed for both PGA-CM-PA and PA-CM-PA. The thermal unfolding experiment monitors the spectral maximum as temperature is increased at 223 nm at the positive ellipticity peak of PGA-CM-PA and PA-CM-PA. The thermal unfolding curve of PGA-CM-PA and PA-CM-PA shown in figure 7.4 red and blue lines respectively

gave a typical sigmoidal transition associated with the cooperative denaturation of triple-helical conformation to single-stranded structure.

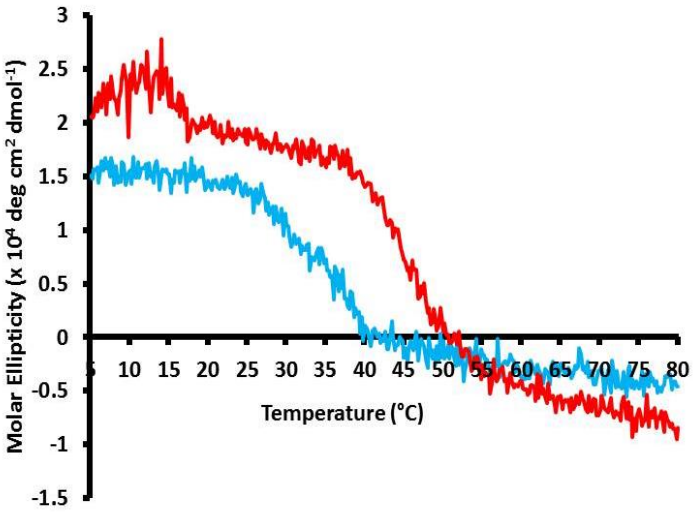

Figure 7.4: CD melting curve spectra of CM-PAs: PGA-CM-PA (red line) and PA-CM-PA (blue line) showing typical sigmoidal transition associated with the cooperative denaturation of triple-helical conformation to single-stranded structure. Thus, confirming that CM-PA forms a triple-helix.

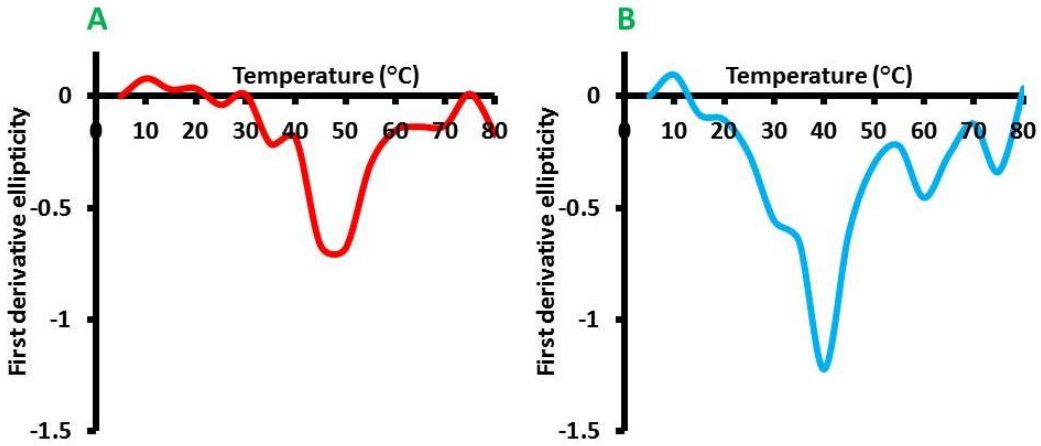

Figure 7.5: First derivative CD melting curve spectra of CM-PAs: PGA-CM-PA (red line) and PA-CM-PA (blue line) showing the melting temperature as 50°C and 40°C respectively.

The first derivative of the melting curve for a 5mM solution of PGA-CM-PA and PA-CM-PA sample in water as shown in figure 7.5 A and B was plotted. The major transition temperature for PGA-CM-PA was found to be at 50°C whereas

for PA-CM-PA was found to be at 40°C. This indicates that the tight β-sheet packing enabled the stabilization of collagen triple-helix in PGA-CM-PA nanofibers.

7.2.6. Mechanical properties characterization

PGA (construct with 10 % PGA-CM-PA and 90 % PGA-PA) and PA (construct with 10 % PGA-CM-PA and 90 % PGA-PA) hydrogels were characterized for their mechanical properties by rheological studies using AR-G2 rheometer. Strain sweep graphs were taken to determine the linear visco-elastic region of the hydrogels.

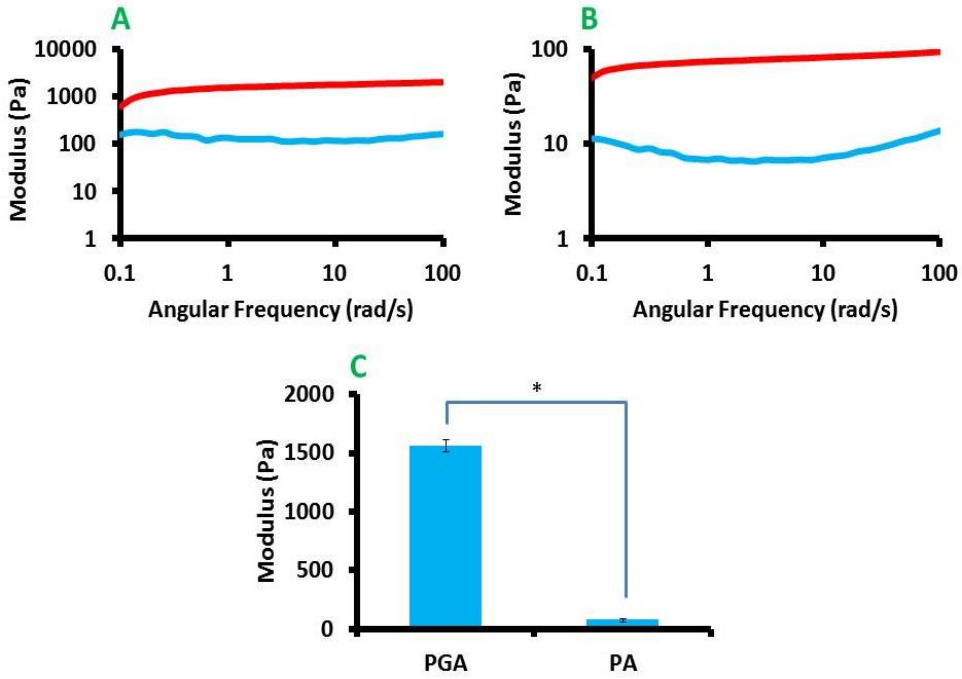

Figure 7.6: Representative frequency sweep curves showing storage modulus, G' (red line) and loss modulus, G" (blue line) for rheological characterization of self-assembled CM-PA nanofiber hydrogels (A) PGA (construct with 10% of PGA-CM-PA and 90% of PGA-PA) and (B) PA (construct with 10% of PA-CM-PA and 90% of PA-PA) formed after charge screening using salt trigger. (C) G' values of PGA and PA nanofiber hydrogels at a frequency of 1 rad/s. *P<0.05 (Student's t-test).

Then, the frequency sweep tests were carried out in the linear visco-elastic region. The frequency sweep tests were carried out to inspect the microstructure of the material, specifically, the strength of the material. The frequency sweep tests yielded two material responses i.e. storage modulus (G') and loss modulus (G"). The G' is the elastic solid like behavior and the G" is the viscous response. From the frequency sweep graphs shown in figure 7.6 A and B, it is evident that the PGA and PA hydrogels differ in their G' and G" responses. However, for both hydrogels, G' was found to be greater than their respective G" for all the frequency range. Physically, in a material, at the microstructure level, there are forces between the molecules. These forces holding the microstructure can be broken by application of external force. When the applied external force is smaller than the microstructural forces then the G' is greater than G'', such a material is said to be elastic. This shows that the material has some capacity to store energy and to regain to some extent its original form which it had before application of external force. However, the material is not ideal elastic as some of the mechanical energy is dissipated as indicated by G''. Thus, the behavior of both PGA and PA hydrogels is indicative of dominant elastic nature over viscous nature at all frequency range (Liu et al. 2013).

As shown in figure 7.6 C, the G' values of PGA and PA hydrogels at a frequency of 1 rad/s were compared to determine the relative hydrogel strengths. G' of PGA was found to be significantly higher compared to that of PA hydrogel by about 20 times. This difference is attributed to difference in stiffness of the individual PA

design. The difference in the stiffness of the individual PA is due to the peptide sequence difference in the β-sheet region of the PA (Pashuck et al. 2010). This difference results in the difference in the twisting of the β-sheets resulting in the difference in the stiffness. The twisting of the β-sheet is observed by the red shift values in the CD spectrum. From the CD spectrum, it is observed that alanine repeat PA nanofibers are more twisted than alanine and glycine repeat PA (Section 7.2.4) However, in nature, alanine repeat sequence sequences are known to form stronger β-sheets than alternating alanine and glycine repeats. In alanine repeat sequence, tight packing between the alanine sequences with hydrophobic interactions of methyl side chain groups prevents the voids in the structure, but, in the alternating alanine and glycine residues, voids are introduced by the glycine residues (Xiao et al. 2009). Hence, it is probable that the additional flexibility offered by the alternating glycine residue might result in the formation of higher hydrogen bonding between residues in the tight core resulting in less twisted and stiffer nanofiber.

7.2.7. Fibroblasts culture within sequence modified hydrogels

L929 fibroblast cells were cultured within PGA and PA nanofiber hydrogels. The morphology of the fibroblast cells were studied under optical microscope as shown in figure 7.7. Fibroblast cells within PGA hydrogels exhibited typical fibroblast flat spindle shape morphology on Day 5 and fibroblasts within PA hydrogels showed rounded morphology on Day 5. The rounded morphology of fibroblasts on PA hydrogels can be attributed to lack of mechanical strength of PA

hydrogel and flat spindle shape morphology of fibroblasts within PGA can be atributed to the presence of sufficient mechanical strength of PGA hydrogel (Discher et al. 2005; Elter et al. 2011).

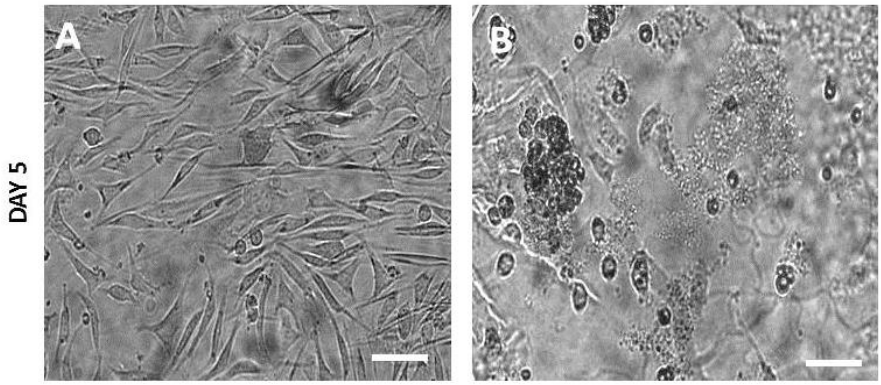

Figure 7.7:Optical light microscope images of fibroblasts within self-assembled CM-PA nanofiber hydrogels (A) PGA (construct with 10% of PGA-CM-PA and 90% of PGA-PA) and (B) PA (construct with 10% of PA-CM-PA and 90% of PA-PA) formed after charge screening using salt trigger on Day 5. The scale of the images is 100 microns.

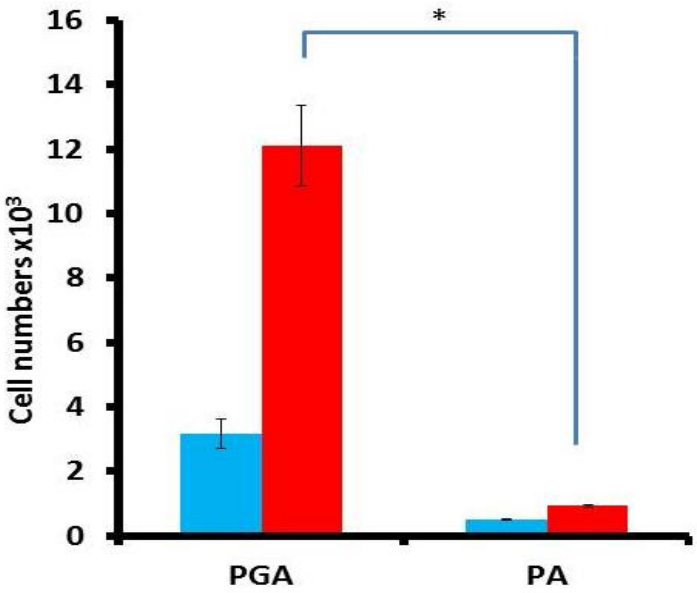

Figure 7.8: Cell proliferation assay of fibroblasts within self-assembled CM-PA nanofiber hydrogels (A) PGA (construct with 10% of PGA-CM-PA and 90% of PGA-PA) and (B) PA (construct with 10% of PA-CM-PA and 90% of PA-PA) formed after charge screening using salt trigger on Day3 (blue columns) and Day 7 (red columns). *P<0.05 (Student's t-test).

The cell proliferation on the above constructs is quantified using MTT assay for

Day 3 and Day 7 and plotted in the graph as shown in figure 7.8 and Student's t-test with 95% confidence level was used for the analysis of significance. There is significant difference in the cell numbers of within PGA and PA hydrogels on Day 7. The significantly higher cell numbers on PGA hydrogels over PA hydrogels can be attributed to the presence of appropriate mechanical cue at the nano-scale level and collagen mimetic biochemical cue.

7.3. Conclusion

Single tail peptide amphiphile design has versatile capabilities to be tuned for presenting varying biochemical and mechanical cues. The versatility of peptide amphiphile designs is attributed to its modular design with each segment with role to play. Peptide amphiphile can be tuned for their mechanical properties by varying the sequence in the β-sheet segment of the peptide region. Thus, collagen mimetic peptide amphiphile designs modified with spider silk and silkworm silk conserved crystalline amino acid sequences in the β-sheet segment of peptide amphiphile offer varying material properties specifically varying mechanical strengths. This design essentially de-couples the biochemical and mechanical cue of the nanofiber. Both collagen mimetic peptide amphiphile hydrogels confirm the role of cell instructive sequence GFOGER for cell adhesion and cell proliferation. However, collagen mimetic peptide amphiphile design modified with silkworm silk's conserved sequence of alternating glycine and alanine repeats forms mechanically stiffer hydrogels than the design with spider silk's conserved sequence of alanine repeats and this difference results in difference in the cell

morphology of the fibroblast cell, eventually reflecting it in the cell viability and proliferation. These results emphasize the need for the scaffolds to possess appropriate mechanical cue in the nanoscale level specific to the tissue. In essence, collagen mimetic peptide amphiphile design modified with silkworm silk's conserved sequence of alternating glycine and alanine repeats offers a novel design for collagen mimics with the potential to be used for in-situ tissue engineering and regenerative biomedical applications and for drug testing purposes.

CHAPTER 8

CONCLUSIONS AND FUTURE PROSPECTS

The research findings and conclusions from each study will be presented as an overview. In particular, the development of cell-instructive collagen mimetic peptide amphiphile hydrogel scaffold with appropriate biochemical and mechanical cue for fibroblast cell culture will be covered.

In addition, further prospects of the developed collagen mimetic peptide amphiphile hydrogel for tissue engineering and regenerative approaches will also be proposed.

8.1. Development of collagen mimetic peptide amphiphile scaffold designs

In this work, we have developed collagen mimetic peptide amphiphile hydrogel scaffold designs through various approaches. These approaches were (i) Fabrication of semi-interpenetrating network hydrogel of collagen mimetic peptide amphiphile and poly(ethylene glycol) diacrylate to introduce bulk mechanical strength to the collagen mimetic peptide amphiphile hydrogel (chapter 5), (ii) Fabrication of covalently modified glutaraldehyde cross-linked collagen mimetic peptide amphiphile hydrogel to introduce mechanical strength on the nanoscale level by formation of nanofiber bundles (chapter 6), and (iii) Fabrication of sequence modified collagen mimetic peptide amphiphile hydrogel, where the sequence is derived from the mechanically strong natural fiber – silk (chapter 7). Following the various fabrication techniques, we further characterized the collagen mimetic peptide amphiphile hydrogel scaffolds in terms of the scaffolds' microstructures, mechanical properties and other physical parameters in line with the scaffold design. Through these characterizations, we were able to ensure that the scaffolds were fabricated properly and the mechanical stiffness achieved for the scaffold was physiologically relevant for L929 fibroblast cell culture. Upon confirmation, these scaffold designs were employed for fibroblast cell culture to understand the influence of the scaffold cues on the fibroblast cell adhesion, morphology and proliferation. All the scaffold designs essentially de-couple the mechanical and biochemical cues of the scaffold, thus, enabling to understand the effect of each cue.

In summary, the 2D architecture obtained by K-CM-PA nanofiber coating on cell culture plate provided high fibroblast cell numbers with ideal fibroblast morphology of 6.6 x 10^3. In this construct, the fibroblast cells grew in their typical morphology owing to the presence of cell instructive GFOGER collagen mimetic sequence from CM-PA and the mechanical strength in the nanoscale level from the short K-PA and at the microscale level from the surface of the culture plate. Hence, the aim to study the necessity and to achieve a 3D architectural scaffold that can provide cell instructive GFOGER collagen mimetic sequence and mechanical strength at both nanoscale and microscale level was developed.

3D architecture of S-IPN hydrogel of mixed PA i.e. K-CM-PA and PEGDA gave high fibroblast cell numbers of 2.9 x 10^3 with ideal fibroblast morphology. With the S-IPN of PA and PEGDA, it was concluded that the presence of cell instuctive collagen sequence alone doesn't ensure favourable fibroblast cell growth. In addition to cell instructive biochemical cue appropriate tissue specific mechanical properties is imperative. The scaffold design also reveals the importance of mechanical cue in nanoscale level to be favorable for fibroblast cells than microscale level.

Further, 3D architecture of cross-linked K-CM-PA nanofiber gels gave high fibroblast cell numbers of 9.5 x 10^3 with ideal fibroblast morphology. In these constructs, nanoscale mechanical cue required for the fibroblast cells was achieved by cross-linking the nanofibers to each other and forming fiber bundles.

Fibroblasts cultured on these scaffold with varying mechanical strength displayed the required fibroblast morphology on the scaffold possessing the mechanical strength close to its physiological conditions.

Finally, by understanding the need of both collagen cell instructive biochemical cue and mechanical strength approprite to the physiological conditions in the nanoscale level led to fabrication of sequence modified CM-PA hydrogel inspired from the mechanically strong natural fiber – silk. In the desired PGA construct very high fibroblast cell numbers 12.1 $x10^3$ were obtained with ideal fibroblast morphology. Indeed, this scaffold design provided the necessary cell cues i.e. nano-topography, biochemical and mechanical cues required for the favorable fibroblast cell culture. In a gist, the fibroblast cell numbers in various constructs providing typical fibroblast morphology is tabulated in table 8.1.

Table 8.1: Comparison of fibroblast cell numbers on various constructs that provide typical fibroblast morphology.

Construct providing typical fibroblast morphology	Nanofiber coated K-CM-PA	1% hydrogel K-CM-PA	S-IPN K-CM-PA-PEGDA	Cross-linked 1 PA : 1 Glt	PGA
Fibroblast cell number ($x10^3$)	6.6 At Day 7	-	2.9 At Day 7	9.5 At Day 7	12.1 At Day 7

Overall, the aim to achieve a collagen mimetic peptide amphiphile hydrogel with appropriate mechanical cue for the culture of fibroblast cells for biomedical applications is met. However, in comparison to the collagen coated construct which has cell numbers of 15.7 x 10^3 at Day 5 even CM-PA nanofiber with modified

silkworm's silk fibroin peptide sequence i.e. PGA-CM-PA, doesn't come close. This indicates that the a combination of two or more tissue specific cell instructive peptide sequences, such as RGD and DGEA are needed along with GFOGER for better mimicking collagen ECM for effective cell adhesion and cell proliferation.

8.2. Novelty

This study to the best of my knowledge is the first study to focus on the biological cellular behavior of fibroblasts on the shorter fragment of collagen i.e. collagen mimetic peptide containing the collagen specific cell binding region i.e. "glycine (G) – phenylalanine (F) – hydroxyproline (O) – glycine (G) – glutamine (E) – arginine (R)" (GFOGER) incorporated in a functional design of a nanofiber in a hydrogel. This study is also the first to study the effect of CM-PA hydrogels with varying mechanical strength on the behavior of fibroblasts.

The novelty of the study is also in the design strategy of the hydrogel in the form of semi-interpenetrating network of PEGDA and CM-PA to study the effect of varying mechanical cues.

This study is also the first study to understand the effect of tunable mechanical properties of CM-PA with varying peptide sequences in the form of a hydrogel for the cellular interactions with fibroblasts.

8.3. Future Prospects

This work started off with a bigger aim to obtain a collagen mimetic peptide amphiphile hydrogel skin equivalent scaffold for wound healing applications which is the perfect replacement for all the existing collagen-based skin equivalent products. However, the approach to use CM-PA hydrogel in its original designed form by our group (Luo et al. 2011) wasn't feasible (Chapter 4) as the scaffold requirements for fibroblast cells are varied from that is offered in the original scaffold design. Thus, these new scaffold designs open the door to explore the use of CM-PA hydrogels for skin equivalent products.

The design of semi-interpenetrating network hydrogel of CM-PA and PEGDA has been successfully employed in this study to examine the role of the cell instructive GFOGER sequence and the effect of microscale mechanical strength for fibroblast cell culture. However, this design is not viable for the intended application of skin equivalent because of its relatively low cell proliferation capability in comparison with other design constructs as shown in table 8.1.

The design of covalently modified glutaraldehyde cross-linked collagen mimetic peptide amphiphile hydrogel to introduce mechanical strength on the nanoscale level by formation of nanofiber bundles. This design definitely confirmed the need for the material to possess mechanical strength on the nanoscale level, but, the use of this material as skin equivalent will be hindered due to the use of glutaraldehyde as the chemical cross-linker. Glutaraldehyde has toxic nature due

to its ubiquitous cross-linking ability with specific functional groups of amino acids. This design limits the in-situ fabrication capability and 3D cell culture capability by cell encapsulation of peptide amphiphile system due to the presence of glutaraldehyde. In addition, the presence of uncross-linked glutaraldehyde in the constructs has the potential to cause adverse effect to the in-situ tissues.

The design of sequence modified collagen mimetic peptide amphiphile hydrogel, where the sequence is derived from the mechanically strong natural fiber – silk is an ideal design to carry forward. This design taps the tremendous advantages of peptide amphiphile system and has the capability to provide all the necessary cell instructive cues like biochemical, nano-topographical and mechanical. Also, the design of the hydrogel construct can be modified to include two or more cell instructive PA sequences containing collagen derived peptide sequences such as DGEA and RGD in the epitope region, interspersed with PGA-CM-PA peptide amphiphile sequence. In such a hydrogel construct, the biological cell instructive ability can be further enhanced, thus, enabling to mimic collagen functional capability even more closely. Then, to further the desire to develop a collagen mimetic skin equivalent, the first step would be to culture human dermal fibroblast cells and keratinocyte cells. This study should focus on cell proliferation and cell functional behavior of the cells on the scaffold in 3D cell encapsulated configuration.

Apart from the use of CM-PA hydrogel for skin tissue engineering, it can be used

for various organ tissue engineering such as liver, cornea, lungs, brain and so on. In addition, the collagen mimetic peptide amphiphile hydrogel can be used as a scaffold for *in vitro* drug testing tools like the organ-on-chip designs. However, uses of collagen mimetic peptide amphiphile hydrogel for these applications have to researched upon. This study only provides a preliminary examination of how scaffold can be customized to provide cell instructive cues.

BIBLIOGRAPHY

Akbal, C., S. D. Lee, S. C. Packer, M. M. Davis, R. C. Rink, and M. Kaefer (2006). “Bladder augmentation with acellular dermal biomatrix in a diseased animal model,” Journal of Urology 176; 1706–1711.

Alenghat, F. J., and D. E. Ingber, (2002), “Mechanotransduction: all signals point to cytoskeleton, matrix, and integrins.” Science STKE: Signal Transduction Knowledge Environment 119; Pe6.

Altman G.H., F. Diaz, C. Jakuba, T. Calabro, R. L. Horan, J. Chen, H. Lu, J. Richmond and D. L. Kaplan (2003). “Silk-based biomaterials” Biomaterials 24: 401–416.

Angeloni, N. L., C. W. Bond, Y. Tang, D. A. Harrington, S. Zhang, S. I. Stupp, K. E. McKenna and C. A. Podlasek (2011). "Regeneration of the cavernous nerve by Sonic hedgehog using aligned peptide amphiphile nanofibers." Biomaterials 32(4): 1091-1101.

Annabi N., J. W. Nichol, X. Zhong, C. Ji, S. Koshy, A. Khademhosseini, F. Dehghani (2010). “Controlling the Porosity and Microarchitecture of Hydrogels for Tissue Engineering.” Tissue Engineering Part B 16(4): 371-383.

Beier, J.P., D. Klumpp, M. Rudisile, R. Dersch, J. H. Wendorff., O. Bleiziffer., A. Arkudas., E. Polykandriotis, R. E. Horch.and U. Kneser (2009). “Collagen matrices from sponge to nano: new perspectives for tissue engineering of skeletal muscle,” BMC Biotechnology 9(34): 216-23.

Bella, J., B. Brodsky and H. M. Berman (1995). "Hydration structure of a collagen peptide." Structure 3(9): 893-906.

Bhowmick, N. A., E. G. Neilson, and H. L. Moses (2004). “Stromal fibroblasts in cancer initiation and progression.” Nature 432: 332-337.

Boccafoschi, F., N. Rajan, J .Habermehl, and D. Mantovani (2007). “Preparation and Characterization of a Scaffold for Vascular Tissue Engineering by Direct-Assembling of Collagen and Cells in a Cylindrical Geometry,” Macromolecular Bioscience 7(5): 719–726.

Boranic, M., J. Jakic-Razumovic, S. Stanovic, A. Kljenak, and I. Fattorini (1999). “Skin cell culture: utilization in plastic surgery and laboratory studies.” Lijecnicki vjesnik 121(4-5):137-43.

Bozkurt A. R. Deumens, C. Beckmann, L. O. Damink, F. Schügner, I. Heschel, B.

Sellhaus, J. Weis, W. Jahnen-Dechent, G. A. Brook, and N. Pallua (2009). "In vitro cell alignment obtained with a Schwann cell enriched microstructured nerve guide with longitudinal guidance channels," Biomaterials 30: 169–179.

Bradshaw M., D. Ho, M. W. Fear, F. Gelain, F. M. Wood and K. S. Iyer (2014). "Designer self-assembling hydrogel scaffolds can impact skin cell proliferation and migration." Scientific Reports 4:6903.

Brakebusch, C., and R. Fassler (2003). "The integrin-action connection, an eternal love affair." EMBO Journal 22: 2324–2333.

Branchet, M.C., S. Boisnic, and C.Francès (1990). "Skin thickness changes in normal aging skin." Gerontology 36: 28-35.

Briceno, P.C., D. Bihan, M. Nilges, S. Hamaia, J. Meseguer, A. García-Ayala, R.W. Farndale, and V. Mulero (2011). "A role for specific collagen motifs during wound healing and inflammatory response of fibroblasts in the teleost fish gilthead sea bream," Molecular Immunology 48(6-7): 826–834.

Brigham M. D., A. Bick, E. Lo, A. Bendali, J. A. Burdick and A, Khademhosseini (2009). "Mechanically Robust and Bioadhesive Collagen and Photocrosslinkable Hyaluronic Acid Semi-Interpenetrating Networks." Tissue Engineering: Part A 15(7).

Brooke. N. Mason., P. C. Joseph, and Cynthia A. "Engineering Biomaterials for Regenerative Medicine: Novel Technologies for Clinical Applications,": Book - Reinhart-King S.K. Bhatia (ed.)

Canty, E.G., and K. E. Kadler (2005). "Procollagen trafficking, processing and fibrillogenesis." Journal of Cell Science 118: 1341–1353.

Carlson, M.A., A. K. Prall, J. J. Gums, A. Lesiak, and V. K Shostrom (2009). "Biologic variability of human foreskin fibroblasts in 2D and 3D culture: implications for a wound healing model," BMC Research Notes 2: 229 -235.

Chan B. K., C. C. Wippich, W. Chia-Jung, P. M. Sivasankar and G. Schmidt (2012). "Robust and Semi-Interpenetrating Hydrogels from Poly(ethylene glycol) and Collagen for Elastomeric Tissue Scaffolds." Macromolecular Bioscience 12 (11): 1490-1501

Chandrasekaran. A. R., **J.** Venugopal, **S.** Sundarrajan, **S.** Ramakrishna (2011). "Fabrication of a nanofibrous scaffold with improved bioactivity for culture of human dermal fibroblasts for skin regeneration." Biomedical Materials 6(1): 015001.

Chen Y., H. Gan, and Y. W. Tong, (2014) “Mechanical Role of Nephila Clavipes Dragline Elastic Motifs in Self-Assembling Silk-Mimetic Peptide Hydrogel” (Submitted)

Chou, P.Y., and G. D. Fasman, (1974). "Prediction of Protein Conformation," Biochemistry 13, 222-245.

Chow, L. W., R. Bitton, M. J. Webber, D. Carvajal, K. R. Shull, A. K. Sharma and S. I. Stupp (2011). "A bioactive self-assembled membrane to promote angiogenesis." Biomaterials 32(6): 1574-1582.

Chung, H. K., and T. G. Park (2009). “Self-assembled and nanostructured hydrogels for drug delivery and tissue engineering.” Nanotechnology Today 4(5):429–437.

Clark, R. A., (1996). “The molecular and cellular biology of wound repair,” New York, NY: Plenum Press.

Cui, H., M. J. Webber, and S. I. Stupp, (2010). “Self-assembly of peptide amphiphiles: from molecules to nanostructures to biomaterials.” Biopolymers 94 (1): 1-18.

Cunniff P. M., S. A. Fossey, M. A. Auerbach, J. W. Song, D. L. Kaplan, W. W. Adams, R. K. Eby, D. Mahoney, and D. L. Vezie (1994). “Mechanical and thermal properties of dragline silk from the spider Nephila clavipes.” Polymers for Advanced Technologies 5:401–10.

Cushing, M. C., and K. S. Anseth, (2007). “Hydrogel Cell Cultures.” Science 316: 1133-1134.

Da Rocha, Azevedo B., H. Chin-Han, and F. Grinnell (2012). “Fibroblast cluster formation on 3D collagen matrices requires cell contraction—Dependent fibronectin matrix organization.” Experimental Cell Research 319(4): 546–555.

Daley W.P., S. B. Peters, and M. Larsen (2008). “ Extracellular matrix dynamics in development and regenerative medicine,” Journal of Cell Science 121, 255–264.

Davis, K. A., and K.S. Anseth (2002). “Controlled release from crosslinked degradable networks.” Critical Reviews in Therapeutic Drug Carrier Systems 19: 385–423.

De Rosa M. M. Carteni, O. Petillo, A. Calarco, S. Margarucci , F. Rosso, A. De Rosa, E. Farina, P. Grippo, and G. Peluso (2004). “Cationic Polyelectrolyte Hydrogel Fosters Fibroblast Spreading, Proliferation, and Extracellular Matrix Production: Implications for Tissue Engineering,” Journal of cellular

physiology 198: 133–143.

Delon, I., and N. H. Brown (2007). “Integrins and the actin cytoskeleton.” Current Opinions Cell Biology 19: 43–50.

Di Lullo, A. G., S. M. Sweeney, J. Körkkö., L. Ala-Kokko, and J. D. San Antonio (2002). "Mapping the Ligand-binding Sites and Disease-associated Mutations on the Most Abundant Protein in the Human, Type I Collagen". Journal of Biological Chemistry 277 (6): 4223–4231.

Discher, D.E., J. Paul, W. Yu-li (2005). “Tissue Cells Feel and Respond to the Stiffness of Their Substrate,” Science 310: 1139-1143.

Drury, J.L., and D. J. Mooney, (2003). “Hydrogels for tissue engineering: scaffold design variables and applications.” Biomaterials 24:4337–4351.

Du, C., C. Du, F. Z. Cui, W. Zhang, Q. L. Feng, X. D. Zhu, and K. de Groot (2000). “Formation of calcium phosphate/collagen composites through mineralization of collagen matrix,” Journal of Biomedical Materials Research A 50: 518–527.

Eckes, B., M. C. Zweers, Z. G. Zhang, R. Hallinger, C. Mauch, M. Aumailley, and T. Krieg (2006). “Mechanical tension and integrin alpha 2 beta 1 regulate fibroblast functions.” Journal of Investigative Dermatology 11:66–72.

Edalat, F., I. Sheu, S. Manoucheri, and A. Khademhosseini (2012). “Material strategies for creating artificial cell-instructive niches.” Current Opinion in Biotechnology 23: 820–825.

Elaine, F., and S. Raghavan (2002). “Getting under the skin of epidermal morphogenesis.” Nature Reviews Genetics 3: 199-209.

El-Sherbiny, I. M., & Yacoub, M. H. (2013). “Hydrogel scaffolds for tissue engineering: Progress and challenges.” Global Cardiology Science & Practice 3: 316–342.

Elter P., T. Weihe, R. Lange, J. Gimsa, and U. Beck (2011). “The influence of topographic microstructures on the initial adhesion of L929 fibroblasts studied by single-cell force spectroscopy.” European Biophysics Journal 40:317–327.

Emsley, J., C.G.Knight, R.W.Farndale, and M.J.Barnes (2004). “Structure of the Integrin α2β1-binding Collagen Peptide.” Journal of Molecular Biology 335(4): 1019 - 1028.

Fallas, J.A., L. E. O'Leary, J. D. Hartgerink (2010). “Synthetic collagen mimics: self-assembly of homotrimers, heterotrimers and higher order structures.”

Chemical Society Reviews 39: 3510–3527.

Farahani, R.M., and L. C. Kloth (2008). “The hypothesis of ‘biophysical matrix contraction’: wound contraction revisited,” International Wound Journal 5, 477–482.

Fisher, M. B., and R. L. Mauck (2013). "Tissue engineering and regenerative medicine: recent innovations and the transition to translation." Tissue Engineering Part B, Reviews 19(1): 1-13.

Frantz, C., K. M. Stewart, and V. M. Weaver (2010). “The extracellular matrix at a glance.” Journal of cell science 123: 4195-4200.

Fraser, R. D. B., MacRae, T. P., and Suzuki, E *(*1979*).* “Chain conformation in the collagen molecule.” Journal of Molecular Biology 129: 463-481.

Gaharwar, A. K., S. A. Dammu, J. M. Canter, C. J. Wu, and G. Schmidt, (2011). “Highly extensible, tough, and elastomeric nanocomposite hydrogels from poly(ethylene glycol) and hydroxyapatite nanoparticles.” Biomacromolecules 12 (5), 1641-1650.

Gaharwar, A. K., C. P. Rivera, C. J. Wu, and G. Schmidt (2011). “Transparent, elastomeric and tough hydrogels from poly(ethylene glycol) and silicate nanoparticles.” Acta Biomaterialia 7 (12), 4139-4148.

Geckil, H., F. Xu , X. H. Zhang, S. Moon, and U. Demirici (2010). “ Engineering hydrogels as extracellular matrix mimics.” Nanomedicine 5(3):469–484.

Gjorevski, N., and C. M. Nelson (2009). “Bidirectional extracellular matrix signaling during tissue morphogenesis.” Cytokine Growth Factor Reviews 20: 459–465.

Gobin, A. S., and J. L. West, (2002). “Cell migration through defined, synthetic ECM analogs.” The FASEB Journal 16 (7), 751-753.

Gore T., Y. Dori, Y. Talmon, M. Tirrell and H. Bianco-Peled, (2001). “Self-Assembly of Model Collagen Peptide Amphiphiles”, Langmuir 17: 5352-5360.

Gosline, J. M., P. A. Guertte, C. S. Ortlepp, and K. N. Savage. (1999).”The mechanical design of spider silk: from fibroin sequence to mechanical function.” Journal of Experimental Biology 202:3295–3303.

Gregory, H., A. F. Diaz, C. Jakuba, T. Calabro, R. L. Horan, J. Chen, Helen Lu, John Richmond, and David L. Kaplan (2003). “Silk-based biomaterials” Biomaterials 24: 401–416.

Griffith, M., W. B. Jackson, N. Lagali, K. Merrett, F. Li and P. Fagerholm (2009). "Artificial corneas: A regenerative medicine approach." Eye 23: 1985–1989.

Grinnell, F., (2003). " Fibroblast biology in three-dimensional collagen matrices." Trends in Cell Biololgy 13: 264–269.

Guarino, V., A. Gloria, R. De Santis, and L. Ambrosio, (2010). "Biomedical Applications of Hydrogels Handbook." Springer, Heidelberg, p. 227.

Guo, Hui., J. Zhang, T. Xu , Z. Zhang, J. Yao , and Z. Shao (2013). "The Robust Hydrogel Hierarchically Assembled from a pH Sensitive Peptide Amphiphile Based on Silk Fibroin." Biomacromolecules, 14 (8): 2733–2738.

Hamdan, M. l. Blanco, A. Khraisat, and I. F.Tresguerres (2006). "Influence of titanium surface charge on fibroblast adhesion." Clinical Implant Dentistry and Related Research 8(1): 32-38.

Harris, A. K., P. Warner and D. Stopak (1984). "Generation of spatially periodic patterns by a mechanical instability: a mechanical alternative to the Turing model." Journal of Embryology & Experimental Morphology 80: 1-20.

Hartgerink J. D., E. Beniash, and S. I. Stupp (2001). "Self-Assembly and Mineralization of Peptide-Amphiphile Nanofibers." Science 294(5547): 1684-1688.

Hartgerink J. D., E. Beniash, and S. I. Stupp (2002). "Peptide-amphiphile nanofibers: A versatile scaffold for the preparation of self-assembling materials." Proceedings of the National Academy of Sciences 99(8): 5133-5138.

Hirsch, S. G., and R. J. Spontak (2002). "Temperature-dependent property development in hydrogels derived from hydroxypropyl." Polymer 43(1): 123-129.

Hodgkinson, T., X. F. Yuan, and A. Bayat (2014). "Electrospun silk fibroin fiber diameter influences in vitro dermal fibroblast behavior and promotes healing of ex vivo wound models." Journal of Tissue Engineering 18 (5): online version.

Hoffman, A. S., (2002). "Hydrogels for biomedical applications." Advanced Drug Delivery 43(1):3–12.

Huang, Y., L. Ren, and Y. Qin (1998). "Observation of cicatricial fibroblasts in culture and its biological properties." Chinese Journal of Reparative and Reconstructive Surgery 12(6): 332-5.

Huh, D., B. D. Matthews, A. Mammoto, M. M. Zavala, H. Y. Hsin, and D. E. Ingber (2010). "Reconstituting Organ-Level Lung Functions on a Chip." Science 328(5986): 1662-1668.

Huh, D., G. A. Hamilton and D. E. Ingber (2011). "From 3D cell culture to organs-on-chips." Trends in Cell Biology 21: 745-754.

Hulmes, D. J. S., (2002). "Building collagen molecules, fibrils, and suprafibrillar structures." Journal of Structural Biology 137: 2–10.

Hunt, N. C., and L. M. Grover (2010). "Cell encapsulation using biopolymer gels for regenerative medicine." Biotechnology Letters 32(6):733–742.

Janmey, P.A., and R. T. Miller (2011). "Mechanisms of mechanical signaling in development and disease." Journal of cell science 124: 9-18.

Jefferson, E. A., E. Locardi and M. Goodman (1998). "Incorporation of achiral peptoid-based trimeric sequences into collagen mimetics." Journal of the American Chemical Society 120(30): 7420-7428.

Jiang, D., J. Liang, and P. W. Noble (2007). "Hyaluronan in tissue injury and repair." Annual Review of Cell and Development Bioliology 23: 435–461.

Jiang, H., and F. Grinnell (2005). "Cell-matrix entanglement and mechanical anchorage of fibroblasts in three-dimensional collagen matrices," Molecular Biology of the Cell 16(11): 5070-5076.

Jimenez, P. A., and S. E. Jimenez (2004). "Tissue and cellular approaches to wound repair." American Journal of Surgery 187(5A): 56S-64S.

Jin, R., and P. J. Dijkstra (2010). Biomedical Applications of Hydrogels Handbook (Eds: R. M. Ottenbrite, K. Park, T. Okano), Springer, Heidelberg 2010, p. 203.

Jonker, A. M., D. Lowik, and J. C. M. van Hest (2012). "Peptide- and Protein-Based Hydrogels." Chemistry of Materials 24 (5): 759–773.

Jung, J. P., J. L. Jones, S. A. Cronier, and J. H. Collier (2008) "Modulating the Mechanical Properties of Self-Assembled Peptide Hydrogels via Native Chemical Ligation." Biomaterials 29(13): 2143–2151.

Juliano, R. L., S. Haskill, and N. Carolina (1993). "Signal Transduction from the Extracellular Matrix." The Journal of Cell Biology120: 577–585.

Kadler, K. E., (1995). "Extracellular matrix 1: fibril-forming collagens." Protein Profile 2: 491–619.

Karamichos, D., N. Lakshman, and W. M. Petroll, (2007). "Regulation of corneal

fibroblast morphology and collagen reorganization by extracellular matrix mechanical properties." Investigative Ophthalmology and Visual Science 48(11): 5030–5037.

Karr, J., (2008). "Utilization of living bilayered cell therapy (Apligraf) for heel ulcers." Advanced Skin Wound Care 21, 270–274.

Kennedy, S. B., E.R. de Azevedo, W.A. Petka, T.P. Russell, D.A. Tirrell and M. Hong (2001). "Dynamic Structure of a Protein Hydrogel: A Solid-State NMR Study." Macromolecules 34(25): 8675-8685.

Khew, S. T., and Y. W. Tong (2007). "The Specific Recognition of a Cell Binding Sequence Derived from Type I Collagen by Hep3B and L929 Cells." Biomacromolecules 8: 3153-3161.

Khew, S. T., and Y. W. Tong (2007). "The specific recognition of a cell binding sequence derived from type I collagen by Hep3B and L929 cells." Biomacromolecules 8(10): 3153-31561.

Khew, S. T., and Y. W. Tong (2008). "Template-Assembled Triple-Helical Peptide Molecules: Mimicry of Collagen by Molecular Architecture and Integrin-Specific Cell Adhesion." Biochemistry 47(2): 585-596.

Khew, S. T., Z. X. Hao, and Y. W. Tong (2007). "An integrin-specific collagen-mimetic peptide approach for optimizing Hep3B liver cell adhesion, proliferation, and cellular functions." Tissue Engineering 13(10): 2451-2463.

Kim, J. B., (2005). "Three-dimensional tissue culture models in cancer biology." Seminars in Cancer Biology 15: 365-377.

Kim, S. H., J. Turnbull, and S. Guimond (2011). "Extracellular matrix and cell signalling: the dynamic cooperation of integrin, proteoglycan and growth factor receptor." The Journal of endocrinology 209: 139-51.

Knight, C. G., L. F. Morton, D. J. Onley, A. R. Peachey, A. J. Messent, P. A. Smethurst, D S. Tuckwell, R. W. Farndale and M. J. Barnes (1998). "Identification in collagen type I of an integrin α2β1-binding site containing an essential GER sequence." Journal of Biological Chemistry 273: 33287-33294.

Koide, T., D. L. Homma, S. Asada, K. Kitagawa (2005). "Self-complementary peptides for the formation of collagen-like triple-helical supramolecules." Bioorganic and Medical Chemistry Letters 15(23): 5230–3.

Kopecek, J., (2007). "Hydrogel biomaterials: a smart future." Biomaterials 28(34):5185–5192.

Kotch, F. W., R. T. Raines, (2006). "Self-assembly of synthetic collagen triple-helices." Proceedings of the National Academy of Sciences 103(9): 3028–3033.

Kuhn, K., (1987). "The classical collagens: types I, II and III. In Structure and Function of Collagen Types, Mayne R, Burgeson RE (eds) "Academic Press. 1–42.

Langer, R. and J. P. Vacanti (1993). "Tissue engineering." Science 260(5110): 920-926.

Lecuit, T., and P. F. Lenne (2007). " Cell surface mechanics and the control of cell shape, tissue patterns and morphogenesis." Nature Reviews Molecular Cell Biology 8:633–644.

Lee, H. J., Y. Christopher, T. Chansakul, N. S. Hwang, S. Varghese, S. M. Yu, and J. H. Elisseeff (2008). "Enhanced Chondrogenesis of Mesenchymal Stem Cells in Collagen Mimetic Peptide-Mediated Microenvironment." Tissue Engineering Part A 14(11): 1843 - 1851.

Lee, J., M. J. Cuddihy, and N. A. Kotov (2008). "Three-dimensional cell culture matrices: state of the art." Tissue Engineering Part B 14(1):61–86.

Lee, S. S., E. L. Hsu, M. Mendoza, J. Ghodasra, M. S. Nickoli, A. Ashtekar, M. Polavarapu , J. Babu , R. M. Riaz, J. D. Nicolas, D. Nelson, S. Z. Hashmi, S. R. Kaltz, J. S. Earhart, B. R. Merk , J. S. McKee , S. F. Bairstow, R. N. Shah, W. K. Hsu, and S. I. Stupp (2004). "Gel Scaffolds of BMP-2-Binding Peptide Amphiphile Nanofibers for Spinal Arthrodesis." Advanced Healthcare Materials online version.

Lee, W.F., and Chen, Y.J. (2001). "Studies on preparation and swelling properties of the N-isopropylacrylamide-chitosan semi-IPN and IPN hydrogels." Journal of Applied Polymer Science 82: 2487.

Leikina, E., M.V. Mertts, N. Kuznetsova, S. Leikin (2002). "Type I collagen is thermally unstable at body temperature." Proceedings of the National Academy of Sciences 99: 1314–1318.

Lesley, E. R. O'Leary., F. A. Jorge, B. L. Erica, K. K. Marci, and H. D. Jeffrey (2011). "Multi-hierarchical self-assembly of a collagen mimetic peptide from triple-helix to nanofiber and hydrogel." Nature Chemistry 3: 821-827.

Li, Y., M. Qin, and Y. Cao, (2014). "Designing the mechanical properties of peptide-based supramolecular hydrogels for biomedical applications." Science China Physics, Mechanics & Astronomy 57 (5): 849-858.

Liang, Y., J. Jeong, R. J. DeVolder, C. Cha, F. Wang, Y. W. Tong and H. Kong

(2011). "A cell-instructive hydrogel to regulate malignancy of 3D tumor spheroids with matrix rigidity." Biomaterials 32(35): 9308-9315.

Liao, S., M. Ngiam, C. K Chan, and S Ramakrishna (2009). “Fabrication of nanohydroxyapatite/collagen/osteonectin composites for bone graft applications.” Biomedical Materials 4, 25019.

Lin, C., and A.T. Metters (2006). “Hydrogels in controlled release formulations: Network design and mathematical modeling,” Advanced Drug Delivery Reviews 58: 1379–1408.

Liu, S. Q., R. Tay, M. Khan, P. L. R. Ee, J. L. Hedrick , and Y. Y. Yang (2010). “Synthetic hydrogels for controlled stem cell differentiation.” Soft Matter 6(1):67–81.

Liu, F., J. D. Mih, and B. S. Shea (2010). “Feedback amplification of fibrosis through matrix stiffening and COX-2 suppression.” Journal of Cell Biology 90(4): 693–706.

Liu, M., Y. Zhang, J. Li and C. Zhou (2013). "Chitin-natural clay nanotubes hybrid hydrogel." International Journal of Biological Macromolecules 58: 23-30.

Liu, Y., S. Bharadwaj , S. J. Lee, A. Atala , and Y. Zhang (2009). “Optimization of a natural collagen scaffold to aid cell-matrix penetration for urologic tissue engineering.” Biomaterials 30: 3865–3873.

Lucero, H. A., and H. M. Kagan (2006). “Lysyl oxidase: an oxidative enzyme and effector of cell function.” Cellular and Molecular Life Science 63: 2304–2316.

Lutolf, M. P., (2009). “Biomaterials: Spotlight on hydrogels.” Nature Materials 8(6):451–453.

Luo, J. and Y. W. Tong (2011). “Self-Assembly of Collagen-Mimetic Peptide Amphiphiles into Biofunctional Nanofiber.” ACS Nano 5(10): 7739-7747.

Ma, P. X. ,(2008). “Biomimetic Materials for Tissue Engineering.” Drug Delivery 60: 184.

MacNeil S., (2008). “Biomaterials for tissue engineering of skin” Materials Today (11) 5: 26-35.

Madhan, B., J. Xiao, G. Thiagarajan, J. Baum, and B. Brodsky (2008). “NMR monitoring of chain specific stability in heterotrimeric collagen peptides.” Journal of the American Chemical Society 130: 13520–13521.

Madison, K. C., (2003). "Barrier function of the skin: "la raison d'être" of the epidermis." Journal of Investigative Dermatology 121 (2): 231–41.

Mann, B. K., and J. L. West, (2002). "Cell adhesion peptides alter smooth muscle cell adhesion, proliferation, migration, and matrix protein synthesis on modified surfaces and in polymer scaffolds." Journal of Biomedical Materials 60(1):86-93.

Mellott, M. B., K. Searcy, and M. V. Pishko, (2001). "Release of protein from highly cross-linked hydrogels of poly(ethylene glycol) diacrylate fabricated by UV polymerization." Biomaterials 22: 929 - 941.

Meng Q., Y. Kou, X. Ma, L. Guo, and K. Liu (2014). "Nanostructures from the self-assembly of α-helical peptide amphiphiles." Journal of Peptide Science 20: 223–228.

Metcalfe, A. D., and W. J. F. Mark (2007). "Tissue engineering of replacement skin: the crossroads of biomaterials, wound healing, embryonic development, stem cells and regeneration." Journal of the Royal Society Interface 4: 413–437.

Migneault I., C. Dartiguenave, M. J. Bertrand, and K. C. Waldron (2004). "Glutaraldehyde: behavior in aqueous solution, reaction with proteins, and application to enzyme crosslinking." BioTechniques 37: 790-802.

Molnar, J., K. S. Fong, Q.P. He, K. Hayashi, Y. Kim, S. F. Fong, B. Fogelgren, K. M. Szauter, M. Mink, and K. Csiszar (2003). "Structural and functional diversity of lysyl oxidase and the LOX-like proteins." Biochimestry Biophysica Acta 1647: 220–224.

Moreo, K., (2005). "Understanding and overcoming the challenges of effective case management for patients with chronic wounds." The Case Manager 16 (2): 62–3, 67.

Moulin, V. J., (2013). "Reconstitution of skin fibrosis development using a tissue engineering approach." Methods in Molecular Biology 961: 287-303.

Myllyharju, J., (2005). "Intracellular post-translational modifications of collagens." Top Current Chemistry 247: 115–247.

Oh, J. K., (2010). "Engineering of nanometer-sized cross-linked hydrogels for biomedical applications." Canadian Journal of Chemistry 88(3):173–184.

Olde Damink, L. H. H., P. J. Dijkstra, M. J. A. Van Luyn, P. B. Van Wachem, P. Nieuwenhuis, and J. Feijen (1995). "Glutaraldehyde as a crosslinking agent for collagen-based biomaterials." Journal of Materials Science: Materials In Medicine 6: 460-472.

Paramonov, S. E., H. W. Jun, and J. D. Hartgerink (2006). “Modulation of peptide-amphiphile nanofibers via phospholipid inclusions.” Biomacromolecules 7(1): 24–36.

Park, H., M. Radisic, J. O. Lim, B. H. Chang, and G. Vunjak-Novakovicet (2005). “A novel composite scaffold for cardiac tissue engineering.” *In vitro* Cellular and Development Biology Animal 41(7): 188-196.

Pashuck E.T., H. Cui and S. I. Stupp (2009). “Tuning Supramolecular Rigidity of Peptide Fibers through Molecular Structure.” Journal of American Chemical Society 132(17): 6041–6046.

Peppas, N. A., J. Z. Hilt, A. Khademhosseini and R. Langer (2006). “Hydrogels in Biology and Medicine: From Molecular Principles to Bionanotechnology.” Advanced Materials 18: 1345.

Peppas, N.A., P. Bures, W. Leobandung, and H. Ichikawa (2000). “Hydrogels in pharmaceutical formulations,” European Journal of Pharmaceutics and Bio pharmaceutics 50: 27–46.

Peyton, S. R., C. M. Ghajar, C. B. Khatiwala, and A. J. Putnam (2007). “The emergence of ECM mechanics and cytoskeletal tension as important regulators of cell function.” Cell Biochemistry and Biophysics 47: 300–320.

Proksch, E., J. M. Brandner, and J. M. Jensen (2008). "The skin: an indispensable barrier." Experimental Dermatology 17 (12): 1063–72.

Rafat, M., T. Matsuura, F. Li and M. Griffith (2009). “Surface modification of collagen-based artificial cornea for reduced endothelialization.” Journal of Biomedical Materials Research 88: 755–768.

Rajangam, K. H., A. Behanna, M. J. Hui, X. Han, J. F. Hulvat, J. W. Lomasney, and S. I. Stupp (2006). “Heparin binding nanostructures to promote growth of blood vessels.” Nano Letters 6: 2086–2090.

Rajangam, K., A. S. Michael, A. R. Mark and S. I. Stupp (2008). “Peptide Amphiphile Nanostructure-Heparin Interactions and their Relationship to Bioactivity.” Biomaterials 29(23): 3298-3305.

Reed, M. J., N. S. Ferara, and R. B. Vernon (2001). “Impaired migration, integrin function, and actin cytoskeletal organization in dermal fibroblasts from a subset of aged human donors.” Mechanisms of Ageing and Development 122: 1203–1220.

Rhee, S., and F. Grinnell (2007). “Fibroblast mechanics in 3d collagen matrices,” Advanced Drug Delivery Reviews 59(13): 1299-1305.

Rippon, W. B., and A. G. Walton (1971). “Optical Properties of the Polyglycine II Helix.” Biopolymers 10: 1207–1212.

Robinson, K. G., T. Nie, A. D. Baldwin, E. C. Yang, K. L. Kiick, R. E. Akins, (2012). “Differential effects of substrate modulus on human vascular endothelial, smooth muscle, and fibroblastic cells” Journal of Biomedical Materials 100A:1356–1367.

Rothamel, D., F. Schwarz, A. Sculean, M. Herten, W. Scherbaum, J. Becker (2004). “Biocompatibility of various collagen membranes in cultures of human PDL fibroblasts and human osteoblast-like cells.” Clinical Oral Implants Research 15: 443–449.

Rousseau, M., C. D. Hernandez, M. West, A. Hitchcock, and M. Pe´zolet (2007). “Nephila clavipes spider dragline silk microstructure studied by scanning transmission x-ray microscopy.” Journal of the American Chemical Society. 129:3897–3905.

Sakakibara, S., K. Inouye, K. Shudo, Y. Kishida, Y. Kobayashi, and D.J. Prockop (1973). “Synthesis of (Pro-Hyp-Gly)$_n$ of defined molecular weights. Evidence for the stabilization of collagen triple-helix by hydroxyproline.” Biochimica et Biophysica Acta 303(1):198-202.

Santos, E., R. M. Hernández, J. L. Pedraz, and B. Orive G (2012). “Novel advances in the design of three-dimensional bio-scaffolds to control cell fate: translation from 2D to 3D.” Trends in Biotechnology 30(6): 331-41.

Sargeant, T. D., M. S. Oppenheimer, D. C. Dunand, and S. I. Stupp (2008). “Titanium Foam-Bioactive Nanofiber Hybrids for Bone Regeneration.” Journal of Tissue Engineering and Regenerative Medicine 2(8): 455–462.

Sawhney, A. S., C. P. Pathak, and J. A. Hubbell (1993). “Bioerodible hydrogels based on photopolymerized poly(ethyleneglycol)-co-poly(alpha-hydroxyacid) diacrylate macromers.” Macromolecules 26 (4), 581-587.

Schulz, R. M., (2008). “Cartilage tissue engineering by collagen matrix associated bone marrow derived mesenchymal stem cells.” Bio-medical Materials and Engineering 18(1): 55-70.

Sechriest, V. F., Y. J. Miao, C. Niyibizi, A. Westerhausen-Larson, H. W. Matthew, C. H. Evans, F. H. Fu and J. K. Suh (1999). “GAG-augmented polysaccharide hydrogel: A novel biocompatible and biodegradable material to support chondrogenesis.” Journal of Biomedical Materials Research 49(4): 534 – 554.

Sen, C. K., G. M. Gordillo, S. Roy, R. Kirsner, L. Lambert, T. K. Hunt,

F. Gottrup, G. C Gurtner, and M. T. Longaker (2009). “Human Skin Wounds: A Major and Snowballing Threat to Public Health and the Economy.” Wound Repair and Regeneration 17(6): 763–771.

Seow, W. Y., and C. A. E. Hauser (2013). "Tunable Mechanical Properties of Ultrasmall Peptide Hydrogels by Crosslinking and Functionalization to Achieve the 3D Distribution of Cells." Advanced Healthcare Materials 2(9): 1219-1223.

Shoichet, M. S., (2010). “Polymer Scaffolds for Biomaterials Applications.” Macromolecules 43: 581.

Shoulders, M. D., and R.T. Raines (2009). “Collagen structure and stability.” Annual Review of Biochemistry 78: 929–958.

Silva, G. A., C. Czeisler, K. L. Niece, E. Beniash, D. A. Harrington, J. A. Kessler and S. I. Stupp (2004). "Selective Differentiation of Neural Progenitor Cells by High-Epitope Density Nanofibers." Science 303(5662): 1352-1355.

Slaughter, B.V., S. S. Khurshid, O. Z. Fisher, A. Khademhosseini, and N. A. Peppas, (2009). “Hydrogels in regenerative medicine.” Advance Materials 21(32–33): 3307–3329.

Sun L., and Z. Xiaojun, (2012). “A self-assembling peptide RADA16-I integrated with spider fibroin uncrystalline motifs.” International Journal of Nanomedicine 2012:7 571–580.

Sun,W., H. Lin, B. Chen, W. Zhao, Y. Zhao, and J. Dai (2007). “Promotion of peripheral nerve growth by collagen scaffolds loaded with collagen-targeting human nerve growth factor-beta.” Journal of Biomedical Materials Research Part A 83: 1054–1061.

Takahashi, Y., M. Gehoh, and K. Yuzuriha (1999). “Structure refinementand diffuse streak scattering of silk (Bombyx mori).” International Journal of Biology and Macromolecules 24:127–138.

Taraban, M. B., S. Ramachandran, I. Gryczynski, Z. Gryczynski, J. Trewhella, and Y. B. Yu (2011). “ Effects of chain length on oligopeptide hydrogelation.” Soft Matter 7(6): 2624–2631.

Tedder, M. E., J. L, B. Weed, C. Stabler, H. Zhang, A. Simionescu, and D. T. Simionescu (2009). “Stabilized collagen scaffolds for heart valve tissue engineering.” Tissue Engineering Part A 15: 1257–1268.

Thompson, S. A., P. W. Burridge, E. A. Lipke, M. Shamblott, E. T. Zambidis, and L. Tung (2012). “Engraftment of human embryonic stem cell derived

cardiomyocytes improves conduction in an arrhythmogenic in vitro model." Journal of Molecular and Cellular Cardiology 53: 15-23.

Tovar, J. D., R. C. Claussen, and S. I. Stupp (2005). "Probing the interior of peptide amphiphile supramolecular aggregates." Journal of the American Chemical Society 127 (20): 7337-7345.

Trabbic-Carlson, K., L. A. Setton and A. Chilkoti (2003). "Swelling and Mechanical Behaviors of Chemically Cross-Linked Hydrogels of Elastin-like Polypeptides," Biomacromolecules 4(3): 572-580.

Trottier, V., G. Marceau-Fortier, L. Germain, C. Vincent, and J. Fradette (2008). "FATS collection: Using human adipose-derived stem/stromal cells for the production of new skin substitutes." Stem Cells 15(6): 1257–1268

Tysseling, V. M., V. Sahni, E. T. Pashuck, D. Birch, A. Hebert, C. Czeisler, S. I. Stupp and J. A. Kessler (2010). "Self-assembling peptide amphiphile promotes plasticity of serotonergic fibers following spinal cord injury." Journal of Neuroscience Research 88(14): 3161-3170.

Tysseling-Mattiace, V. M., V. Sahni, K. L. Niece, D. Birch, C. Czeisler, M. G. Fehlings, S. I. Stupp and J. A. Kessler (2008). "Self-assembling nanofibers inhibit glial scar formation and promote axon elongation after spinal cord injury." Journal of Neuroscience 28(14): 3814-3823.

Van der Rest, M., and R. Garrone (1991). "Collagen family of proteins." FASEB Journal 5: 2814–2823.

Vendamme, R., S. Y. Onoue, A. Nakao, and T. Kunitake, (2006). "Robust free-standing nanomembranes of organic-inorganic interpenetrating networks." Nature Materials 5: 494-501.

Verderio. E. A., T. S. Johnson, and M. Griffin (2005). "Transglutaminases in wound healing and inflammation." Progess in Experimental Tumor Research 38: 89–114.

Wang, N., and D. E. Ingber, (1994). "Control of cytoskeletal mechanics by extracellular matrix, cell shape, and mechanical tension." Biophysics Journal 66: 2181–2189.

Watt, F. M., (1988). "The epidermal keratinocyte." Bioessays 5:163-167.

Webber, M. J., J. Tongers, M. A. Renault, J. G. Roncalli, D. W. Losordo and S. I. Stupp (2010). "Development of bioactive peptide amphiphiles for therapeutic cell delivery." Acta Biomaterialia 6(1): 3-11.

Webber, M. J., J. Tongers, C. J. Newcomb, K. T. Marquardt, J. Bauersachs, D. W.

Losordo, and S. I. Stupp (2011). "Supramolecular nanostructures that mimic VEGF as a strategy for ischemic tissue repair." Proceedings of the National Academy of Sciences 108(33):13438-43.

Weng, L., A. Gouldstone, Y. Wu, and W. Chen, (2008). "Mechanically strong double network photocrosslinked hydrogels from N,N-dimethylacrylamide and glycidyl methacrylated hyaluronan." Biomaterials 29:2153.

Wichterle, O., and D. Lim (1960). "Hydrophilic gels for biological use." Nature 185:117–118.

Williams, D.F., (1999). "The Williams Dictionary of Biomaterials." Liverpool University Press.

Williams, D. F., (2014). "The Biomaterials Conundrum in Tissue Engineering." Tissue Engineering : Part A 20(7-8): 1129-1131

Winterswijk, P. J. V., and Erik Nout (2007). "Tissue Engineering and Wound Healing: An Overview of the Past, Present, and Future." Wounds 19(10): 277-284.

Wozniak, M.A., and C. S. Chen (2009). "Mechanotransduction in development: a growing role for contractility." Nature reviews Molecular cell biology 10: 34-43.

Xiao S., W. Stacklies, M. Cetinkaya, B. Markert, and F. Gräter (2009). "Mechanical Response of Silk Crystalline Units from Force-Distribution Analysis." Biophysical Journal 96: 3997–4005.

Xu, X., Y. Jin, Y. Liu, X. Zhang, and R. Zhuo (2010). "Self-assembly behavior of peptide amphiphiles (PAs) with different length of hydrophobic alkyl tails." Colloids and Surfaces B:Biointerfaces 81(1): 329–335.

Yamazaki, C. M., S. Asada, K. Kitagawa, and T. Koide (2008). "Artificial collagen gels via self-assembly of de novo designed peptides." Biopolymers 90 (6):816–823.

Yamazaki, C. M., Y. Kadoya, K. Hozumi, H. Okano-Kosugi , S. Asada, K. Kitagawa, M. Nomizu, and T. Koide, (2010). "A collagen-mimetic triple-helical supramolecule that evokes integrin-dependent cell responses." Biomaterials 31: 1925–1934.

Zhang, J., R. Hao, L. Huang, J. Yao, X. Chen and Z. Shao, (2011) "Self-assembly of a peptide amphiphile based on hydrolysed Bombyx mori silk fibroin." Chemical Communications (Cambridge) 47(37): 10296-10298.

Zhang, S., M. A. Greenfield, A. Mata, L. C. Palmer, R. Bitton, J. R. Mantei, C.

Aparicio, M. O. De La Cruz and S. I. Stupp (2010). "A self-assembly pathway to aligned monodomain gels." Nature Materials 9(7): 594-601.

Zheng, L., J. Sun, X. Chen, G. Wang, B. Jiang, H. Fan, and X. Dong (2009). "In vivo cartilage engineering with collagen hydrogel and allogenous chondrocytes after diffusion chamber implantation in immunocompetent host." Tissue Engineering Part A 15(8): 2145-2153.

Zhu, J., (2010). "Bioactive modification of poly(ethylene glycol) hydrogels for tissue engineering." Biomaterials 31(17):4639–4656.

Zhu, J., C. Tang , K. Kottke-Marchant and R. E. Marchant (2009). "Design and Synthesis of Biomimetic Hydrogel Scaffolds with Controlled Organization of Cyclic RGD Peptides," Bioconjugate Chemistry 20(2): 333-339.

Zhu, J., and R. E. Marchant (2011). "Design properties of hydrogel tissue-engineering scaffolds." Expert Review of Medical Devices 8(5): 607–626.

APPENDIX A

LIST OF PUBLICATIONS

Journal publications

1. Sundar S., Chen Y., Tong Y. W. (2014). "Delivery of therapeutics and molecules using self-assembled peptides." Current Medicinal Chemistry. 21(22):2469-2479.

2. Sundar S., Tong Y. W. "Role of mechanical strength in collagen mimetic peptide amphiphile hydrogels investigated with polymer network design" (in preparation)

3. Sundar S., Zhu M., Tong Y. W. "Investigation of nanoscale tuning of mechanical strength using cross-linked collagen mimetic gels" (in preparation)

4. Sundar S., Tong Y. W. "Nature inspired silk conjugated collagen mimetic peptide amphiphile hydrogels" (in preparation)

Conference publications

1. Sushmitha Sundar, Yen Wah Tong, 2013, 15th Asian Pacific Confederation of Chemical Engineering Congress, Korea.

2. Sushmitha Sundar, Yen Wah Tong, 2013, 7th East Asian Consortium on Biomedical Engineering, Taiwan.

3. Sushmitha Sundar, Yen Wah Tong, 2014, 2nd IBN International Symposium, Singapore.

4. Sushmitha Sundar, Yen Wah Tong, 2014, 3rd Hong Kong International Conference on Engineering and Applied Sciences, Hong Kong.

APPENDIX B

Table B.1: Letter codes of naturally occurring and non-natural (marked with *) amino acids.

Aminoacids	**3 letter code**	**1 letter code**
Alanine	Ala	A
Arginine	Arg	R
Asparagine	Asn	N
Aspartic acid/ Aspartate	Asp	D
Cysteine	Cys	C
Glutamine	Gln	Q
Glutamic Acid/ Glutamate	Glu	E
Glycine	Gly	G
Histidine	His	H
Hydroxyproline*	Hyp*	O*
Isoleucine	Ile	I
Leucine	Leu	L
Lysine	Lys	K
Methionine	Met	M
Phenylalanine	Phe	F
Proline	Pro	P
Serine	Ser	S
Threonine	Thr	T
Tryptophan	Trp	W
Tyrosine	Tyr	Y
Valine	Val	V